

Kasper Keskinen

ENERGY STORAGES IN HIGH-POWER STATCOM APPLICATIONS

Master of Science Thesis
Faculty of Information Technology and Communication Sciences
Examiner: Doctoral researcher Joni Markkula
Examiner: Associate professor Tomi Roinila
June, 2022

ABSTRACT

Kasper Keskinen: Energy storages in high-power STATCOM applications
Master of Science Thesis
Tampere University
Master's Degree Programme in Electrical Engineering
June 2022

Renewable energy sources are connected to the electric grid at an increasing pace. Previously synchronous generators have been the basis of stable grid operation, but nowadays and in the future, synchronous generators are being replaced by renewable energy sources that are grid connected using power electronics converters. Replacement of synchronous machines can cause for example decrease of inertia which can make the power grid more vulnerable to stability issues. To avoid such problems, new control methods have been developed to maintain stable grid operation in a situation where synchronous machines are not present. Grid-forming control method is being applied to a static synchronous compensator (STATCOM) compensation device that is traditionally used just for reactive power compensation, but for inertial response also active power injection and absorption are required.

STATCOM can provide active power response if the device has sufficiently large energy storage for active power injection and absorption. Previously capacitors have been used as the capacitors have a long lifetime of well over 10 years, fast response time and can tolerate high voltages. In reactive power compensation the capacitors have been used to provide voltage for the modular multilevel converter in order to be able to inject or absorb reactive power. Nowadays transmission system operators have showed interest in STATCOM devices that are capable of active power injection and absorption. However, the energy density of capacitors is quite low, so more cost and size effective solutions need to be investigated which presents the main objective of this thesis. The new energy storage should be safe, capable of producing high power output and have larger stored energy than previously. In addition, the size, complexity and cost should be minimal.

Supercapacitors, Li-ion batteries, superconducting magnetic energy storages, flywheels and Li-ion capacitors were identified as possible energy storage options. Based on characteristics of each energy storage option, supercapacitors and Li-ion batteries are seen as the best options. Closer analysis of the supercapacitors and Li-ion batteries has been made using commonly used simulation models. Especially different supercapacitor models can have significant differences that will affect the sizing and ratings. Battery sizing was done using LTO cell parameters while supercapacitor sizing was done based on 3200 F cell. Simulating the behavior of the energy storage as a part of STATCOM model showed that the voltage change during the start of discharge and charge can be significantly large. Based on the decreasing voltage characteristics of batteries and supercapacitors during discharge, it is seen that a DC-DC converter should be used as it will also have a significant effect on the overall costs. Major difference between batteries and supercapacitors is that the equivalent series resistance of batteries is much larger. Charging and discharging rate of batteries is lower than with supercapacitors which means that many more parallel battery strings are needed to limit the current experienced by one cell in common DC-link implementation. Benefit of using batteries is that the voltage during discharge and charge is very linear with a small slope unlike with supercapacitors. Voltage change for batteries during short charging and discharging is small because the batteries are oversized in terms of energy for the given power requirement. Based on simple calculations, the initial investment to buy the energy storage is smaller with batteries than with supercapacitors.

Keywords: STATCOM, energy storage, supercapacitor, battery energy storage, energy storage simulations

The originality of this thesis has been checked using the Turnitin OriginalityCheck service.

TIIVISTELMÄ

Kasper Keskinen: Energiavarastot suurtehoisissa STATCOM-sovelluksissa
Diplomityö
Tampereen yliopisto
Sähkötekniikan diplomi-insinöörin tutkinto-ohjelmaa
Kesäkuu 2022

Uusiutuvien energialähteiden verkkoyhteydet lisääntyvät kovaa vauhtia. Aiemmin sähköverkon tapapainosta ovat huolehtineet suuret tahtigeneraattorit, mutta nykyään ja tulevaisuudessa tahtigeneraattoreita korvataan uusiutuville energialähteillä, jotka kytketään sähköverkkoon tehoelektronikan avulla. Tahtigeneraattoreiden korvaaminen saa aikaan lisääntyviä sähkövoimajärjestelmän ongelmia, kuten inertian vähenemisen ja siitä johtuvat mahdolliset stabiiliusongelmat. Ongelmien välttämiseksi on kehitetty uudenlaista säätötapaa, joka pystyisi muodostamaan ja ylläpitämään sähköverkon tilanteessa, jossa tahtigeneraattoreita ei ole. Uutta säätötapaa sovelletaan muun muassa staattiseen synkronikompensointiin (STATCOM), jolla perinteisesti kompensoidaan vain loistehoa, mutta inertivasteen kannalta myös suuri pätötehon injektio ja absorptio ovat keskeisiä.

STATCOM kykenee tuottamaan pätötehovasteen, kunhan laitteella on käytettävissään tarpeeksi suuri energiavarasto pätötehon varastoimiseksi. Aiemmin STATCOM:n energiavarastot ovat koostuneet kondensaattoreista. Kondensaattorit ovat pitkäikäisiä ja kestävät suhteellisen korkeita jännitteitä. Lisäksi kondensaattorin pystyy lataamaan ja purkamaan hetkessä, joka on tärkeää, jos teho halutaan käyttöön nopeasti. Kondensaattorin energianvarastointikyky on varsin pieni sen viemään tilaan ja hintaan nähden. Aiemmin kondensaattorit ovatkin lähinnä toimineet loistehon luomisen vaatiman jännitteen lähteenä. Nykyään kantaverkkoyhtiöt ovat kuitenkin kiinnostuneet pätötehon injektioon ja absorptioon kykenevistä STATCOM:eista, jolloin energiavaraston kokoa tulee suurentaa. Uuden energiavaraston tulisi olla suuritehoinen ja energiamäärältään huomattavasti suurempi kuin aiemmin. Lisäksi energiavaraston koko ja kustannukset tulisi minimoida, jonka takia aiemmin hyödynnetyille kondensaattoreille halutaan kartoittaa vaihtoehtoisia ratkaisuja.

Vaihtoehtoisiksi on tässä työssä kartoitettu superkondensaattorit, Li-ioni akut, suprajohtava magneettinen energiavarasto, vauhtipyörä ja Li-ioni kondensaattori. Työssä suoritetun vertailun avulla on todettu, että etenkin superkondensaattori ja Li-ioni akku ovat käyttökelpoisia ratkaisuita. Kummankin vaihtoehdon osalta tulee kuitenkin pitää mielessä energiavaraston ja STATCOM:n rajoitteet kuten turvallisuus, hinta sekä virta- ja jänniterajat. Energiavarastojen tarkempaa analyysiä on suoritettu hyödyntämällä yleisesti käytössä olevia superkondensaattori- ja akkumalleja. Etenkin superkondensaattorimallien välillä on suuri eroja, jotka vaikuttavat huomattavasti energiavaraston mitoittamiseen ja kustannuksiin. Li-ioni akun osalta karkea mitoitus tehtiin hyödyntämällä LTO-akkukemialla ja superkondensaattorin osalta mitoitus tehtiin käyttämällä 3200 F kennon tietoja hyväksi. Akkujen ja superkondensaattorien simulointi osana STATCOM:a paljasti, että riippuen energiavaraston jännitteestä, voi jännitteenalennus purkauksen alkaessa ja sen aikana olla huomattavan suuri. Jännitekäytöksen takia tulisi hyödyntää hakkuria, jotta STATCOM:n jännite pysyisi mahdollisimman vakiona ja näin helpottaisi laitteen säätöä. Simulaatiotuloksista myös huomaa, että akun sisäresistanssi on huomattavasti suurempi verrattuna superkondensaattorin sisäresistanssiin. Tämä tarkoittaa, että rinnakkaisia akkuhaaroja pitää hyödyntää monin kerroin yhteisen DC-linkin implementaatioissa verrattuna superkondensaattoreihin. Akun hyöty on kuitenkin purkauksen aikaisen jännitteen tasaisuudessa, koska suuren tehon saavuttamiseksi tulee akkuja kytkeä niin monta sarjaan ja rinnan, että ylimääräinen energiakapasiteetti takaa pienen jännitemuutoksen purkauksen ja lataamisen aikana. Alustavien laskelmien perusteella akkujen osakustannus on pienempi kuin superkondensaattorien.

Avainsanat: STATCOM, energiavarasto, superkondensaattori, akku, energiavarastosimulaatiot

Tämän julkaisun alkuperäisyys on tarkastettu Turnitin OriginalityCheck –ohjelmalla.

PREFACE

This thesis was written in the New Product Introduction (NPI) unit of Grid Solutions FACTS unit based in Tampere. From Tampere University, examiners associate professor Tomi Roinila and doctoral researcher Joni Markkula guided me through the thesis process. From General Electric, Anssi Mäkinen served as the supervisor. In addition to examiners, the NPI project team guided me through the process with their comments and suggestions. I would like to thank the examiners and NPI team for their valuable insights, suggestions and overall support.

This thesis served as a nice introduction to the NPI process, topic of grid-forming STATCOMs and especially supercapacitors. The thesis merely scratched the surface of the grid-forming STATCOM topics, but it showed what are the upcoming key questions that need to be solved. In addition to the energy storage evaluation, the control, topology and actual implementation of the system are fascinating challenges that are merely mentioned in this thesis.

As my studies are coming to their end, I would like to thank all of the great teachers I had the pleasure to learn from. Especially studies related to power grid dynamics, power electronics and control theory were among my favorites. I want to thank myself for having the courage to do the decisions I made during the studies that led me to this thesis experience and hopefully to a great start as an electrical engineer. During the thesis I had a pleasure of measuring supercapacitor cells which would not have been possible without the help from Minh Tran, so thank you as well. The biggest thanks I want to give to my family for always believing in what I do even when I had my own doubts. I also want to thank my friends for providing so much entertainment and discussion outside the studies. Lastly, I cannot put into words the amount of gratitude and love I have for my fiancé Matilda. Thank you for always being my favorite "Boss".

Tampere, 3.6.2022

Kasper Keskinen

CONTENTS

1. INTRODUCTION	1
2. STATCOM AND ENERGY STORAGES	4
2.1 STATCOM	4
2.2 High-level energy storage requirements and integration options	10
2.3 Energy storage technologies for STATCOM applications	15
2.4 Electrochemical batteries	16
2.5 Li-ion battery	20
2.6 Supercapacitor	24
2.7 Other energy storage technologies	33
3. ENERGY STORAGE MODELLING AND DESIGN	35
3.1 Battery modelling	35
3.2 Supercapacitor modelling	46
4. STATCOM SIMULATIONS	67
4.1 STATCOM models	67
4.2 Energy storage sizing	69
4.3 Submodule simulation results	74
4.4 Common DC-link simulation results	76
4.5 Switching STATCOM model simulation results	78
5. CONCLUSIONS	80
REFERENCES	83

LIST OF SYMBOLS AND ABBREVIATIONS

AC	Alternating current
BESS	Battery energy storage system
BMS	Battery management system
BOL	Beginning of life
CAES	Compressed air energy storage
CPE	Constant phase element
DC	Direct current
DOD	Depth of discharge
DSBC	Double-star bridge cell
DSCC	Double-star chopper cell
DSHC	Double-star hybrid cell
EDL	Electrical double layer
EDLC	Electrochemical double-layer capacitor
EES	Electrical energy storage
EIS	Electrochemical impedance spectroscopy
EOL	End of life
HPPC	Hybrid pulse power characterization
HSS	Hybrids storage system
IGBT	Insulated gate bipolar transistor
IGCT	Integrated gate commuted thyristor
LCO	Lithium cobalt oxide
LFP	Lithium iron phosphate
LIB	Lithium-ion battery
LIC	Lithium-ion capacitor
Li-ion	Lithium-ion
LMO	Lithium manganese oxide
LNO	Lithium nickel oxide
LTO	Lithium titanate oxide
MMC	Modular multi-level converter
MW	MathWorks
NaS	Sodium-Sulfur
NCA	Lithium nickel cobalt aluminum oxide
NiCd	Nickel-Cadmium
NiMH	Nickel-Metal hydride
NMC	Lithium nickel manganese cobalt oxide
NPI	New product introduction
PCC	Point of common coupling
PHES	Pumped hydro energy storage
PT	Power transformer
SDBC	Single-delta bridge cell
SEI	Solid electrolyte interphase
SMES	Superconducting magnetic energy storage
SOC	State of charge
SOH	State of health
SVC	Static var compensator
SSBC	Single-star bridge cell
STATCOM	Static synchronous compensator
TSO	Transmission system operator
VSC	Voltage source converter
A	Surface area of a capacitor plate

A_i	Interfacial area between electrode and electrolyte
C	Capacitance
C_{batt}	Battery charge
C_{cell}	Cell capacitance
C_{GC}	Gouy-Chapman's capacitance
C_H	Helmholtz's capacitance
C_o	Initial capacitance
C_{series}	Series connection capacitance
C_{SM}	Submodule capacitance
C_T	Double layer capacitance
c	Molar concentration
d	Capacitor plate separation distance, molecular radius
E	Strength of electric field, source voltage of the battery
E_{avb}	Available supercapacitor energy
E_{batt}	Battery energy
E_c	Energy of supercapacitor charged to a voltage
$E_c(u_c)$	Energy of the supercapacitor charged to voltage u_c
E_{exp}	Potential at the end of exponential zone
E_{full}	Potential at fully charged voltage
E_{load}	Energy realized to the load
E_{losses}	Energy dissipated as losses
E_{nom}	Potential at the end of nominal zone
E_{OC}	Open circuit voltage of a battery
$E_{SC,min}$	Minimum supercapacitor energy
$E_{SC,nom}$	Nominal supercapacitor energy
E_{arm}	Average energy stored in phase arm
E_{max}	Maximum arm voltage
E_{nom}	Arm nominal energy
E_{tot}	Total energy
E_{vR}	Generated voltage of the STATCOM VSC
E_0	Constant voltage
F	Faraday's constant
H	Inertia constant
I	Moment of inertia, current
i_C	Capacitor current
i^*	Low frequency current dynamics
it	Extracted capacity
I_{batt}	Battery current
$I_{ch/dch}$	Charge or discharge current
$I_{cut-off}$	Cut-off current
$I_{max,CL}$	Maximum current based on carbon loading
I_{max}	Maximum current
$I_{sc,max}$	Maximum supercapacitor current
$I_{SM,max}$	Maximum submodule current
$I_{SM,min}$	Minimum submodule current
I_c	Current towards the STATCOM
J	Machine inertia
j	Imaginary unit
k_{CL}	Carbon loading coefficient
k_{dc}	Submodule time average scaling factor
k_{max}	Upper limit of the energy storage voltage
k_c	Voltage dependent capacitance coefficient
L	Inductance

L_s	Series inductance
m_a	Switching pattern
N	Number of submodules in series, dispersion factor
N_e	Number of electrode layer
n_p	Number of parallel connected cells
n_s	Number of series connected cells
OCV	Open circuit voltage
P	Active power
P_{batt}	Battery power
P_{max}	Supercapacitor peak power
P_{nom}	Nominal Submodule power
P_{sc}	Supercapacitor bank power
pe	Peukert's coefficient
Q	Reactive power, total charge
Q_+	Positive charge
Q_0	Battery capacity
Q_{BoL}	Beginning of life capacity
Q_{cut}	Charge at the end of discharge curve
Q_{exp}	Charge at the end of exponential zone
Q_{nom}	Charge at the end of nominal zone
R	Ideal gas constant, resistance
R_0	Resistance of second order equivalent circuit model
R_{C0}	Time dependent resistance
R_{cell}	Cell resistance
R_{dc}	Low frequency resistance
R_f	Leakage resistance
R_i	Internal resistance
R_{int}	Constant battery resistance
R_{pol}	Polarization resistance
S	Apparent power
T	Operational temperature
t_{dsc}	Discharge time
t	Time
U_{batt}	Battery voltage
$U_{c,max}$	Maximum supercapacitor voltage
$U_{c,min}$	Minimum supercapacitor voltage
u_c	Charged voltage of supercapacitor
V	Electric difference
V_0	Voltage when HPPC pulse is applied
V_1	Voltage at after 1 second of discharge
V_{init}	Initial voltage
V_{max}	Maximum voltage
V_{min}	Minimum voltage
V_{ref}	Reference voltage
$V_{SC,min}$	Minimum supercapacitor voltage
$V_{SC,max}$	Maximum supercapacitor voltage
V_{SC}	Maximum supercapacitor voltage
V_{series}	Series connection voltage
V_{sub}	Medium voltage connection voltage
V_{dc}	DC voltage
V_s	Voltage at the main transformer
V_{vR}	VSC voltage
X_l	Inductor reactance

$x(t)$	State variable
$\dot{x}(t)$	Change of state variable
$u(t)$	Input signal
$y(t)$	Output signal
α	Charge transfer coefficient
γ	Angle of the current towards the STATCOM
ε	Relative permittivity of electrolyte material
ε_0	Permittivity constant
τ	RC network time constant
ω	angular velocity
ω_{max}	Maximum angular velocity
ω_{min}	Minimum angular velocity
δ_{vR}	Angle of the VSC voltage
ΔE_{max}	Maximum amount of excess energy
ΔV	Over potential
ΔV_x	Voltage difference over the inductor

1. INTRODUCTION

Power-electronics have become increasingly applied to connect renewable energy sources to the power grid. Such a high penetration of power-electronics-based devices have started to change the dynamics of the power grid causing negative effects to the power system. These negative effects can be, for example, decrease of inertia, faster voltage fluctuations, volatile load flow patterns, power quality problems, reduction of transient stability margins, lack/excess of reactive power, low short-circuit power levels and loss of devices in fault-ride-through situations [1]. Classically large centralized synchronous generators have provided system stability and robustness but with the increase of renewable energy the distributed converters are replacing synchronous machines. Because of this replacement, there is a need for control concepts that allow power-electronics converters to have characteristics comparable to synchronous machines in order to maintain the stability and robustness of the power system. [1]

Conventionally power-electronics converters have been connected to the grid by applying grid-following control concept. This means that the direct current-alternating current (DC-AC) inverter uses measurement information of the frequency, amplitude and phase of the grid voltage and injects current according to the measurements so that the desired active and reactive powers are fed with the desired frequency to the power system. A major drawback of grid-following control is that the control concept can only be used in networks where a synchronous machine provides the voltage reference for synchronization. In a network where synchronous generators do not exist, the grid-following concept cannot be used or there needs to be a grid-forming converter present. [2]

To enable more renewable energy generation to a grid with a high penetration of power-electronics based devices a new control concept, called grid-forming control, for the converters should be applied. Grid-forming control allows the converter to behave as a voltage source with controllable frequency so that the other grid-following converters can be synchronized to the produced voltage. Currently, the grid-forming concept is being implemented to a static synchronous compensator (STATCOM). A STATCOM with an energy storage allows for fast injection and absorption of reactive and active power independent from the actual voltage at the connection point [2]. In addition to reactive and active power control, a STATCOM can be also used for other tasks, such as improving the voltage stability and power factor [3]. A STATCOM is part of flexible alternating

current transmission systems (FACTS) family of devices. An overview of different FACTS devices and conventional compensation systems are shown in Figure 1.

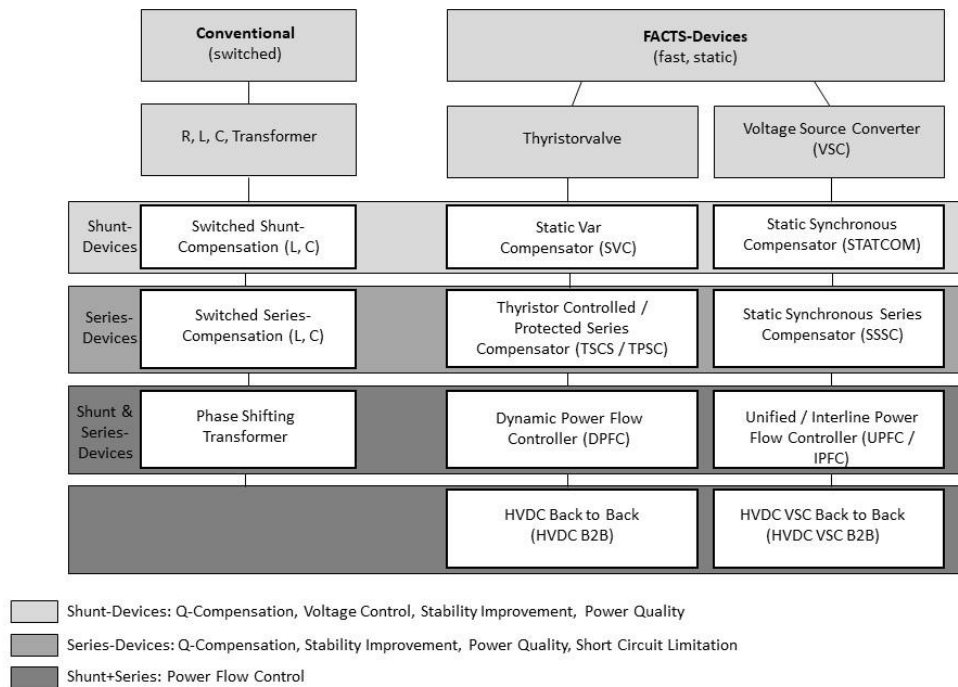


Figure 1. Overview of FACTS and conventional compensation devices. Modified from [4]

Based on the grid-forming control concept, the converters can provide inertia to the power system by injecting active power [1]. However, the active power capability of a STATCOM is limited by its energy storage. Currently, many STATCOMs utilize capacitors, but the energy content of a capacitor is not sufficient for a high active power output for a couple of seconds. To increase the active power capability of a STATCOM, different energy storage options have been researched. In this thesis the main focus has been given to Li-ion batteries and supercapacitors because of their fast response time to provide full power, high power density, energy density, scalability and proven implementation [5].

The objectives of this thesis can be divided into three parts. The first objective is to analyze different energy storage options for STATCOM applications. Energy storages are compared based on a few key criteria that are seen as the most important for STATCOM applications, such as response time, lifetime, cost, and energy density. In addition, the energy storage should be able to meet the power, energy and response time requirements imposed by transmission system operators (TSO). The second objective is to model the electro-dynamic behavior of chosen energy storage options based on popular modelling techniques. In a STATCOM application, especially the accurate control of the current and voltage are important factors that the model should address as they have an impact on the integration of the energy storage to the device. The third

and final objective is to see how the energy storage works together with the existing STATCOM simulation model and determine if the energy storage can fulfil the requirements.

The remainder of the thesis is organized as follows. Chapter 2 presents the basic structure and operation of STATCOM. In addition, a literature review of different high-power energy storages is given. The number of energy storages is narrowed down based on the energy storage characteristics and requirements from a STATCOM application. Especially Li-ion batteries and supercapacitors are analyzed in more detail. Chapter 3 focuses on modelling the chosen energy storages for the STATCOM application. The modelling focuses on the basic electrical behavior of the storage, and thus, does not consider the thermal and lifetime characteristics. Chapter 4 presents a simulation model for the STATCOM together with the chosen energy storage and the main simulation results. Finally, Chapter 5 draws conclusion and possible future research subjects.

2. STATCOM AND ENERGY STORAGES

This chapter focuses on different energy storage options. Before analyzing the options, STATCOM structure and operation principles are introduced to explain different energy storage integration possibilities. Because many STATCOMs utilize capacitors as the energy storage, a short introduction to the capacitor and its inapplicability for high active power applications is discussed. In addition, high-level energy storage requirements are introduced that will limit the energy storage options. Focus on the energy storage comparison is given to batteries and supercapacitors.

2.1 STATCOM

STATCOM is a voltage-source-converter (VSC) based device that compensates reactive power and provides voltage support to a power system. STATCOM consists of an energy storage device that is connected to the power system using a VSC. [6] VSC is self-commutated converter that connects high voltage alternating current and high voltage direct current systems using high-power electronic devices, such as insulated gate bipolar transistors (IGBTs) or integrated gate commutated thyristor (IGCTs) [7]. VSCs can generate AC voltages without the need to rely on AC system, meaning VSCs can operate as grid-forming converters. Self-commutation means that the converter switch can be turned on by applying a control signal to the gate of the switch when collector-emitter voltage is positive. Removing the control signal causes the switch to turn off [8]. A basic representation of a grid-connected STATCOM is shown in Figure 2. In addition to the VSCs, STATCOM consists of a DC-link capacitor, a smoothing reactor, and a transformer. A controller is needed to control the VSC switches so that the device operates as intended. The controller receives voltage measurement information through a power transformer (PT) and based on the measurements and reference voltage V_{ref} , computes a control error. Based on the control error, a modulator feeds a switching pattern m_a to the VSC.

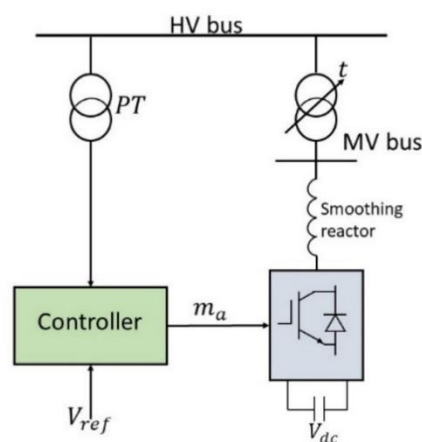


Figure 2. Basic STATCOM representation

2.1.1 STATCOM topologies

STATCOM VSCs can have many different topologies depending on the applications. Usual topologies are 2-level and 3-level converters for lower voltage levels and modular multi-level converter (MMC) for high voltage and high-power applications [9]. In high-power applications the voltage and current requirements over a 2- or 3-level converter would be too high, so a modular structure should be used where modules, also known as submodules, are connected in series and/or parallel. A submodule is shown in Figure 3 and MMC STATCOM topology in Figure 4. The series and/or parallel connection of submodules is called a valve. A valve module is shown in Figure 5. Due to the high voltage in high-power applications, key properties of MMCs structure are that the modules are series connected so that the overall connection point voltage can be reached while the module voltages are relatively low. Adding more modules increases the output voltage, so the MMC systems is easily scalable and can be made redundant. In addition, having many voltage levels means that the harmonic filter size can be reduced [6][10]. In this thesis MMC topology is used for the aforementioned reasons.



Figure 3. STATCOM submodule [11]

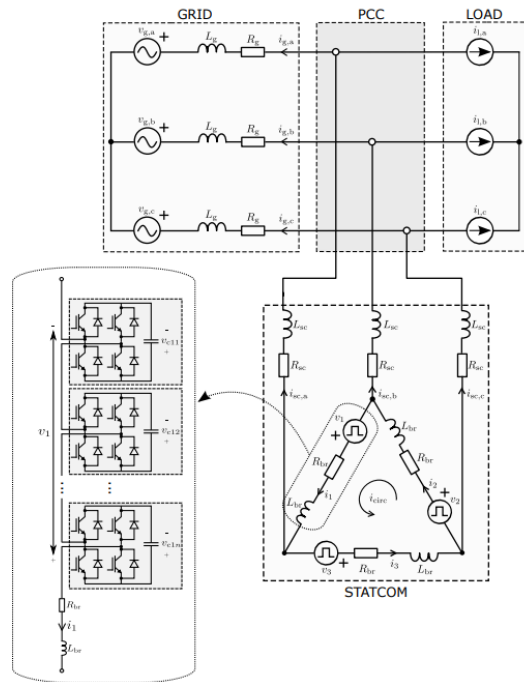


Figure 4. Delta connected full-bridge MMC STATCOM [12]



Figure 5. MMC STATCOM valve module [11]

Within the MMC structure, one submodule can be implemented either as half-bridge or full-bridge topology. Other submodule topologies exist but they are not discussed in this thesis. The half-bridge topology consists of a fully controllable upper and lower switch cells connected antiparallel to a diode. The full-bridge topology consists of two half-bridge VSCs that are connected in parallel via the DC-side. The benefit of the full-bridge VSC is that the generated AC-side voltage is twice the voltage of a half-bridge VSC if both topologies have the same DC-side voltage. This means that the same DC-side voltage is used more effectively in a full-bridge VSC. In addition, the full-bridge topology is also a 3-level converter as it can produce three output levels [9]. The disadvantage of full-bridge topology is that with more switches, the losses and cost increase [13]. A comparison of half-bridge and full-bridge structures is shown in Figure 6.

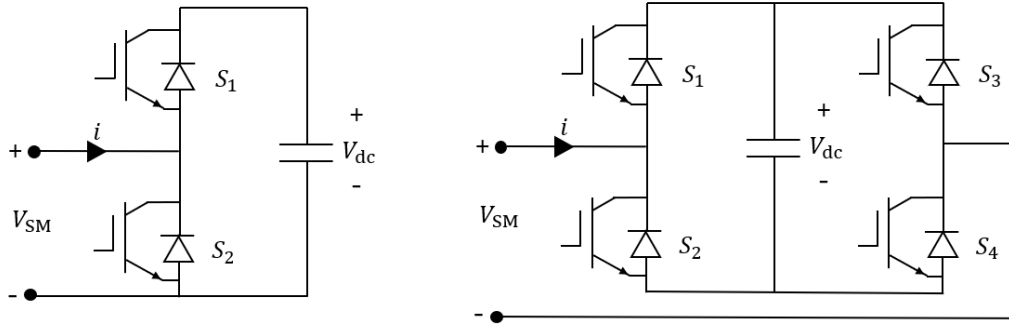


Figure 6. Half-bridge and full-bridge submodule topology

In addition to submodule structure, the MMC STATCOM can be built in many topologies based on how the phase legs are connected. Most popular topologies for energy storage integration include single-star bridge cell (SSBC), single-delta bridge cell (SDBC), double-star chopper cell (DSCC), double-star bridge cell (DSBC) and double-star hybrid cell (DSHC) shown in Figures 7 and 8 [14].

All topology options have their pros and cons related to the voltage and current ratings, ability to work in an unbalanced grid, how easy it is to implement balancing and how the energy storage can be implemented. For example, the star configurations can have advantage over the delta connected configurations in positive-sequence reactive power control while the delta configuration allows for negative-sequence compensation by letting a zero-sequence current to circulate inside the delta [15]. According to the star delta transformation, the delta structure has higher current capability than the star configuration, but the star configuration has the advantage in voltage rating as in the star connection the phase legs are connected between phase voltage and neutral, so less series connected modules are needed to create the required voltage [16].

Related to the energy storage implementation, all the mentioned configurations allow for distributed energy storage implementation into the submodule cells, but the double-star topologies allow also for centralized energy storages [14]. The benefit of a distributed energy storage integration is that the energy storage voltage can be lower and a possible failure in one submodule is easier to isolate than in a centralized design. The drawbacks of a distributed energy storage integration include possible thermal management issues, complex control structure, maintenance difficulties, a lot of required DC-cable and possible difficulty of enabling additional storage after commissioning [14].

The centralized energy-storage option is possible with DSCC, DSBC and DSHC topologies. The difference between the mentioned topologies is in the employed cell type. Figure 8 shows a general topology for centralized integration of energy storage. The advantage of the centralized implementation is that the energy storages can be placed to a separate space where the maintenance and temperature control is easy to implement. In addition, in case of malfunction the destruction of the energy storage will not affect the STATCOM valves. For isolation, the centralized option requires a DC disconnecter. Drawback is that the energy storage needs to operate at a much higher voltage level compared to a distributed topology unless a high voltage converter is used. [14]

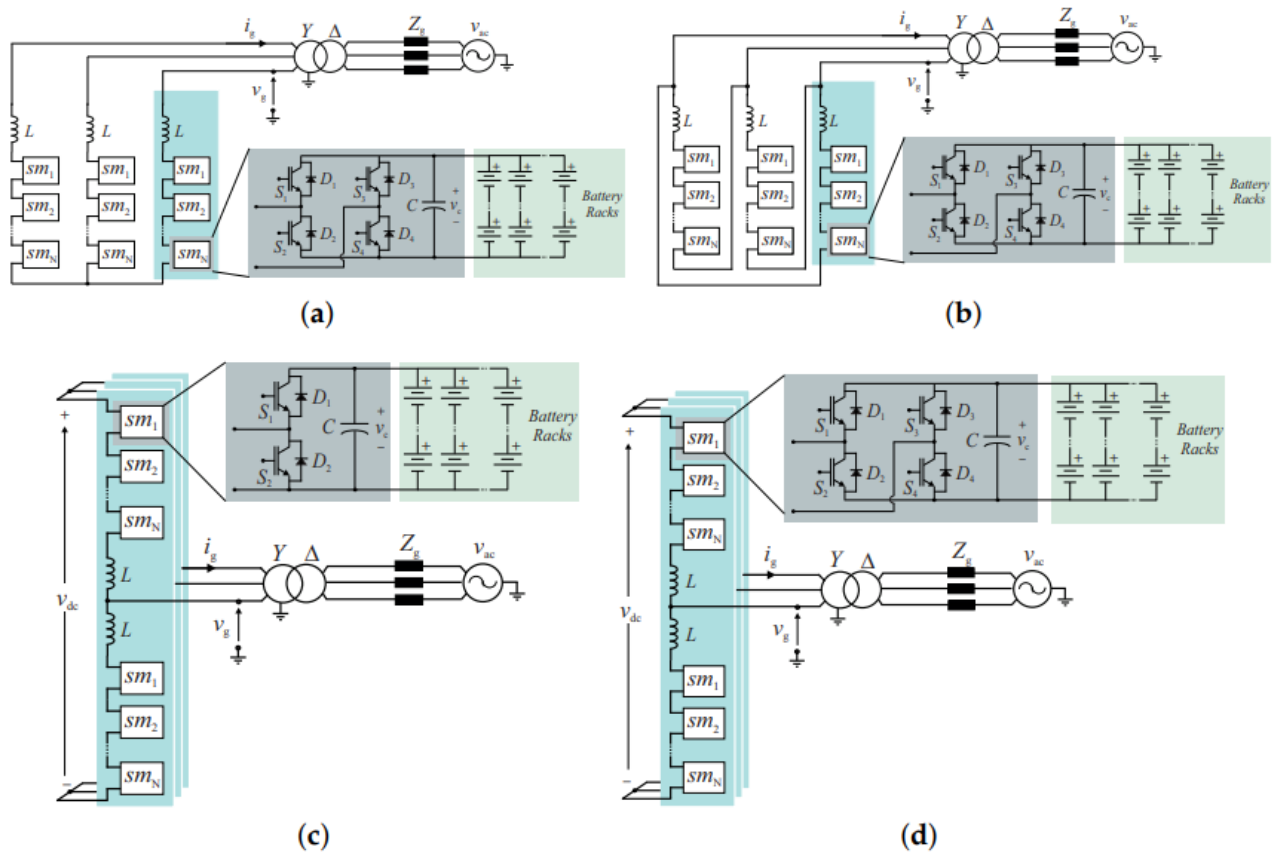


Figure 7. STATCOM topologies for distributed energy storage integration: a) SSBC, b) SDBC, c) DSCC and d) DSBC [14]

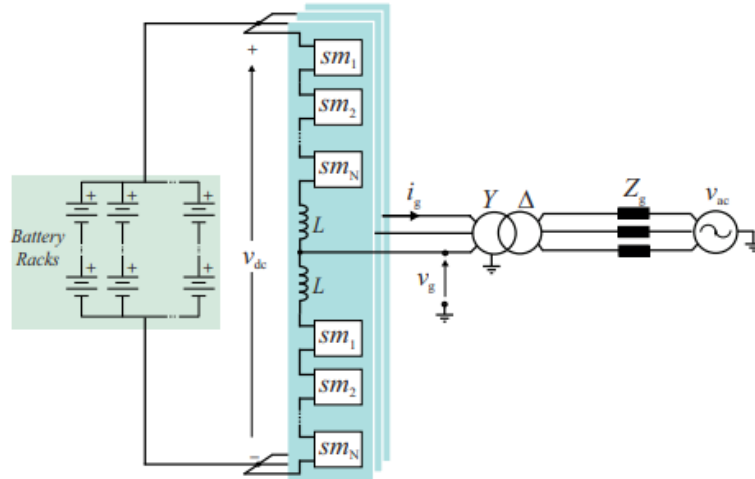


Figure 8. Centralized energy storage topology. Possible for DSCC, DSBC and DSHC topologies [14]

2.1.2 STATCOM operation basics

The operation of a STATCOM is based on the voltage difference between the compensator and the point of common coupling (PCC). If the compensator voltage, meaning the STATCOM voltage, is higher, then the STATCOM injects a current towards the PCC. In this operational condition the STATCOM acts like a capacitor generating reactive power. If the compensator voltage is smaller than the PCC voltage, then there is a current flow towards the STATCOM. In this case the STATCOM acts like an inductor and absorbs reactive power. [17] Figure 9 shows a simple circuit representation that can be used as the basis on analyzing STATCOM operation. In the figure V_s represents the voltage at the main transformer with an angle of zero degrees, I_c is the current towards the STATCOM with angle γ , ΔV_x is the voltage difference over the inductor, E_{vR} represents the generated voltage of the STATCOM VSC and V_{dc} is the DC-link voltage.

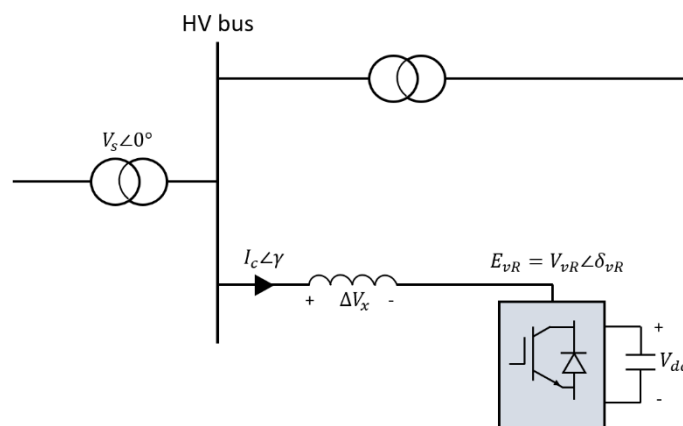


Figure 9. Simplified single-line diagram of a STATCOM

Figure 10 presents the space vector representation for leading and lagging operation.

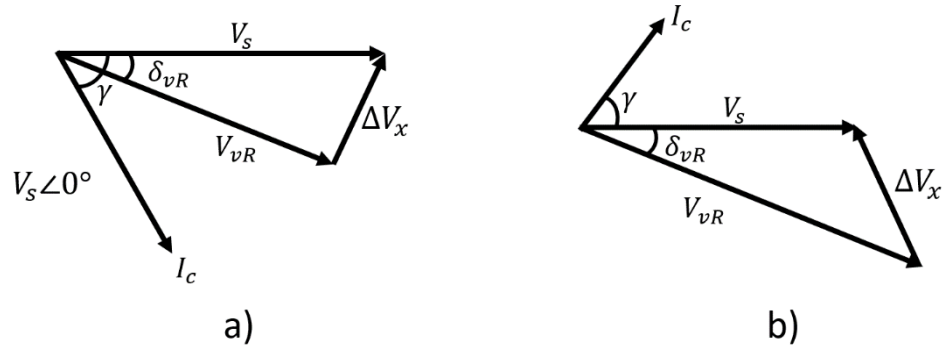


Figure 10. Leading a) and lagging b) space vector representations of STATCOM

Based on Figure 9, following equations for active and reactive powers can be defined [17]

$$P = \frac{V_s V_{vR}}{X_l} \sin(\delta_{vR}) \quad (1)$$

$$Q = \frac{V_s^2}{X_l} - \frac{V_s V_{vR}}{X_l} \cos(\delta_{vR}) \quad (2)$$

where V_{vR} is the VSC voltage, δ_{vR} is the angle of the voltage and X_l depicts the inductor reactance.

Using (1) and (2) as well as Figure 10, it is clear to see that the current flowing between STATCOM and PCC is controlled by the voltage difference. The reactive power of the STATCOM is controlled by varying the amplitude of the STATCOM voltage and active power is controlled by changing the phase of the STATCOM voltage.

Traditionally only a small DC-link capacitor is used as the main objective of the STATCOM is to control the reactive power and not active power. For this task a small DC-link capacitor has been sufficient as the capacitor itself is not used to produce reactive power, unlike in static var compensator (SVC) [18]. However, with a larger energy storage also active power can be controlled. During normal operation, δ_{vR} is kept slightly larger than zero so that there is a small active power flow to the STATCOM so that it can compensate for the losses in the VSC [17].

2.2 High-level energy storage requirements and integration options

Rough estimates of the energy storage requirements can be made based on valve ratings, energy storage ratings and TSO demands. Requirements differ based on where the energy storage is placed. However, the common requirements independent of topology are based on power and energy. As a first estimate, the demanded active power requirement given for the STATCOM is 100 MW for 1.25 seconds. For a shorter time period greater power can be demanded, 200 MW for 0.5 seconds. Based on these numbers, the maximum energy is 34.72 kWh. It should however be noted that these requirements are minimum requirements and based on one TSO, so having easily scalable device is important.

In addition to energy and power requirements, the energy storage should be able to charge and discharge in a fast manner. The requested output power profile can be highly uneven with a lot of fast fluctuations, so the energy storage cannot be designed only for a constant power output but rather the energy storage needs to be able to tolerate many charge/discharge cycles. For batteries, so called micro cycling, where the depth of discharge (DOD) is small, might not be as harmful as deep discharges. In STATCOM application, if a large phase jump occurs, the DOD might be deep which could limit the usability of the energy storage and reduce lifetime of some battery chemistries if the battery capacity is not large. Also, need for maintenance should be minimal.

An important aspect is also the safety of the energy storage, as energy storages have upper and lower limits for their operation window as well as common failure mechanisms that need to be addressed. For Li-ion batteries, a failure can lead to a thermal runaway that causes a fire or in worst case an explosion [19]. Supercapacitors on the other hand are much safer as electric and thermal abuse mainly causes pressure build up that causes a safety valve to open [20]. Safety is also related to where the energy storage is implemented as with a concentrated DC-link implementation possible destruction of energy storage might not affect the STATCOM valves unlike the submodule implementation. Related to safety, there needs to be a possibility to disconnect the energy storage from the STATCOM, meaning that the integration should be done using a switch or a converter.

If the energy storage unit is implemented into the common DC-link in a double-star configuration, then the energy storage unit should provide the previously mentioned energy and withstand a voltage up to the medium voltage connection rating. Thus, the voltage can be between 30-75 kV if a half-bridge converter without DC-DC converter is used. If full-bridge converters are used, then the voltage can be reduced as long as the valve current is not too high. It should be noted that the energy storages are not designed for such a high voltage difference to ground. In the STATCOM application, energy storage insulation is an important topic that needs to be addressed if common DC-link energy storage integration is chosen.

In a submodule implementation, the limiting voltage and current values are based on the VSC and energy storage limits. For this thesis the approximate VSC current limit of a few kA in rms can be used for analyzing and sizing the energy storage. Usually, the maximum series voltage without insulation is around 1-2 kV for the energy storages so it can be seen as the voltage rating of the submodule. If the energy storage is connected in parallel with the submodule DC-link capacitor, shown as C1 in Figure 11, with a DC-DC converter, then the 1-2 kV voltage rating is applicable for the converter as well. If the already used capacitor C1 is replaced by the energy storage, then the voltage profile of the storage is very important as it defines how many submodules are needed to produce the required STATCOM voltage and how the voltage control needs to be implemented. If the already existing capacitor is not replaced, but rather the energy storage is connected in parallel, then the energy storage can be seen as an additional capacitance and/or

energy capacity. In the latter case, the already existing capacitor can behave as a power buffer so that the energy storage does not need to react instantly to the requested active power.

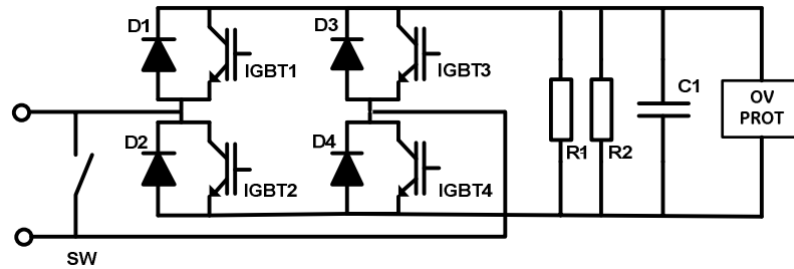


Figure 11. Full-bridge valve submodule [11]

In addition to common DC-link or submodule implementation, there is a third integration option. The third option is to connect a separate energy storage unit to the same coupling transformer as the STATCOM. This option would ensure that the changes to the existing STATCOM structure would be minimal as the added active power demand is fulfilled entirely from a separate energy storage unit that is not connected to the STATCOM in any way. The disadvantages in this solution would be the increased cost as the energy storages would require many separate DC/AC converters. Also, the control systems of STATCOM and energy storage system should be designed carefully to operate together with each other. The converter should be able to produce voltages of 30-75 kV. This third integration option is not studied further in this thesis. The main requirements are collected to Table 1.

Table 1. Energy storage requirements

Power	100 MW for 1.25 s and 200 MW for 0.5 s
Energy	34.72 kWh
Submodule voltage range	1-2 kV
Submodule nominal current	A few kA
STATCOM voltage	30-75 kV

2.2.1 Capacitor

Most current STATCOMs use capacitors at the DC-link of the submodules, as depicted in Figure 11, to provide excellent output voltage waveforms at low switching frequencies [21]. Capacitor stores energy in the electric field and can release the stored energy quickly. Figure 12 presents a typical parallel plate capacitor.

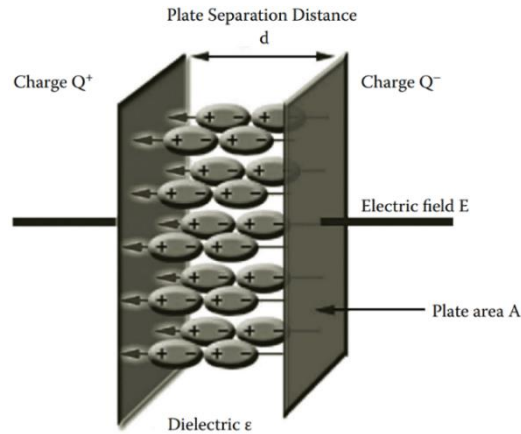


Figure 12. Charged parallel plate capacitor [22]

Based on Figure 12, the electric difference V between the two plates is given by the strength of the electric field E and the separation distance d as [22]

$$V = Ed = \frac{Q_+d}{\epsilon_0 A} \quad (3)$$

where $\epsilon_0 = 8.8542 \cdot 10^{-12} \frac{C^2}{Nm^2}$ is permittivity constant, Q_+ is positive charge and A is surface area of a plate.

Capacitance C can be given as

$$C = \frac{Q}{V} = \frac{\epsilon_0 A}{d} \quad (4)$$

where Q is total charge given as $Q = |Q_+| + |Q_-|$.

The voltage change of a capacitor is dictated by the current and capacitance based on

$$\frac{du_c}{dt} = \frac{i_c}{C} \quad (5)$$

where i_c is the capacitor current in amperes and C is capacitance in farads.

STATCOM does not use capacitor as a reactive power source but rather the capacitor is used to maintain constant DC voltage for inverter. Capacitor can be used for active power exchange, but the active power needs to be controlled to zero on average unless an external energy storage system is used. [23] Based on previous experience at Grid Solutions, capacitors represent a major cost of a submodule and takes the majority of the VSC volume.

To understand the limitation of capacitors, a short comparison to synchronous machine is given. Synchronous machines have energy stored in the rotor. Based on the apparent power, angular speed and inertia, an inertia constant H can be derived based on [24]

$$H = \frac{J\omega^2/2}{S} \quad (6)$$

where J is machine inertia, ω is angular speed and S is apparent power.

Typical values for synchronous machine inertia constants are 1-3 seconds, which depicts the amount time the machine can provide energy at a specific power. For STATCOM, a similar inertia constant can be defined as [24][25]

$$H_{\text{STATCOM}} = \frac{cV_{\text{DC}}^2/2}{s} \quad (7)$$

where V_{DC} is DC voltage.

Typical value for STATCOM inertia constant is around 0.5-5 ms, so the STATCOM does not have a lot of stored energy and is mostly designed for reactive power control. STATCOMs that are designed for unbalanced load operation can have much larger capacitors to avoid large voltage ripples due to power oscillations at the second harmonic [24].

The capacitance value can be chosen based on the amount of nominal energy. Energy stored in a submodule capacitor in an MMC STATCOM can be given as [21]

$$E_{\text{sub}} = \frac{1}{2} CV_{\text{sub}}^2 \quad (8)$$

where $V_{\text{sub}} = \frac{V_{\text{d}}}{N}$, V_{d} can be the common DC-link voltage or medium voltage connection voltage and N is the number of submodules.

Nominal energy storage in one arm of the STATCOM is simply related to the number of submodules connected in series as [21]

$$E_{\text{nom}} = \frac{N}{2} CV_{\text{sub}}^2 \quad (9)$$

Average energy stored in a phase arm is given by [21]

$$E_{\text{arm}} = \frac{1}{2} \frac{C}{N} k_{\text{dc}}^2 V_{\text{d}}^2 \quad (10)$$

Where k_{dc} is a scaling factor affecting the time average voltage of submodules.

Maximum voltage that can be stored per arm is given by [21]

$$E_{\text{max}} = \frac{V_{\text{d}}^2}{2N} k_{\text{max}}^2 C \quad (11)$$

where k_{max} is the upper limit of the energy storage voltage. For a supercapacitor the factor k_{max} should not exceed unity.

Maximum amount of excess energy is $\Delta E_{\text{max}} = E_{\text{max}} - E_{\text{arm}}$ and from the solution the size for minimum capacitance solved as [21]

$$C_{\text{min}} = \frac{2N\Delta E_{\text{max}}}{V_{\text{d}}^2(k_{\text{max}}^2 - k_{\text{dc}}^2)} \quad (12)$$

According to (12), if the energy requirement is in the scale of 100 MW, the capacitance value would need to be very large. For large energy storages, capacitors are not a good choice as the energy density and capacitance are more than thousand times smaller than that of supercapacitor. [5] This means that the physical space requirements, number of capacitors needed to fulfil

the energy requirement, cost and discharge time for only such a short period of time rule capacitors out from further analysis.

2.3 Energy storage technologies for STATCOM applications

Electrical energy storage (EES) technologies convert energy from one form to a more storable form. The energy is stored in a medium until it is released again when needed. [26] EESs can be divided into high energy/extended discharge and high power/rapid discharge categories based on the energy and power capability of the device. STATCOM applications can benefit from both storage types depending on how much power for how long is required, but the requirements presented in Chapter 2.2 suggest that mainly high-power technologies are needed. In addition to classifying EESs based on their power and energy capabilities, another classification can be made based on the form of stored energy. In the latter classification the main forms of stored energy are mechanical, electrochemical, electrical, thermochemical, chemical, and thermal [26]. Figure 13 presents some example storage technologies based on the form of stored energy.

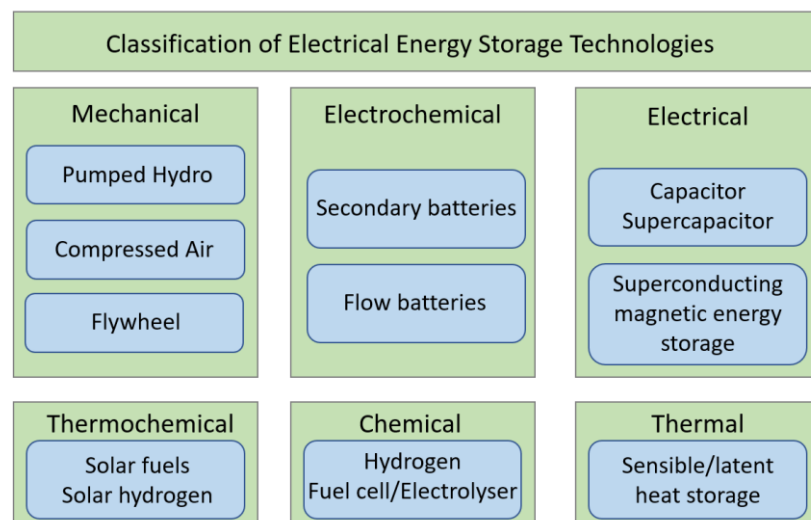


Figure 13. Energy storage classification based on the form of stored energy [26]

Currently the research regarding high-power storage technologies is concentrated to supercapacitors, superconducting magnetic energy storage (SMES) and flywheels [5]. From this list, the focus in this thesis will be on supercapacitors. High energy storage devices comprise pumped hydro energy storages (PHES), compressed air energy storage (CAES) and electrochemical batteries [5]. From this list only electrochemical batteries are seen as viable solutions for STATCOM applications.

In this thesis the energy storages are compared based on a few key energy storage characteristics. The chosen characteristics are energy density, power density, specific energy, specific power, daily self-discharge, lifetime in years, lifetime in cycles, discharge efficiency, cyclic efficiency, response time and temperature region. Values of these characteristics for different energy storage technologies are introduced in Appendix A.

Looking at appendix A, the most importance should be given to response time, lifetime, cycling time, energy and power density. Less importance should be given to specific energy and specific power, as STATCOM is a stationary device, so weight of the energy storage is not seen as a limiting factor. Other important factors that were not included into table of Appendix A would be cost, maintenance frequency, safety and technological maturity. Based on Appendix A, in addition to batteries and supercapacitors, flywheels and SMES seem to have great characteristics for STATCOM applications. Short summary of the disadvantages of flywheels and SMES are given in section 2.7.

It should be noted that in some applications both high power and energy are needed. In these situations, one energy storage solution might not be able to fulfil both requirements. For those situations so called hybrid storage systems (HSS) are needed where one energy storage is responsible for providing high power bursts while the other supports the energy demand [27]. One example would be to combine a supercapacitor with a fuel cell or a battery.

Especially related to the batteries, an important factor is the behavior of the output voltage with respect to the available charge and the effects of temperature. Appendix A introduced broad operating temperatures for some energy storages but in reality the supercapacitors and more so batteries start to have significant efficiency drops, lifetime reduction and inability to charge before the absolute temperature limits shown in Appendix A are reached [28]. In addition to temperature, also the operating window and charge/discharge rate affect the battery lifetime regardless of the chemistry, design or technology [29]. More detailed behavior of battery characteristics are analyzed next for the most promising battery chemistries.

2.4 Electrochemical batteries

In this thesis emphasis will be given to electrochemical secondary batteries that have the appropriate characteristics for STATCOM applications. Secondary battery differs from a primary battery by being rechargeable many times. This means that secondary batteries have reversible chemical reaction. [30] Popular battery choice for many high-power applications are Lithium-ion (Li-ion) batteries which have been applied to FACTS applications before [31]. Other battery chemistries include Nickel-Cadmium (NiCd) batteries, Nickel-Metal hydride (NiMH) batteries, Lead-Acid batteries and Sodium-Sulfur (NaS) batteries. For high-power-density applications Li-ion, NaS and NiCd represent the leading technologies. [32]

2.4.1 Battery operating principle

Main elements of battery cell include the negative and positive electrodes, separator and an electrolyte. Next, a short description of the operation of a Li-ion battery is given as they are seen as one the most viable and fastest evolving chemistry for STATCOM applications.

When battery is charging, the lithium ions are deintercalated from the layers of positive electrode material and intercalate into the layers of negative electrode material [30]. In a discharge process, the flow of lithium ions is reversed, and electrons are released by the negative electrode. In discharge process, negative electrode is oxidized, and positive electrode is reduced. In this oxidation/reduction process, known as redox process, chemical energy is converted to electrical energy [30]. Electrolyte functions as a carrier substance for the lithium ions that connects the electrodes [30]. Separator allows the lithium ions through but blocks the flow of electrons so that the electrons must flow to the active material via the external load or source, current collectors and binder material. A basic representation of a Li-ion battery is shown in Figure 14.

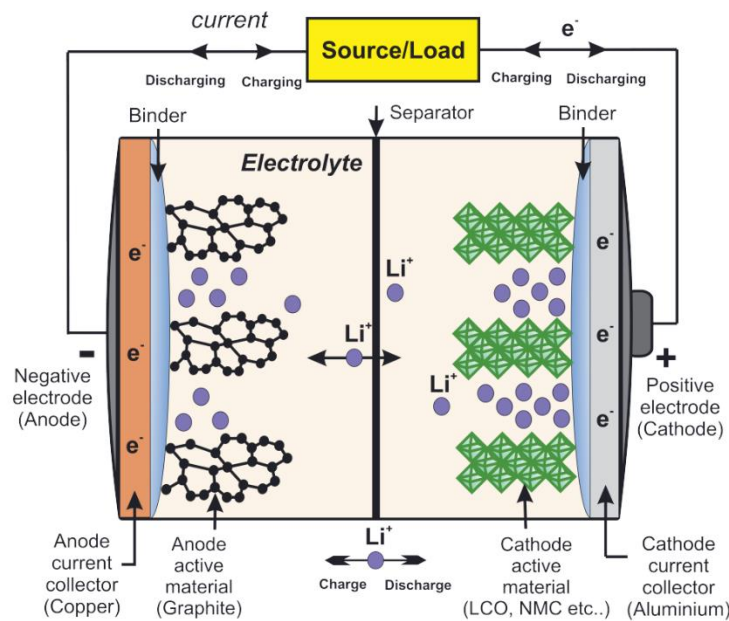


Figure 14. Li-ion battery while charging/discharging [33]

In batteries, the energy is stored as active material in the conducting electrode. Release of the energy requires oxidation/reduction reaction which is a slow process when compared to the operation principle in capacitors and supercapacitors. [34] Electrochemical batteries can offer energy over a long time range but the charging time and cyclic life is limited when compared to supercapacitors. For STATCOM applications, the cyclic lifetime, depth of discharge, charging and discharging rates and safety are important factors. Many of the battery chemistries, including Li-ion batteries, have a reported response time of less than 5 ms [35]. Response time means the duration of time to reach full discharge state starting from no discharge state.

It should be noted that typically batteries are not designed to release all the stored energy in a few seconds. Usually, batteries are designed for discharge times from 30 minutes to hours. If batteries are used in STATCOMs to fulfil power requirement of a few seconds, then there is extra capacity that is not used in the discharge. This means that with batteries, the STATCOM manufacturer pays for energy capacity that is not used. However, an advantage in energy related oversizing when using batteries is that the state of charge (SOC) will fluctuate only in minor steps as the discharge current for such a short time will not affect the stored energy very much. Related to small SOC changes, also the DOD will remain small if the battery has a significant amount of

stored energy. Additionally, if the STATCOM is fitted with a large energy storage, then the device can also operate under situations where longer active power support is requested without needing to change the configuration. If only the short time high power demands need to be fulfilled, then only very high-power battery cells should be investigated to avoid major energy oversizing.

2.4.2 Battery charging and discharging

Battery charging and discharging is usually depicted with a C-rate that scales the charge/discharge current according to the nominal capacity of the battery. For example, a 2 Ah battery with a discharge current of 2 A would have a 1C-rate as the current is enough to completely discharge the battery in one hour. Batteries with low internal resistance can achieve high discharge rates because the heating of the battery is not as substantial as with higher resistance. In addition to high charging and discharging currents, high cell voltages are seen as an advantage so that less cells are needed to connect in series to achieve proper system-level voltages. As was discussed before, ability to withstand deep discharges can be seen as advantage if the energy storage is not oversized in terms of energy. Comparison based on the discussed key battery characteristics for a few chemistries is presented in Table 2 and Appendix A.

Table 2. *Battery comparison based on key characteristics* [36][37][38][39][40][41][42][43][44][45]

Battery chemistry	Cycle durability (100% DOD)	C-rate (charge/dis- charge)	Cell voltage
Lead-acid	50-100	0.05-0.2	2.1
Nickel-zinc	100 to 50% capacity	0.1-2	1.6
Nickel-iron	5000	0.2	1.5
Nickel-cadmium	500	Up to 20	1.2
Nickel-metal hydride	300-800	5	1.2
Lithium cobalt oxide	500-1000	2-3	3.6
Lithium-titanate	6000-10000	10-75	2.4
Lithium iron phos- phate	2500-12000 to 80% capacity	1-25	3.2
Lithium manganese oxide	300-700	10	3.8

Based on Table 2, emphasis should be given to batteries with high C-rates, but it should be noted that the C-rates are only approximative and also other characteristics need to be compared before choosing an appropriate battery chemistry. Other important factors are cost, voltage profile and safety.

General discharge characteristic of a battery consisting of three sections as is shown in Figure 15. First section depicts exponential voltage drop due to charging. Second section depicts the nominal voltage area where charge can be extracted without dropping below minimum voltage limit. Third zone depicts total discharge of the battery where the remaining voltage drops rapidly. With higher discharge current the battery capacity is depleted faster and based on Peukert's effect, the capacity at high discharge rates is less than with low discharge currents.

Based on Figure 15, empirical models can be obtained, an example is shown in section 3.1.1. Li-ion batteries, excluding lithium iron phosphate, do not have notable hysteresis effect so the charging behavior can be assumed to be equal to the discharging, but this assumption is not true for all battery chemistries [46]. For lead-acid and nickel-cadmium chemistries the behavior can differ so that the exponential voltage drop increases in charging when compared to discharging.

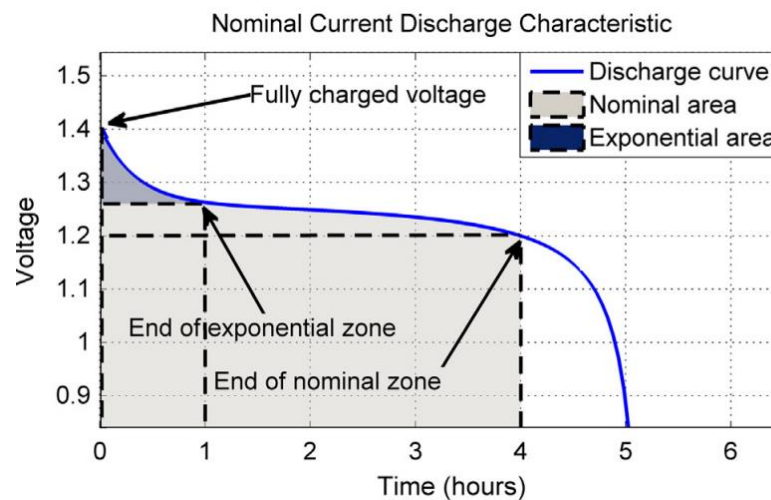


Figure 15. Battery discharge characteristic [47]

For STATCOM connection, a battery that has a wide nominal voltage area is preferred so that the output voltage is constant for as long as possible. If a battery has a narrow nominal voltage range, or the nominal voltage range has a steep constant decline, then the number of connected sub-modules or the DC-DC converter output voltage needs to be increased as the battery voltage starts to decrease. For example, li-ion batteries based on Lithium iron phosphate and graphite are known for their flat nominal voltage area [46]. As a comparison Figure 16 shows a discharge plot of carbon-zinc and alkaline battery where the voltage change is very rapid over the whole discharge curve.

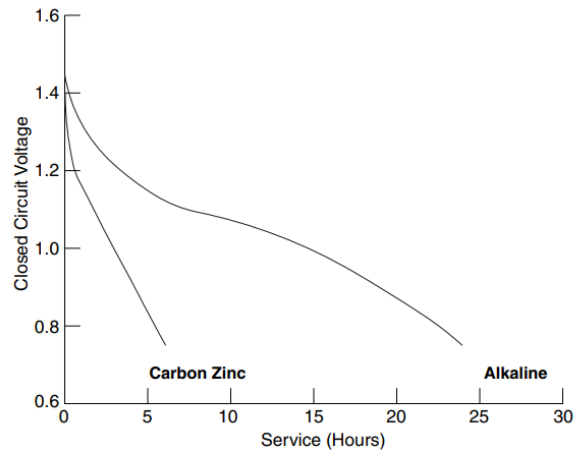


Figure 16. Discharge plot for carbon-zinc and alkaline batteries [48]

Based on the capability of Li-ion batteries to withstand deep discharges and high C-rates, in addition to having an appropriate discharge characteristic for STATCOM applications and rapid development pace, Li-ion battery chemistries are analyzed more in detail next.

2.5 Li-ion battery

Li-ion batteries have many different chemistry options. A comparison of the properties of different chemistries should be made so that the optimal chemistry is chosen. The main chemistries for comparison are:

- Lithium cobalt oxide (LCO)
- Lithium manganese oxide (LMO)
- Lithium nickel oxide (LNO)
- Lithium nickel cobalt aluminum oxide (NCA)
- Lithium nickel manganese cobalt oxide (NMC)
- Lithium iron phosphate (LFP)
- Lithium titanate oxide (LTO)

Comparison is based on specific capacity, nominal voltage, energy density, cyclic life and basic properties [49]. In addition, capability to endure many deep discharges is appreciated. Typically, Li-ion battery price is between 1200-4600 \$/kW and 300-1700 \$/kWh [50]. However, more accurate price information for a few chemistries is shown in Appendix B.

Based on Appendix B, the best chemistries for STATCOM applications are LNO, NMC, LFP and LTO as these chemistries have high power charge/discharge capability, long cyclic life, low cost/cycle and fast response time [49]. Especial emphasis is given to LTO because of its extraordinarily good cycle life at 80% depth of discharges, it has recharge rates up to 10C, allows for rapid recharging without the risk of lithium plating, avoids formation of solid electrolyte interphase (SEI) and the operating temperature range is wide [29][30].

All Li-ion batteries share common advantages and disadvantages when compared to other battery chemistries. Benefits of Li-ion batteries include good electrode stability, high cyclic life, long full discharge time, less maintenance requirement compared to many other battery chemistries, very low self-discharge rate, consistent output power discharge from SOC 80% to SOC 20%, no memory effects, high coulombic efficiency within the SOC range, high energy density, high specific energy, great power/weight ratio and fast response time. [30][51]

Disadvantages of Li-ion batteries include inability for trickle-charging, so identification of full charged state and balancing functions with full charge is hard, high cost due to packaging requirements and internal overcharge protection circuits as well as scarcity of lithium [5] [29] [30] [52]. Compared to supercapacitors, batteries have significantly higher internal resistance, so the heat generation is much greater with large currents. High internal resistance can curtail the amount deliverable power from the battery [53].

2.5.1 Li-ion battery safety

Some Li-ion battery cells can suffer from a thermal runaway caused by mechanical, electrical or thermal abuse. Mechanical abuse in the form of crushing the cell can cause cell deformation that tears the separator and thus causes an internal short circuit. Electric abuse is caused by over discharging or over charging the cell. Electric abuse allows for dendrite growth that can pierce through the separator causing an internal short circuit. Thermal abuse first causes loss of capacity and starts to decompose SEI layer which happens around 60°C. When SEI is decomposed, the anodes directly contact with electrolytes at around 100°C. The reaction releases more heat which causes the melting of separators at 130-140°C. Next, micro internal short circuits start to happen, and the temperature rises to around 240°C when the cathode material, electrolyte and binders decompose. Decomposition quickly increases heat up to 800°C leading to fire as oxygen is released from cathode reactions. At the same time, gaseous products are generated that increase the pressure of the battery and can lead to an explosion. All the described abuse methods can thus cause a thermal runaway and at worst a fire or even an explosion. [19] [54]

Terminal voltage of a Li-ion battery depends on the charge of the battery. The charge should be kept within safety limits related to cut-off voltage and full-charge voltage. Typical voltage profile with the safety limits for one Li-ion battery chemistry is depicted in Figure 17. Charging the battery over full-charge voltage can cause serious safety problems discussed earlier and a reduction of lifetime. Discharging the battery over cut-off voltage can cause the battery to lose some of its charge receiving capability. The amount of charge in ampere hours left within these limits is called capacity of the battery. Charge, power and energy of the battery can be calculated as [55]

$$C_{\text{batt}} = \int_0^{I^{\text{cut-off}}} I dt \quad (13)$$

$$P_{\text{batt}} = U_{\text{batt}} I_{\text{batt}} = IU_0 + I^2 R_i + I^2 R_{\text{pol}}(I) \quad (14)$$

$$E_{\text{batt}} = \int_0^{I^{\text{ch/dch}}} P_{\text{batt}} dt = \int_0^{I^{\text{ch/dch}}} I(t) U_0(t) dt + \int_0^{I^{\text{ch/dch}}} I^2(t) R_i(t) dt + \int_0^{I^{\text{ch/dch}}} I^2(t) R_{\text{pol}}(I, t) dt$$

(15)

where U_{batt} is battery voltage, I_{batt} is battery current, R_1 is internal resistance, R_{pol} is polarization resistance from charge transfer and diffusion effects, $I_{\text{cut-off}}$ is cut-off current in discharge and $I_{\text{ch/dch}}$ is the charge or discharge current.

Battery capacity can be increased by parallel connecting battery cells and the battery system voltage can be increased by series connecting cells. Thus, the overall power and energy can be increased by using both series and parallel connections.

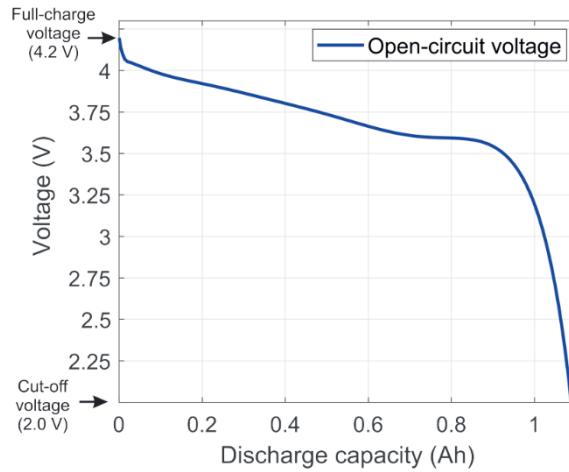


Figure 17. Open circuit voltage of a Li-ion battery [33]

In Appendix B, the given C-rate values are maximum values, but it should be noted that with higher currents, the battery performance starts to suffer. For example, cycling LTO battery with 3 C rate is enough to have noticeable effect on the capacity retention and gas build up as can be seen from Figures 18 and 19 [56]. In addition to the discharge current, also the temperature has major effect on capacity retention and gas build-up.

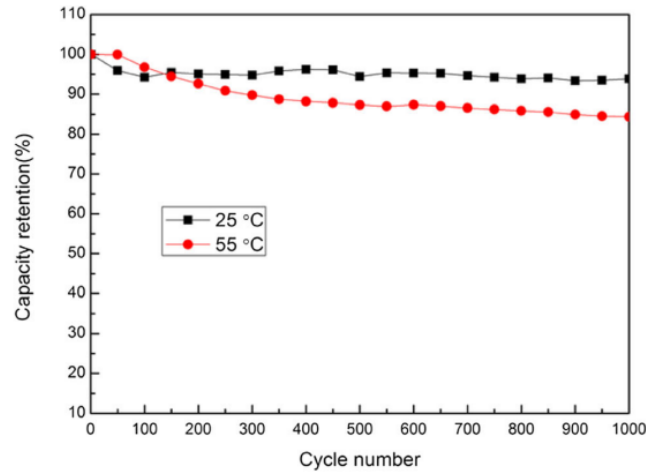


Figure 18. LTO cell capacity retention at 3 C current at different temperatures [56]



Figure 19. LTO cell gas build-up with 3 C current at A) 25°C and B) 55°C after 1000 cycles [56]

The rate of chemical reactions and temperature follow Arrhenius equation, which states that in higher temperature, chemical reactions occur more rapidly. In addition to reaction rates, also ionic conductivity of electrolytes and electrodes are affected. At low temperatures, viscosity of electrolyte increases, and thus ionic conductivity reduces. Internal resistance rises as the directional migration impedance increases. It has been observed that charge-transfer resistance of a discharged battery is much higher than that of charged battery. For this reason, discharging a battery at low temperatures is much easier than charging a battery. Low temperature also introduces lithium plating because the anodes are polarized so that the potential of graphite and other carbon-based anodes are close to the lithium metal. For this reason, intercalation of lithium ions to the anodes is slowed down and the ions are instead deposited to the surface of electrodes. If the plating occurs over a long time, the plating can grow dendrites that penetrate the separator and causes a short circuit as was explained before. [54]

Regarding the safety and performance, benefit of LTO chemistry is that it does not have a SEI-layer, so capacity fade and lithium plating does not occur [57]. Li-ion batteries are modelled in Chapter 3.1 and simulated based on the STATCOM energy storage requirements in Chapter 4.

2.6 Supercapacitor

Supercapacitor, also known as electrochemical double-layer capacitor (EDLC) or ultracapacitor, stores electrical energy using a non-faradic method in the solid-liquid interface between two electrodes that are separated by a separator and immersed in an electrolyte [58]. In non-faradic mechanism a solid-liquid interface is formed where a double-layer effect occurs. In electrical double layer (EDL) the first layer, known as surface layer or inner Helmholtz layer, is formed when surface charge consisting of adsorbed ions are collected on to the electrode. Second layer, known as outer Helmholtz layer, having an opposite polarity consists of dissolved and solvated ions. The two layers are separated by solvent molecules in a monolayer [59]. A simplified figure of a charged supercapacitor based on non-faradic method is shown in Figure 20.

In non-faradic method energy is stored without the use of chemical reaction. Supercapacitors can store energy also using a faradic method where charge is stored using electron charge transfer. Electron charge transfer is caused either by intercalation as in Li-ion battery cells or by redox reaction as in traditional battery cells. Faradic energy storage method is also known as pseudo-capacitance. [60]

Usually, the separator is made of polyolefin to allow for electrolyte intake and porosity [61]. The separator acts as an insulator between the porous electrodes to avoid short circuit but is transparent to the ions. In addition, the separator stores electrolyte into its pores. Both electrodes are connected to current collectors. Difference compared to batteries is that there is no conversion to chemical energy, so the conversion losses are minimal. The main difference compared to capacitors is that the electrodes are layered with activated carbon or carbon nanotubes which greatly increases the surface area. Also, regular capacitor uses dielectric as the insulating material to prevent the flow of electrons while supercapacitor uses an ion-permeable separator, for example graphene membrane. In a supercapacitor the capacitance is voltage dependent, and the charge has time/space redistribution because of electrode porosity unlike in an ideal capacitor model [58].

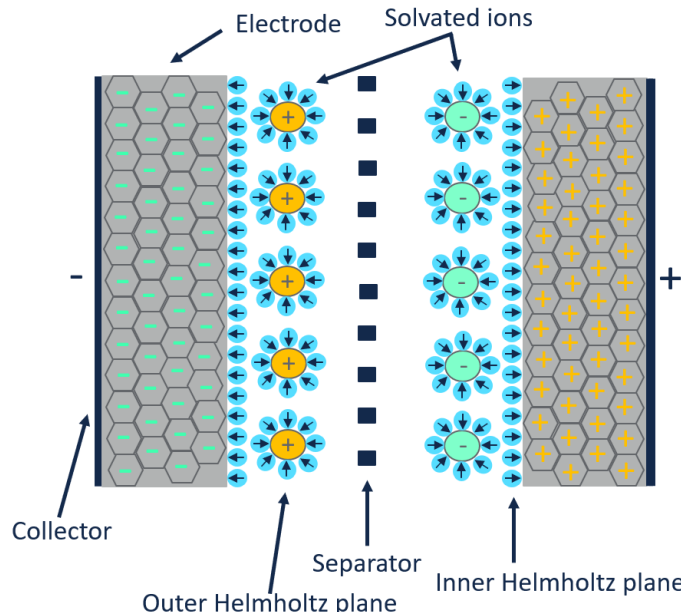


Figure 20. Charged supercapacitor structure

Advantages of supercapacitors are the fast charge-discharge times, possibility for high charge and discharge currents, good stability in terms of charge-discharge cycles, fast response time and high capacitance. An example response time of 11,5 ms to full power has been reported in [62]. Disadvantage is the low energy density, so supercapacitors are viable for only short power outputs [58]. As was discussed, the basic structure of supercapacitor is based on double-layer topology where the activated carbon electrodes have high surface area, creating a large capacitance. In addition, a short distance between the opposite charges increases the already high capacitance that can be up to 6000 F per cell [63][64].

Supercapacitors can be classified to different categories as is shown in Figure 21. In this thesis the term supercapacitor assumes an electric double-layer capacitor structure even though supercapacitor refers in general to a capacitive energy storage device [58].

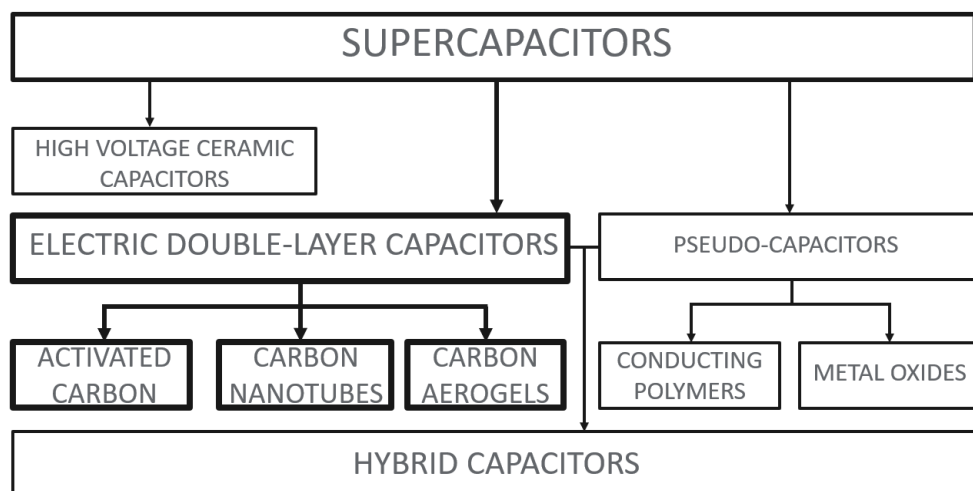


Figure 21. Supercapacitor taxonomy [58]

2.6.1 Supercapacitor performance

Supercapacitor can be seen as a voltage dependent capacitance. The voltage dependency comes from interfacial tension in the double-layer that is caused by charge distribution. Charge distribution depends on potential difference over the material [65]. Voltage controlled capacitance of a supercapacitor can be defined as [58]

$$C(u) = C_0 + k_c u \quad (16)$$

where C_0 is the initial capacitance and k_c is the voltage dependent coefficient representing effects of diffused layer expressed in $\frac{F}{V}$. In many sources, voltage dependent coefficient is depicted as C_v .

Energy of the supercapacitor charged to voltage u_c is [58]

$$E_c(u_c) = \frac{1}{2} \left(C_0 + \frac{4}{3} k_c u_c \right) u_c^2 \quad (17)$$

If the supercapacitor is charged to a maximum voltage of $U_{c,max}$ and discharged to a minimum voltage of $U_{c,min}$ that is greater than zero, the available energy is [58]

$$E_{avb} = \frac{C_0}{2} (U_{C,max}^2 - U_{C,min}^2) + \frac{2}{3} k_c (U_{C,max}^3 - U_{C,min}^3) \quad (18)$$

Because of the internal resistance of supercapacitor, some part of the available energy is dissipated as losses, thus the energy realized for the load is [58]

$$E_{load} = E_{avb} - E_{losses} = \frac{C_0}{2} (U_{C,max}^2 - U_{C,min}^2) + \frac{2}{3} k_c (U_{C,max}^3 - U_{C,min}^3) - \int_0^{t_{dsc}} R_{C0}(t) i_{C0}^2(t) dt \quad (19)$$

where t_{dsc} is discharge time and R_{C0} is time dependent supercapacitor resistance.

The peak power is defined as [58]

$$P_{max} = \frac{U_{C,max}^2}{4R_{C0}} \quad (20)$$

Typically, capacitance values of supercapacitors are between 100-6000 F and voltage ratings range from 2.5-3.0 V. The voltage of single cell is limited as too high voltages start to decompose the solvent. Like batteries, the supercapacitor discharge characteristics depend on the discharge time and the discharge type. An example figure of the supercapacitor module discharged with constant power is presented in Figure 22.

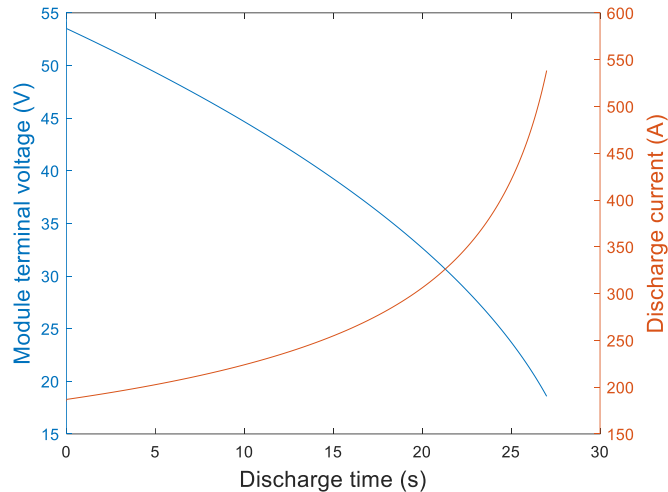


Figure 22. *Supercapacitor module discharge characteristics with constant power of 10 kW*

The maximum voltage of one supercapacitor cell is limited, so to reach high voltages, series connection of cells is needed. For STATCOM application, requiring over 100 MW power output, parallel connections are also required to increase the capacitance. There is a limit for the number of series connected modules based on the voltage creepage, the requirement from the auxiliary circuit and the dielectric strength of the enclosures. If the ground voltage is floating, the voltage limits can be extended. Usually, a series connection maximum voltage of around 1500 V is reported while there is no limit for the number of parallel connected ultracapacitors. [66]

For long lifetime the supercapacitor temperature and voltage need to be controlled. The supercapacitor module voltage can be managed similarly to battery cells by using either passive, active or shunt voltage balancing methods. In passive method, the current from high voltage cells is controlled to the low voltage cells via a voltage dividing resistor. Passive balancing causes more self-discharge losses but is a cheap method. Active method implements a measurement and control unit that actively balances the cell voltages if adjacent cells become out of balance. Active method should only be used if the energy storage consists of a single module. Shunt method implements voltage sensing shunts that balance the cell voltages. Shunt balancing method is a good choice when low self-discharge is needed for series or parallel connected modules [66]. Usually, the balancing method is implemented on a module level, so the end user does not need to implement it.

2.6.2 Supercapacitor lifetime and safety

Supercapacitors can go through hundreds of thousands of deep charge and discharge cycles because of the lack of chemical reaction taking place in electrochemical battery energy storages. The lifetime of a supercapacitor is limited by temperature and voltage. Increased temperature causes higher reactivity of the chemical components and high voltages cause more impurities to undergo the faradic redox reaction as well as increased decompositions of the electrolyte. All

these negative effects cause the capacitance to drop and increase in internal series resistance as well as in the self-discharge rate.

Temperature effects impose a limit to the ripple current as the ripple current should be such that the surface temperature of the module does not increase more than 3°C [66]. As a rule of thumb, the aging increases with a rate of two if voltage increases by 0.1 V or temperature by 10°C . It is observed that voltage increase leads to greater pressure build-up than increase in temperature [67].

Usually, the end-of-life condition for supercapacitors and batteries is a decrease in the capacitance by 20 % or doubling of the internal resistance. It is noted that for supercapacitors the capacitance decrease is usually reached faster than the doubling of internal resistance [20]. Regarding supercapacitor safety, most common failure mechanism is the pressure build up that will lead to a safety valve opening [20]. Compared to many battery chemistries, supercapacitors are thus much safer as the failure does not lead to a thermal runaway. However, if electrolyte is leaking from a supercapacitor and happens to combust, toxic gases can be released that can have negative health effects. Usually over 90 % of the electrolyte is absorbed into the activated carbon layers so in case of a puncture, only minimal amount of electrolyte should leak. The electrolyte is usually made of TEABF₄ quaternary salt compound dissolved in acetonitrile. The electrolyte is flammable if kept in an ignition source or in flame. The chemicals inside the cell can decompose into toxic gasses such as carbon oxides, nitrogen oxides, hydrogen cyanide etc. which should not be inhaled. Substances within the supercapacitor can also be toxic to aquatic life. [68] The electrolyte should not self-ignite under temperatures of 500°C , but still suppression unit should be installed in the site. After modules show end of life (EOL) signs, preferably the whole system is replaced to avoid cell unbalances that could lead to faster aging. Supercapacitors are seen as industrial waste but for example aluminum can be recycled. Under normal operating conditions, supercapacitors represent a very safe technology and thus the normal operation monitoring should focus on maintaining appropriate temperature and voltage to ensure long lifetime. The effect of cell voltage and temperature to the supercapacitor lifetime is shown in Figure 23.

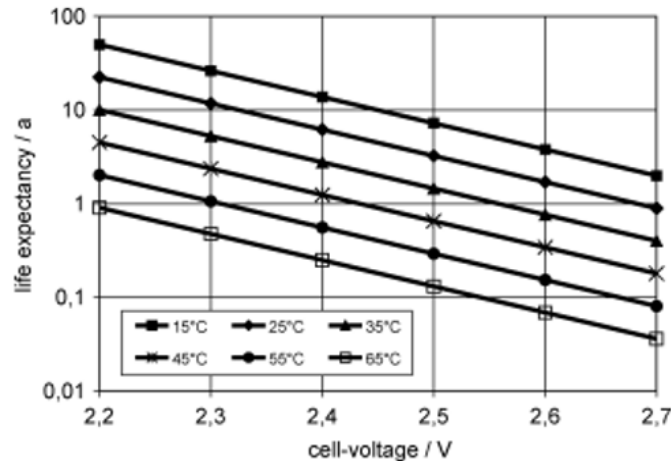


Figure 23. Supercapacitor lifetime expectancy versus operating voltage and temperature [58]

To increase lifetime, reliability and performance, one should use power circuits that do not over-charge or overheat supercapacitors because of high ripple voltages or currents. In addition, supercapacitors cells can be kept at derated voltage values to increase the lifetime. Usual temperature rating for a supercapacitor is between -25°C and 70°C . Normal maintenance consists of visual checks and dirt cleaning once a year in clean operating conditions.

2.6.3 Supercapacitor characteristics

The discharge characteristics are an important factor when analyzing the supercapacitor behavior. Figure 24 presents a general constant current discharge profile of a supercapacitor.

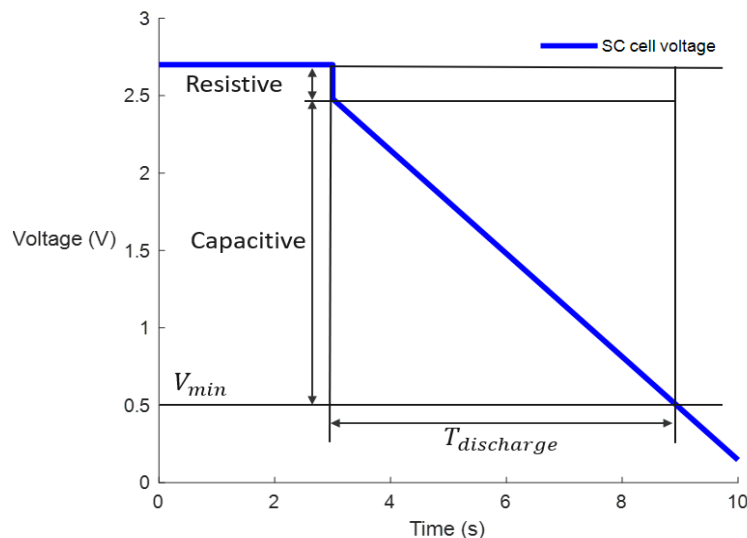


Figure 24. General discharge profile of a supercapacitor at constant current

During constant current discharge the discharge profile consists of a resistive and capacitive voltage drop. Resistive voltage drop is caused by the equivalent series resistance of the supercapacitor and can be calculated as [69]

$$\Delta V_R = R_{\text{cell}} i \quad (21)$$

where R_{cell} is cell resistance and i is current.

Capacitive voltage drop is caused by the change in energy due to discharge and is calculated as

$$\Delta V_C = \frac{dt}{C_{\text{cell}}} i. \quad (22)$$

The total voltage drop during discharge is the sum of the resistive and capacitive voltage drop depicted as

$$\Delta V = \frac{dt}{C_{\text{cell}}} i + R_{\text{cell}} i \quad (23)$$

Based on constant current discharge test, the capacitance and resistance of a simple supercapacitor equivalent model can be solved. Supercapacitor has a constant voltage decrease with constant discharge current during the capacitive voltage drop unlike a battery. It should be noted that with different currents, the capacitance values vary slightly. Constant current discharge modelling assumes a capacitance that is not a function of cell voltage, so the capacitance is assumed to be constant for both charging and discharging. The simple model is shown if Figure 25.

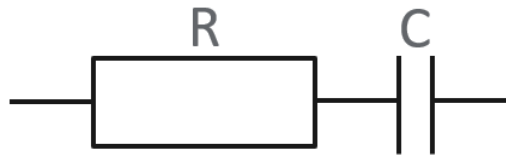
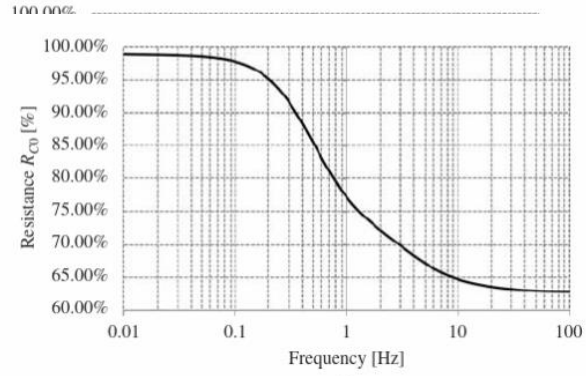


Figure 25. Simple model for supercapacitor

For more accurate models it should be noted that supercapacitor equivalent series resistance and cell capacitance are frequency, voltage and temperature dependent as is shown in Figures 26, 27 and 28.



(a)

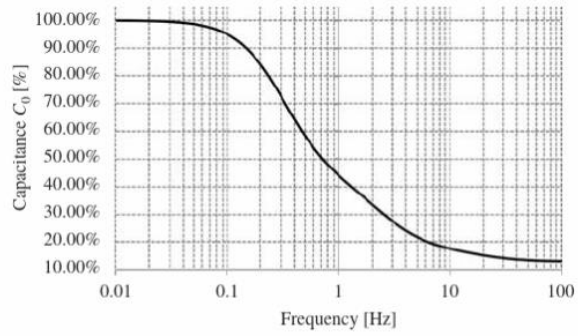
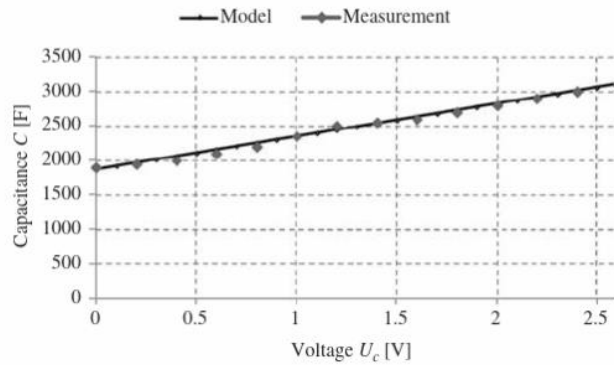


Figure 26. Frequency dependence of supercapacitor equivalent series re-



sistance and capacitance [58]

Figure 27. Voltage dependency of supercapacitor capacitance [58]

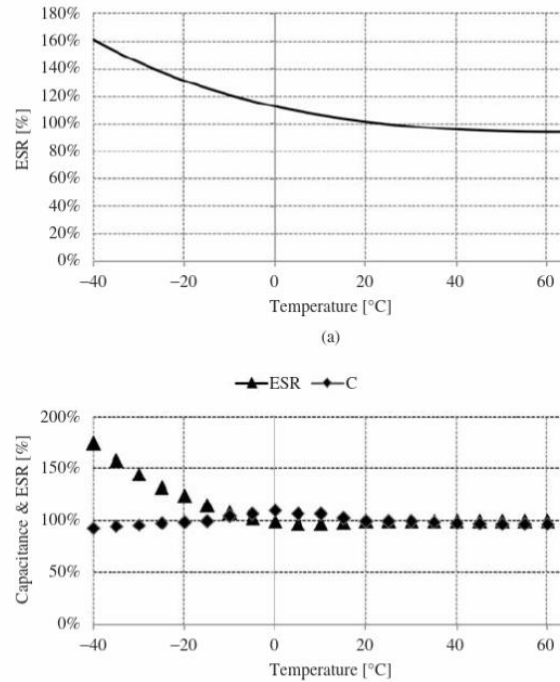


Figure 28. *Temperature dependency of supercapacitor equivalent series resistance and capacitance [58]*

As can be seen from Figures 26, 27 and 28, in high frequencies and low temperatures the performance of the supercapacitor changes drastically. In STATCOM applications the operating temperature is assumed to be close to room temperature or higher and the supercapacitor cooling is assumed to be powerful, so the temperature effect is not considered in supercapacitor simulation models. In reality, high discharge currents produce significant amount of heat through the series resistance which needs to be taken into account in the energy storage design. Frequency effects need to be considered in supercapacitor energy storage sizing and modelling. Behavior of Figure 26 was verified by testing a 3000 F supercapacitor cell that is rated for 3 V. Capacitance behavior is shown in Appendix C.

It should be noted that a regular capacitor has similar frequency behavior as a supercapacitor with the difference that the transition frequency is located on much higher frequencies. This difference of transition frequency is caused by the increased capacitance of supercapacitors. A 3000 F supercapacitor has a transition frequency of 30 – 40 Hz, above which the supercapacitor behaves as an inductor. According to supercapacitor manufacturers the frequency dependency of Figure 26 and Appendix C is not relevant if a DC component is present, and the AC ripple frequency is orders of magnitude above cutoff frequency. For this reason, the capacitance of the supercapacitor system does not collapse if a converter is used. Still, the AC ripple current increases the RMS current and thus causes increased heat generations, so the ripple amplitude should be kept as small as possible. Also, in an MMC application the typical submodule capacitor should be included as it will significantly reduce the losses in the supercapacitor.

2.7 Other energy storage technologies

Based on Appendix A, flywheels and SMES also represent viable energy storage options. Flywheels store energy to the rotor as kinetic energy based on equation [70]

$$E_{\text{use}} = \frac{1}{2}I(\omega_{\text{max}}^2 - \omega_{\text{min}}^2) \quad (24)$$

where I is moment of inertia, ω_{max} is the maximum angular velocity and ω_{min} is the minimum angular velocity.

It is reported that the flywheel cost is around 914 – 1294 \$/kW for a 20 MW system and generally flywheel levelized cost of energy is higher than that of supercapacitors or SMES [71][72]. Flywheels are not considered in more detail because of their mechanical complexity, weight, need for maintenance, cost, high self-discharge, lack of actual STATCOM implementations and possible safety problems [70]. Also, scalability of flywheels is not as simple as with batteries or supercapacitors as flywheels need a vacuum chamber, electric machine and a safety housing for each unit. Based on the reliability and maintenance costs, flywheels have much higher total cost of ownership than supercapacitors [73].

SMES stores electrical energy into a superconducting coil. In a superconducting state the resistive losses in cryogenically stable operation are practically zero. SMES device consists of the superconducting magnet, refrigeration system, cryogenic dewar or cryostat, quench protection system, current switch and current leads. In addition, the SMES requires a power conditioning device that has a bidirectional converter, AC filters, current-voltage choppers and a DC-link capacitor [74]. The amount of stored energy into the superconducting coil follows equation [5]

$$E = \frac{1}{2}Li^2 \quad (25)$$

where L is inductance and i is the current in the coil.

Some simulation studies have been made where SMES is integrated with STATCOM or VSC, e.g., [75], [76] and [77], but the lack of actual implementations, possible safety problems, high cost and maintenance requirements rules the energy storage out from further analysis.

New emerging technology called Li-ion capacitor (LIC) combines the benefits of both Li-ion batteries (LIB) and supercapacitors. LIC can be classified as a hybrid capacitor according to Figure 21. The LIC uses carbon material as the negative electrode which can be doped with Li-ions [78]. Positive electrode resembles that of a supercapacitor as it comprises of activated carbon as can be seen from Figure 29. Main benefits of LIC are increased maximum voltage up to 3.8 V compared to supercapacitors, greatly increased energy density up to 14 Wh/kg, increased safety compared to Li-ion batteries, smaller self-discharge than supercapacitors, great cyclic lifetime of over 100 thousand times and specific power up to 10 kW/kg. In LICs both intercalation and non-faradic reactions occur as the Li-ions are de-intercalated/intercalated from/into the negative electrode while anions are desorbed/absorbed from/into the positive electrode. In LICs the operational

voltage can be high as the potential ranges of the electrodes differ due to different reversible electro-chemical mechanisms.

Main disadvantages compared to EDLCs are that the price per power is higher, power capability is lower, charge and discharge rates are lower and due to larger internal resistance heat losses are greater. Also, LIC technology is not as mature as traditional supercapacitor technology. Based on the listed advantages and disadvantages LICs seem to represent a good potential energy storage solution for the STATCOM. However, in this thesis LICs are not analyzed in more detail.

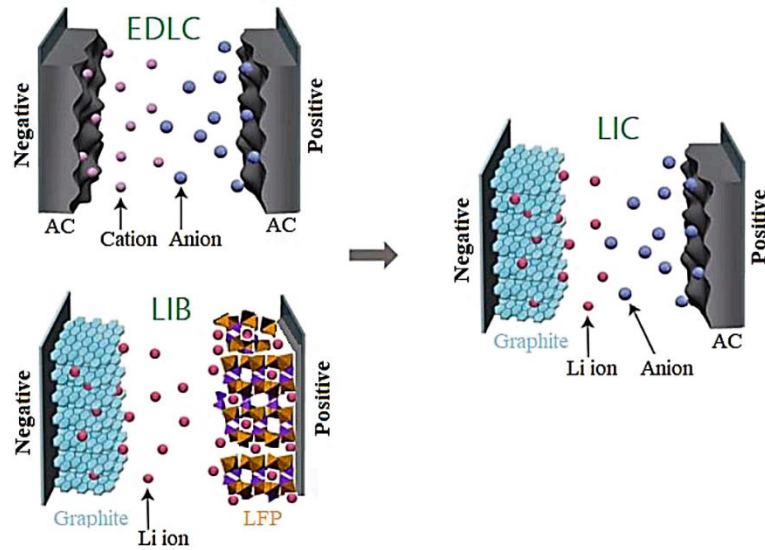


Figure 29. LIC structure combining properties from EDLC and LIB [78]

3. ENERGY STORAGE MODELLING AND DESIGN

In this chapter simulation models for a Li-ion battery and a supercapacitor cell are introduced. Chosen models need to realistically model the effects of energy storage current, SOC and voltage with respect to the demanded power or current over a short-term timescale. Modelling of the aging, capacity fade, and heating are out of the scope of this thesis even if they are important factors affecting the applicability of the energy storage. This chapter presents multiple models ranging from simple, easy to implement and fast to compute to more complex and slower to simulate. The optimal model should describe the required dynamics of the energy storage accurately enough without being computationally too demanding and complex to implement.

Main difference between batteries and supercapacitors come from the mechanism of energy storage. Batteries use slower redox reactions for high energy density but slow kinetics while supercapacitors use the electrostatic storage of charge on electrode surface [79]. This difference in charging and discharging times thus needs to be considered and modelled. In addition, a battery voltage has nonlinear dependence on SOC unlike a supercapacitor. For these reasons battery modelling tends to be more challenging.

3.1 Battery modelling

Battery cell can be modeled as a voltage source where the SOC is dependent on the voltage. For more realistic modelling also state of health (SOH) should be modelled. Both SOC and SOH measurements can be made by the battery management system (BMS) [80].

SOC depicts the amount of charge that can be drawn from a battery, and it is given by

$$SOC = \left(1 - \frac{Q}{Q_0}\right) 100\% \quad (26)$$

where Q is consumed charge and Q_0 is the capacity of the battery.

Tracking of the consumed charge Q is conventionally based on Coulombic counting method. Coulombic counting algorithm is given as [81]

$$SOC(t) = SOC(t_0) - \left(\frac{1}{Q_0} \int_{t_0}^t i_{bat} dt\right) 100\% \quad (27)$$

where Q_0 is nominal capacity, i_{bat} is battery current, t_0 and t depict the time instants between which the SOC is calculated.

Coulomb counting algorithm can produce inaccurate results as the nominal capacity depends on temperature, charge/discharge currents and life cycles that are not considered in the method [33]. For this reason, Coulombic counting is usually used as a part of a more sophisticated method, such as Kalman filters or neural networks [82].

Aging of the energy storage can be modelled using SOH which indicates the actual capacity of the energy storage with respect to the nominal beginning of life (BOL) capacity. SOH is defined as [83]

$$SOH = \frac{Q_0}{Q_{BoL}} 100\% \quad (28)$$

where Q_{BoL} is the capacity at the beginning of battery's life.

SOH estimation is difficult as evaluating the present capacity Q_0 requires time-consuming charge-discharge measurements which limit the normal use of the battery. Because of these difficulties, Q_0 is usually indirectly computed from battery current, voltage, and temperature [33]. Nowadays impedance/resistance measurements have become a popular estimation choice. In this thesis, SOH is not modelled and analyzed because of the complexity and short simulation timescale.

Main reasons for Li-ion battery aging are lithium-plating, corrosion of the electrodes and current collectors as well as the growth of SEI [84]. These effects are accelerated by overcharging, over-discharging, overly high or low SOC levels, current rates and operating temperatures. Battery temperature increase is significant as the internal ohmic resistance can almost double when temperature drops from 25°C to 0°C [85]. In short timescale simulations the aging and effect on SOH are not needed as the importance is in the capability of the battery to meet the current and voltage requirements from the STATCOM application. However, estimation of the end-of-life performance is needed to estimate how the energy storage behaves in a worst-case scenario.

In addition to SOC and SOH, also polarization needs to be addressed by the battery model. Polarization refers to the departure of cell voltage from the open-circuit voltage during charging and discharging. Polarization is mainly caused by slow speed of electrochemical reaction rate compared to electron transfer rate caused by current. In low temperatures, polarization is more severe. A simple model only assumes an instantaneous polarization caused by series resistance but in reality, polarization has more complex behavior. In Li-ion batteries polarization is caused by the slow diffusion of lithium in the cell. More accurate way to model polarization is to use parallel connected resistance and capacitance. Sometimes an impedance is used in the place of polarization resistance to allow for more thorough analysis of the battery using Nyquist-plane plots. [60]

Because battery operation is dependent on many parameters, many battery models utilize look-up tables together with equivalent circuit models. However, look-up tables need many measurements to cover the whole operation range of the battery. In addition, battery aging will change the model parameters, so the original look-up tables need to be updated. One solution is to use online recursive model parameter estimation algorithms. [85] In addition to equivalent circuit models using look-up tables there are many other modelling options which are introduced in Figure 30.

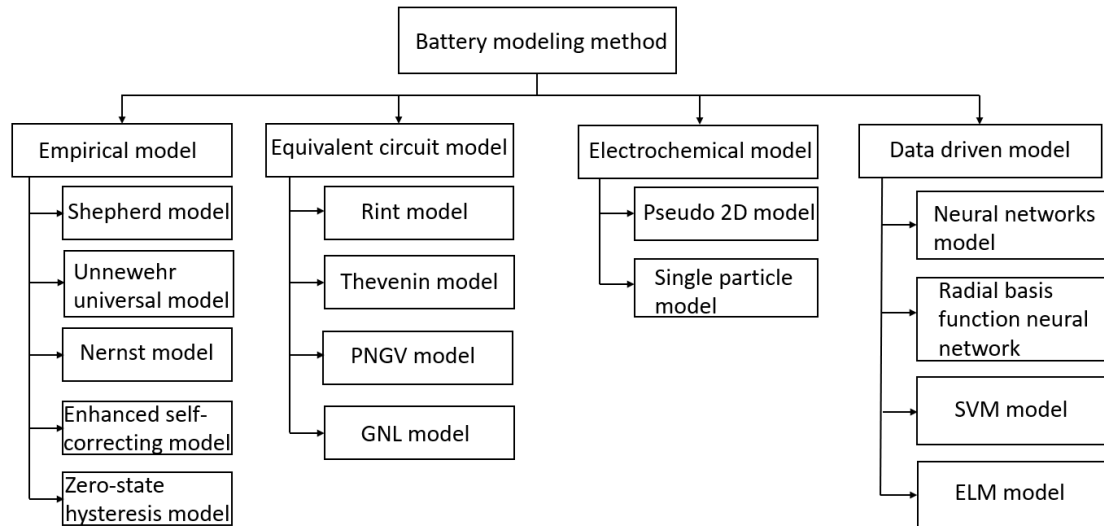


Figure 30. Battery modelling methods, modified from [86]

Empirical models are easiest to setup and execute but the accuracy of the model is the worst out of all modeling methods. On the other hand, electrochemical models are the most accurate but require a lot of information. Benefit of electrochemical models is that they can predict physical cell limitations [87]. Between empirical and electrochemical model, in terms of accuracy, are equivalent circuit models. The accuracy of equivalent circuit models is good enough so that they capture most of the dynamics of batteries. Disadvantage of equivalent circuit models is that the SOC tracking, and runtime prediction is hard [47]. Data driven models are not discussed in this thesis.

In this thesis, an LTO battery is modelled using an empirical and equivalent circuit model. Table 3 presents the battery information.

Table 3. LTO battery information

Rated capacity	13 Ah
Nominal voltage	2.26 V
DC internal resistance	1.6 mΩ
Max C-rate	20 C
Maximum charge/discharge current	260 A

3.1.1 Generic controlled voltage source battery model

Controlled voltage source model is based on the basic equation

$$V_{\text{batt}} = E - R_{\text{int}} I_{\text{batt}} \quad (29)$$

where E is source voltage of the battery, R_{int} is constant resistance and I_{bat} is battery current.

Electrical circuit of the model is shown in Figure 31. The voltage of the battery can be simply calculated based on the charge or discharge current and initial SOC.

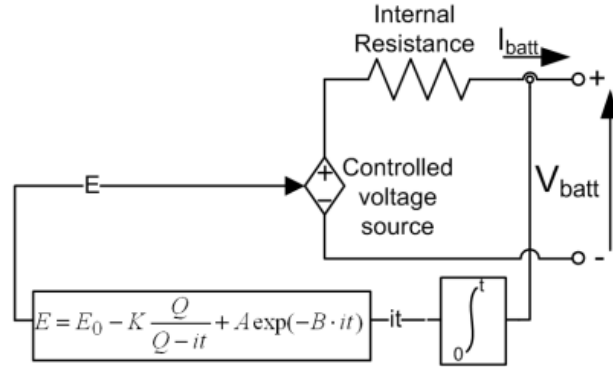


Figure 31. Non-linear voltage source battery model [88]

Controlled voltage source model depicts well the charge and discharge characteristics using an empirical model based on Shepherd's original model [89]. Implementation of the model is easy as the model parameters are derived from battery datasheets. Many variations of controlled voltage source model exist with different number of details. Some models consider the Peukert's equation that models the decrease in capacity with respect to increasing discharge current. Peukert's equation can be written with respect to capacity as [47]

$$Q_1 = Q_0 \left(\frac{I_0}{I_1} \right)^{pe-1} \quad (30)$$

where Q_1 is capacity for discharge current I_1 , I_0 is known current, Q_0 is known capacity and pe is Peukert's coefficient greater than one based on empirical data. In this thesis, Peukert's effect is neglected for simplicity.

Model for open circuit voltage as a function of SOC without the effect of Peukert's equation can be written as [47]

$$E_{OC} = E_0 - K \frac{Q_{cut}}{Q_{cut} - Q} + A e^{(-BQ)} \quad (31)$$

$$A = E_{full} - E_{exp} \quad (32)$$

$$B = \frac{3}{Q_{exp}} \quad (33)$$

$$K = \frac{[E_{full} - E_{nom} + A(e^{(-BQ_{nom}} - 1)](Q_{cut} - Q_{nom})}{Q_{nom}} \quad (34)$$

$$E_0 = E_{full} + K + R_{int} I_0 - A \quad (35)$$

$$Q = \int_0^t -I_{batt} dt = I_{batt} t \quad (36)$$

where E_{full} is potential at fully charged voltage, E_{exp} is potential at the end of exponential zone, Q_{exp} is charge at the end of exponential zone, E_{nom} is potential at the end of nominal zone, Q_{nom} is charge at the end of nominal zone and Q_{cut} is the charge at the end of discharge curve and t is time.

MathWorks has documented that their generic battery model is based on controlled voltage source model. Voltage of the battery depends on the battery type, extracted battery capacity, low frequency current dynamics and battery current. For example, Li-ion battery voltage during discharging and charging can be modelled using equations [90]

$$E_{\text{Li-ion,discharge}}(it, i^*, i) = E_0 - K \frac{Q}{Q-it} i^* - K \frac{Q}{Q-it} it + Ae^{(-itB)} \quad (37)$$

$$E_{\text{Li-ion,charge}}(it, i^*, i) = E_0 - K \frac{Q}{it+0.1Q} i^* - K \frac{Q}{Q-it} it + Ae^{(-itB)} \quad (38)$$

where it is the extracted capacity in Ah, i^* is low frequency current dynamics in A, i is battery current in A, E_0 is constant voltage in V and Q is maximum battery capacity in Ah.

For Li-ion batteries, the MathWorks model also offers equations for temperature effects and aging effects modelling. Simulink model assumes that the internal series resistance of battery is constant, the parameters are derived based on discharging characteristics, Peukert effect and self-discharge is not modelled, and the battery has no memory effect [90]. For series and/or parallel connections, the parameters can be scaled based on Table 4.

Table 4. *Series and/or parallel connection scaling based on one cell*

Parameter	Value
Nominal voltage	$E_{nom} \cdot n_s$
Rated capacity	$Q_{nom} \cdot n_p$
Maximum capacity	$Q \cdot n_p$
Fully charged voltage	$E_{full} \cdot n_s$
Nominal discharge current	$i \cdot n_p$
Internal resistance	$R_{int} \cdot \frac{n_s}{n_p}$
Capacity at nominal voltage	$Q_{nom} \cdot n_p$
Exponential zone	$E_{exp} \cdot n_s, Q_{exp} \cdot n_p$

An example simulation result for one battery cell in discharge and charge conditions is shown in Figure 32. The model parameters were extracted from simulation results that were simulated with the model in section 3.1.2. This was decided as the model parameters for the model in Section 3.1.2 were precisely known, but the datasheet values were not. It was assumed that the simulation results were accurate enough to be the basis of controlled voltage source model parameters. Using the same cell for both models also allow for direct comparison. In the simulation battery capacity was 13 Ah and the charge/discharge current 13 A, so the battery capacity is charged and depleted in one hour which is 3600 seconds.

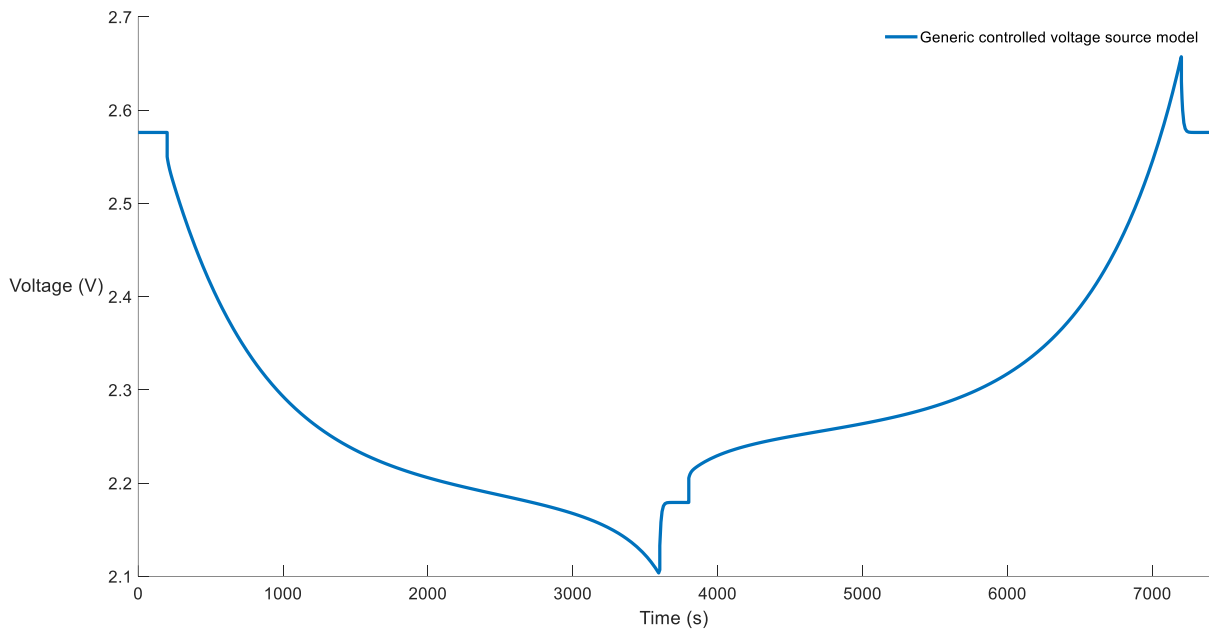


Figure 32. *Generic voltage source model simulation result for a battery cell*

Benefit of the generic voltage source model is that the implementation is easy. Disadvantage is that the model typically only uses SOC as a state variable to avoid algebraic problems. In addition, the charge and discharge characteristics are assumed to be similar, and the model parameters are not temperature dependent.

3.1.2 Second order equivalent circuit model

A popular Li-ion battery model called second order model, Thevenin model or six parameter equivalent circuit model consist of a SOC dependent open-circuit voltage, series resistance and two RC networks where the first RC circuit has smaller time constant than the second. Purpose of the two RC circuits is to model polarization during charge and discharge. Values for the resistances and capacitances need to be measured from discharge tests. Based on the parameter

extraction method, the second order model can be further categorized as either a Thevenin-based or impedance based-model. Equivalent circuit of the second order model is shown in Figure 33.

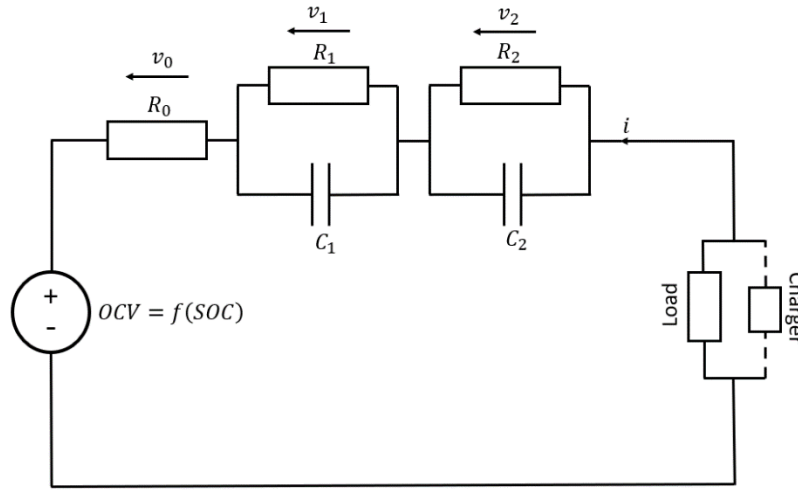


Figure 33. General Li-ion circuit diagram

In Thevenin-based model, the parameters are identified based on time domain current and voltage data. In impedance-based method, the parameters are identified from electrochemical impedance spectroscopy (EIS) measurements in frequency domain. In impedance-based method, the battery equivalent model is shown in Figure 34. In the model, so called constant phase elements (CPE) and ZARC elements are used instead of capacitances. Impedance of the model is given by [91]

$$Z_{2nd\ order} = j\omega L_s + R_s + \frac{1}{\frac{1}{R_1} + (j\omega)^{N_1} Q_1} + \frac{1}{\frac{1}{R_2} + (j\omega)^{N_2} Q_2} \quad (39)$$

where Q_1 and Q_2 are generalized capacitances, L_s and N_2 are dispersion factors, R_s is series resistance, L_s is series inductance and j is imaginary unit.

Based on the two methods, it is clear the Thevenin-based methods are easier to implement as there is no need to first identify the impedance and from impedance the parameters for the model.

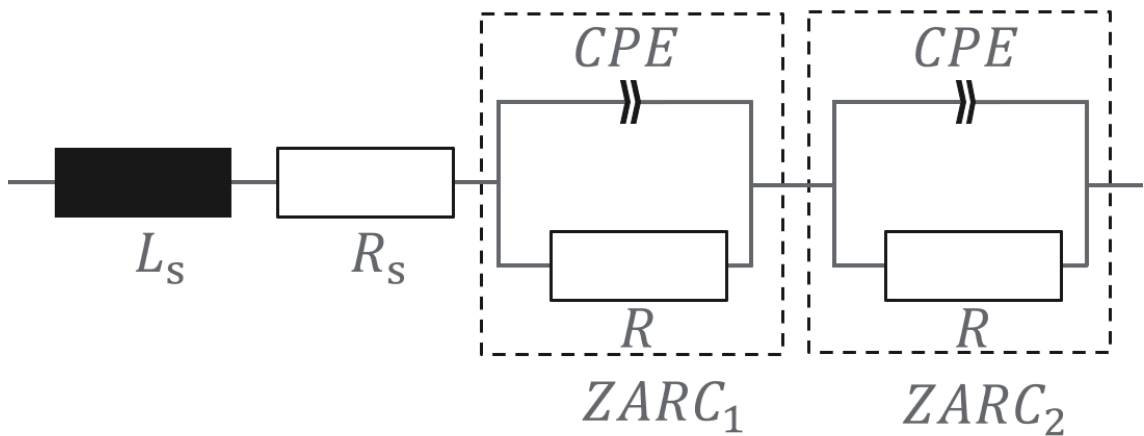


Figure 34. Electrical equivalent circuit based on ZARC elements [91]

Because the model parameters are a function of SOC, the parameters need to be identified for each SOC value, which means many discharge tests. In a discharge test a current pulse is injected to the battery and the voltage response is measured. An illustrative figure of the discharge current pulse method is shown in Figure 35. Discharge pulse method is also known as hybrid pulse power characterization (HPPC).

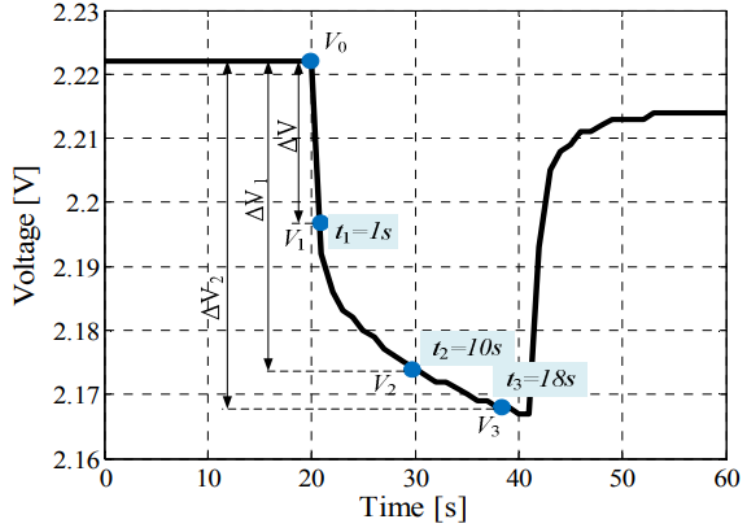


Figure 35. Voltage response of the battery to a discharge current pulse [92]

According to Figure 35, the voltage response can be divided into three separate time windows. From discharge current starting time to one second after, it can be approximated that only the ohmic resistance causes the instantaneous voltage drop. The resistance value can be calculated from

$$R_0 = \frac{\Delta V}{\Delta I} = \frac{V_0 - V_1}{I} \quad (40)$$

where I is the constant discharge current, V_0 is voltage when current pulse is applied and V_1 is voltage after 1 second of discharge.

Values for the two RC networks can be solved using RC network time constants

$$\tau_1 = R_1 C_1 \quad (41)$$

$$\tau_2 = R_2 C_2 \quad (42)$$

Based on the time values in Figure 35, the time constants can be written as

$$\tau_1 = -\frac{t_2 - t_1}{\ln\left(\frac{V_1(t_2)}{V_1(t_1)}\right)} \quad (43)$$

$$\tau_2 = -\frac{t_3 - t_2}{\ln\left(\frac{V_2(t_3)}{V_2(t_2)}\right)} \quad (44)$$

Resistance values for R_1 and R_2 can be solved from

$$R_1 = \frac{V_1 - V_2}{I} \quad (45)$$

$$R_2 = \frac{V_2 - V_3}{I} \quad (46)$$

Using the derived equations for time constants and resistances, the capacitance values can be solved from

$$C_1 = \frac{\tau_1}{R_1} \quad (47)$$

$$C_2 = \frac{\tau_2}{R_2} \quad (48)$$

Total battery cell voltage can be written as

$$V_{sim} = OCV + I(t)R_0 + I(t)R_1 \left(1 - e^{-\frac{t}{\tau_1}}\right) + I(t)R_2 \left(1 - e^{-\frac{t}{\tau_2}}\right) \quad (49)$$

Simulation model parameters can be optimized using least squared error by feeding a similar current to the model and calculating the error between the measured voltage and simulated voltage. Based on the error, the optimization algorithm finds better parameters that produce the smallest error. To avoid overfitting, validation data should be used to test the generality of the identified parameters. After the parameters for different operational points have been identified, they can be applied in the model using lookup-tables.

A Simulink implementation of the model is shown in Figure 36. If a battery pack model is needed, the cell model parameters can be scaled according to the number of series and/or parallel connections as is shown in Figure 36 with the gain blocks. Note that the capacity is multiplied by the number of series connections. Parameters for the simulation model in Figure 36 were taken from [93], in which the model parameters have been identified for a 13 Ah, 2.26 V LTO Li-ion battery using four different discharge currents. The SOC had a resolution of 5% and the temperature was kept constant at 30°C. Discharge current had values 0.25C, 0.5C, 1C, 2C and 4C. Based on the lookup-tables, the model can extrapolate parameter values for even higher currents, but the model results might not be accurate. The created model does not take into account any temperature or cycle-life dependencies. Also, for more realistic model, cell unbalance should be included if long-time simulations are needed. If parameter dependency to temperature and cycling is needed, then more detailed and time-consuming identification is needed.

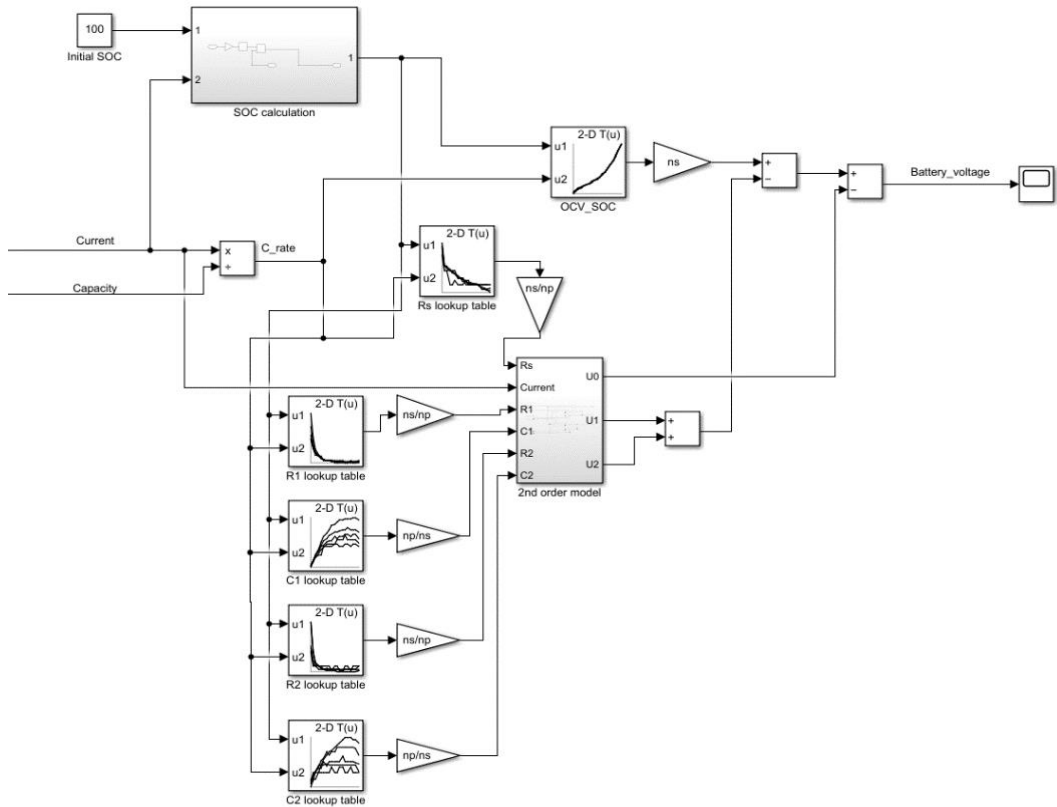


Figure 36. 2nd order battery model using lookup-tables in Simulink

An example simulation of the battery cell voltage is shown in Figure 37. The voltage behavior is not as flat as expected so the parameter extraction for general voltage source model is based on iterative simulations to find the optimal values.

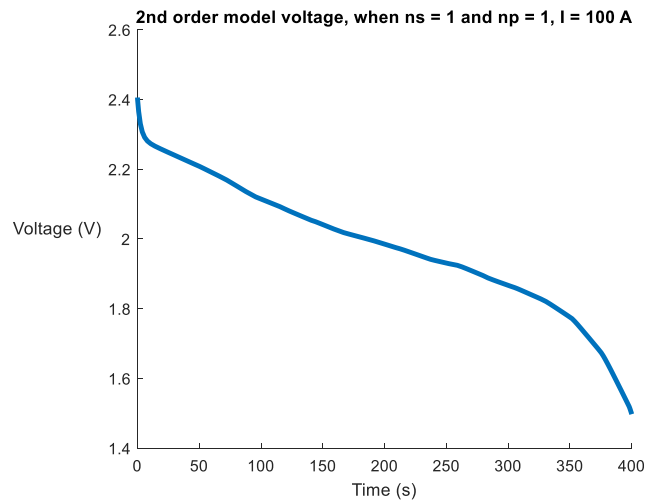


Figure 37. Simulated cell voltage with discharge current of 100 A

3.1.3 Comparing battery model results

Comparison between generic controlled voltage source model and second order model is done to find out which model should be used. Because there are no reference measurements from an

actual battery cell, the comparison is mainly based on how accurately the voltage source and second order model can produce similar and reliable results. Major disadvantage of generic controlled voltage source model is that for the LTO battery that is used, sufficient datasheet information was not available, so the parameter extraction is done based on Figure 37. As the voltage profile of Figure 37 is not as defined as the generic voltage model parameter identification assumes, the identified values can be inaccurate. Based in trial and error, the following parameters in Table 5 were identified.

Table 5. *Identified general voltage source model parameters*

E_{full}	2.55 V
R_{int}	0.002
E_{exp}	2.2 V
E_{nom}	2 V
Q_{nom}	13 Ah
Q_{max}	13.5 Ah
Q_{exp}	7 Ah
A	0.25
B	1.875
K	0
E_0	2.326 V
E_{cut}	1.6 V

The second order model produces accurate results when discharge current close to the identification currents are used as the parameters are identified from actual discharge tests. Based on the simulation results, the voltage profile of the LTO cell is not as flat as was expected. However, the voltage profile does not seem to have a great impact on the final sizing for the STATCOM as the sizing is mainly dictated by the voltage change due to the ESR effect as will be seen in Section 4.2. A major disadvantage of the 2nd order model is that it does not work with charging current so the model can be only used for discharge simulations.

A comparison of the battery voltages is shown in Figure 38 when both models are fed the same current. Only one battery cell is simulated. Based on Figure 38 the two models agree very well when the cell voltage is high. At the end of discharge, there is noticeable difference. Still, the response of the general voltage source model is deemed to be good enough for initial simulations.

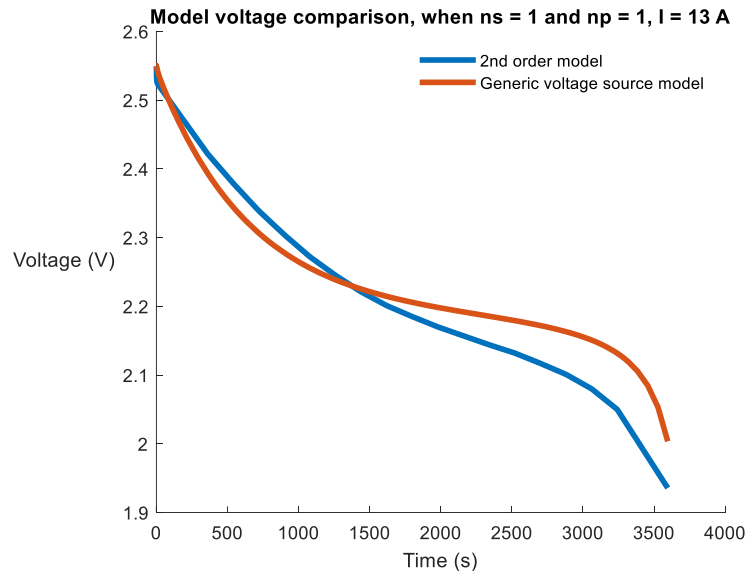


Figure 38. *Battery model comparison with constant discharge current*

Constant power charging and discharging works correctly with the general voltage source model. Second order model can only be used for constant discharge power simulations as the charging simulations produce an error. The two models agree well with each other when multiple cells are connected in series and in parallel. Based on the results, general voltage source model can be used for charge and discharge simulations if accuracy does not need to be very high. For more detailed modelling, an upgraded 2nd order model should be used that works in both charge and discharge conditions and also models the thermal behavior of the cells. For initial discharge tests, both models can produce believable battery voltage, current and SOC behavior. Because of the ability of the controlled voltage source model to work in both charge and discharge situations, it is used in the STATCOM simulations.

3.2 Supercapacitor modelling

Like batteries, supercapacitor models can be categorized to three main classes: mathematical, electrochemical, and electrical. Electrochemical models are formed using partial differential-algebraic equations that have many parameters [94]. Electrochemical models result in very accurate results, but they require a lot of information. Mathematical models can be made to have a good fit with experimental data but the process of defining parameter values is complex. Electric models are used for their ease of implementation. In this thesis supercapacitor modelling concentrates on a few popular equivalent circuit models. Detailed equivalent circuit modelling of a single supercapacitor cell is presented in [58], [64] and [95].

Accurate electrical supercapacitor model consists of infinite number of parallel connected capacitors and resistances. The need for many capacitors and resistors arises from the porous carbon-based electrodes that have a nonlinear relation with capacitance and surface area. Because of the nonuniform structure, an accurate supercapacitor model is the so-called transmission line model which depicted in Figure 39.

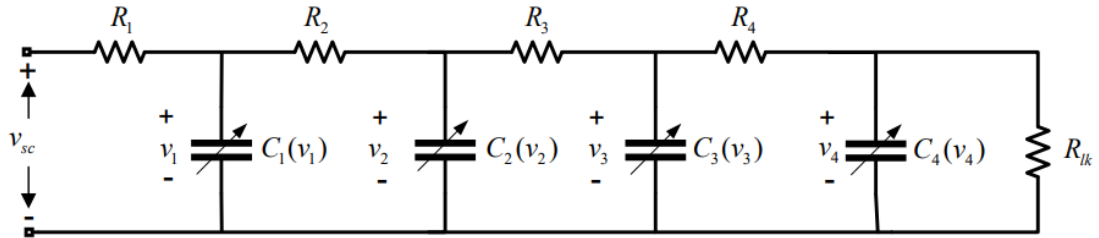


Figure 39. Transmission line model of a supercapacitor [94]

The presented model in Figure 39 is too complicated for most use cases, so simpler models are investigated. Figure 39 only applies to one supercapacitor cell, so a series and parallel connections are needed to achieve the wanted power and energy levels. Voltage in a series connection of supercapacitors is additive, so the series connection has a voltage of [96]

$$V_{\text{series}} = n_s V_{\text{cell}} \quad (50)$$

where n_s is the number of series connected cells.

The same applies for the series equivalent resistance of the cells

$$R_{\text{series}} = n_s R_{\text{cell}} \quad (51)$$

Capacitance of series connected supercapacitors is given as

$$C_{\text{series}} = \frac{C_{\text{cell}}}{n_s} \quad (52)$$

Maximum current flows through the supercapacitor bank when the supercapacitor voltage is at minimum. With a supercapacitor bank power of P_{sc} , the current maximum is

$$I_{\text{sc,max}} = \frac{P_{\text{sc}}}{V_{\text{sc,min}}} \quad (53)$$

To achieve the required maximum current from the supercapacitor, the cells should also be connected in parallel. The number of parallel connected supercapacitor strings is given by

$$n_p = \frac{I_{\text{sc,max}}}{I_{\text{cell}}} \quad (54)$$

Parallel connection of supercapacitor strings increases the capacitance according to

$$C_{\text{parallel}} = n_p C_{\text{series}} \quad (55)$$

Parallel connection decreases the equivalent series resistance based on

$$R_{\text{parallel}} = \frac{R_{\text{series}}}{n_p} \quad (56)$$

For modelling, behavior of the supercapacitor during charge and discharge are important factors. If the current and voltage behavior are deemed unsatisfactory for the application in a direct connection, then a DC-DC converter is needed. If the supercapacitor module characteristics seem to behave nicely from the application point of view, the connection to the STATCOM could be made without the use of converters which would cut down the costs and implementation complexity.

As was the case with batteries, SOC information is needed for monitoring and controlling the supercapacitor. For supercapacitors the SOC can be calculated in simplified cases as [27]

$$SOC = \frac{V_{sc}^2}{V_{sc,max}^2} \quad (57)$$

where V_{sc} is the supercapacitor voltage and $V_{sc,max}$ is the maximum voltage of a supercapacitor.

Coulombic counting method can also be used for supercapacitors. Compared to batteries, supercapacitor SOC is directly related to the terminal voltage, but self-discharge and pseudocapacitance effects can lead to a bias in the estimation. More sophisticated methods for SOC estimation include intelligent models and state-observers. SOH monitoring can be integrated by measuring capacitance, internal resistance and leakage current under different temperatures and voltages using a constant load. [97]

Also, the safety of the supercapacitor is important to include in modelling, so the model should have upper and lower bounds for the currents and voltages. For the maximum current, there are limits for the maximum peak current I_{max} for one second and so-called maximum carbon loading current $I_{max,CL}$ [58]. Current limitations can be depicted as

$$I_{max} = \frac{1}{2} \frac{u_c C_0}{C_0 R_{C_0} + 1} \quad (58)$$

$$I_{max,CL} = C_0 k_{CL} \quad (59)$$

where k_{CL} is carbon loading coefficient and gets a typical value of $70 \frac{mA}{F}$ but it can have values $100-500 \frac{mA}{F}$ under extreme loading.

Typically, the maximum and minimum values for currents and voltages are given in the datasheet, so the limits can be implemented as limiter block in Simulink models. It should be noted that datasheet values are usually conservative, so the values can be exceeded when optimizing the energy storage sizing.

Next, some typical electrical supercapacitor modelling techniques are discussed, and simulation results are presented. All simulation models use SCA3200 cell datasheet information offered by Skeleton Technologies. Basic cell information is presented in Table 6.

Table 6. *Supercapacitor cell information* [98]

Rated capacitance	3200 F
Rated voltage	2.85 V
10ms ESR (DC)	0.14 mΩ
1s ESR (DC)	0.18 mΩ
Energy	3.6 Wh
Specific energy	6.8 Wh/kg
Energy density	9.3 Wh/L
Power, 1s ESR	11.3 kW
Power density, 1s ESR	29 kW/L
Maximum peak current, 1s	2.89 kA

Based on the SCA3200 cells, Skeleton offers modules called SkelMod 102V88F that can be used as a reference design in energy storage sizing. The maximum one second current for 102 V, 88 F module is 2.69 kA which is very close to the individual cell 1 second maximum current.

An important parameter for some models is the factor k_c relating how supercapacitor voltage affects to the capacitance. Usually, datasheets do not have a value for k_c so in this thesis it was assumed to be $470 \frac{F}{V}$.

3.2.1 RC model

Classic equivalent circuit model, also known as RC model, is the simplest electrical model for a supercapacitor. The model presents the supercapacitor as a capacitor C_{sc} in series with resistance R_{sc} . In addition, a leakage resistance R_f can be added in parallel with the capacitor but for short duration simulations it can be neglected as the leakage resistance is much larger than the series resistance. Benefits of the RC model is that the implementation is very easy. All the values can be taken from manufacturers datasheet. [99] Circuit diagram and Simulink implementation of RC model is presented in Figure 40.

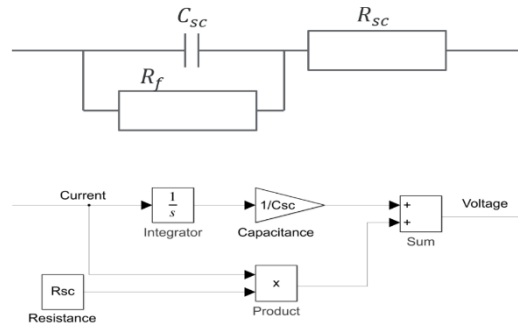


Figure 40. Supercapacitor RC model circuit diagram and Simulink implementation

An example simulation result can be seen in Figure 41 for one supercapacitor cell. Supercapacitor model was controlled by feeding a current shown in Figure 41. SOC of the model was calculated based on (57) and the simulated results are shown in Figure 42.

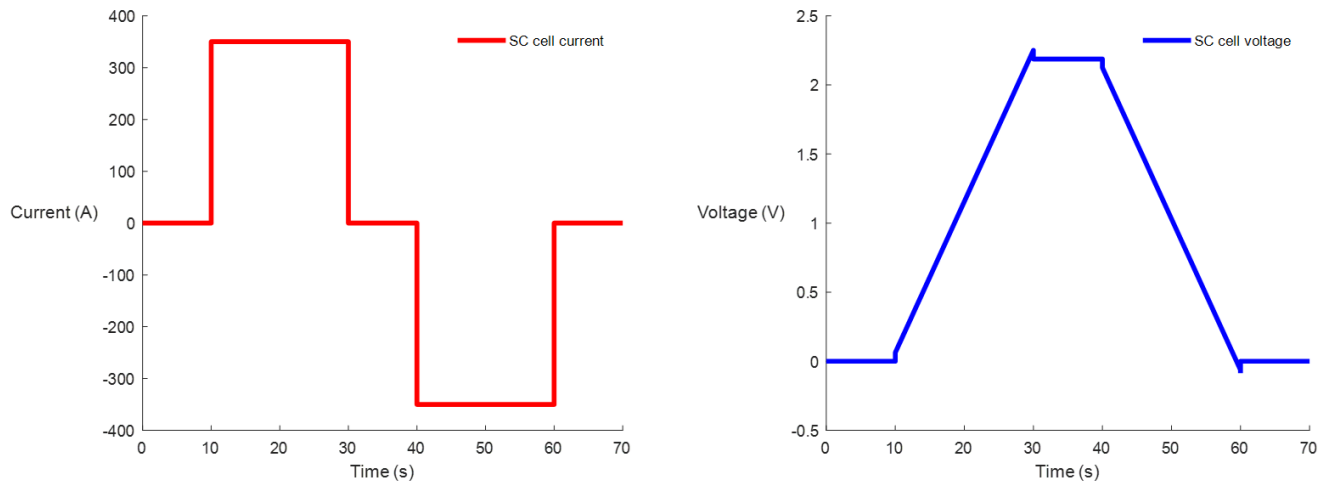


Figure 41. Simulated supercapacitor RC model current and voltage

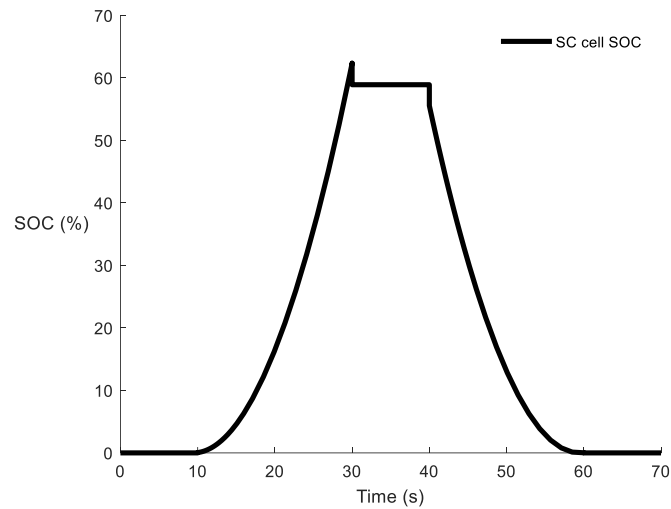


Figure 42. Simulated RC model SOC

From figure 41, the effect of series resistance can be seen as the initial voltage jump when current is applied and switched to negative value. The rate of change of voltage is dictated by the capacitance value. Because the model does not include any inductance, the voltage change is immediate according to the current. The voltage increase is strictly linear during charging and discharging which indicates that the model capacitance is not voltage dependent.

3.2.2 Simplified supercapacitor cell state-space model

For simulation purposes a state-space model is often used. State-space models use state variables to describe a complex system. The system consists of first-order differential equations or difference equations. The state variables are updated according to the measured input-output data. The basic state-space representation can be given as [100]

$$\dot{x}(t) = Ax(t) + Bu(t) \quad (60)$$

$$y(t) = Cx(t) + Du(t) \quad (61)$$

where $\dot{x}(t)$ is the change in the state variables, $y(t)$ is the output, A , B , C and D contain elements with physical significance and $u(t)$ is the input to the system.

Related to the supercapacitor modelling, equation for the change of capacitor voltage can be derived as [58]

$$\frac{du_c}{dt} = i_c \frac{1}{(C_0 + 2k_c u_c)} \quad (62)$$

where u_c is internal voltage of the supercapacitor as a state variable and i_c is the input.

The output equation is

$$u_{c0} = u_c + R_s i_{c0} \quad (63)$$

where u_{c0} is terminal voltage of the supercapacitor.

Based on (62) and (63) a block diagram shown in Figure 43 can be built in Simulink.

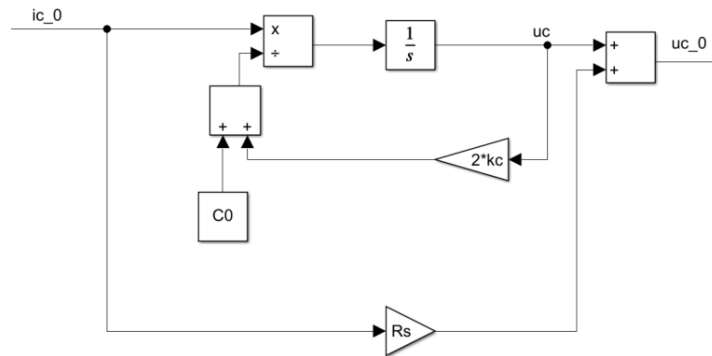


Figure 43. Large signal supercapacitor block diagram

For control system analysis a linear model can be derived that accurately describes the supercapacitor near a chosen operating point. The linearized model in Laplace domain is presented with equations

$$u_c(s) = \frac{(C_0 + 2k_c U_c)}{s(C_0 + 2k_c U_c)^2 + 2k_c I_{c0}} i_{c0}(s) = G_{c0}(s) i_{c0}(s) \quad (64)$$

$$u_{c0}(s) = u_c(s) + R_s i_{c0}(s) \quad (65)$$

A Simulink implementation of the block diagram is shown in Figure 44.

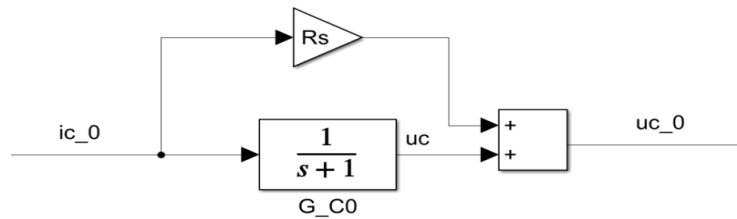


Figure 44. Small signal model of a supercapacitor cell [58]

In the state-space model, the frequency dependency of resistance and capacitance are neglected. For certain frequencies this assumption can cause major error. For example, a current with frequency of 100 Hz is seen as a high frequency signal that has a major effect on the capacitance and resistance. [58] The capacitance of the model consists of a constant capacitance at 0 V and has a value of 1860.5 F. At full voltage, the effect of voltage dependent capacitance increases the capacitance up to 3200 F.

Pros of the state-space model is that it is easy to implement in Simulink on a supercapacitor cell level and the model takes into account the voltage dependent capacitance with the factor k_c . Cons are that the frequency, temperature and voltage effects are not included in the model. Comparing the RC model and simplified state-space model, it is easy to see the similarity. Only difference comes from the voltage dependent capacitance. Because both models are easy to implement, the state-space model should be used if value for the k_c is known.

3.2.3 Simplified series model

In slow discharge application a simplified series model based on equation (16) can be used [95]. In [64] supercapacitors are modelled for power system dynamics studies and thus certain simplifications have been made. The detailed RC circuit of a supercapacitor is shown in Figure 45.

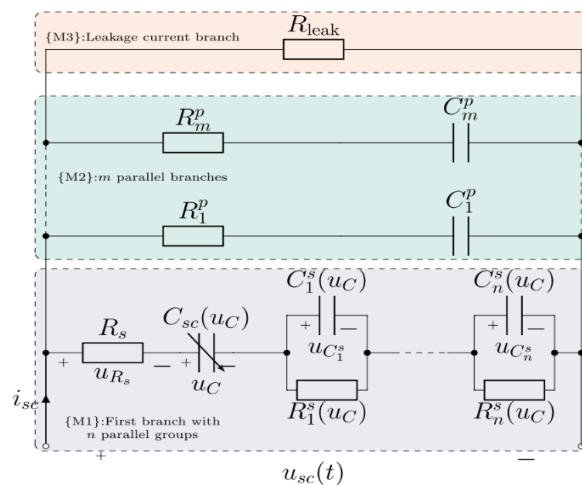


Figure 45. Simplified series model of a supercapacitor cell [64]

Most of the capacitance comes from C_{sc} and only five series connected groups of parallel connection of capacitances and resistances are needed. Also, the number of parallel branches shown

with M2, M3 and so on is limited to two or four as it has been shown that it is sufficient while in theory the number is infinite. Additionally, the equivalent series resistance is assumed to be voltage dependent and determined at high frequencies and the value for R_s is small. The temperature dependency of the cell is neglected because a properly sized cooling system is assumed.

The series connected branches have capacitances and resistances of [64]

$$C_k^s = \frac{1}{2} C_{sc}, k \in \{1 \dots n\} \quad (66)$$

$$R_k^s = \frac{2\tau(u_c)}{k^2 \pi^2 C_{sc}} \quad (67)$$

where $\tau(u_c) = \tau_0 + k_r u_c(t)$ and it can be approximated as $\tau(u_c) \approx 3C_{sc}(R_{dc} - R_s)$.

R_{dc} is a low frequency resistance that needs to be obtained experimentally. The benefit of the model presented in this section is that all of the parameters for the branch M1 in the Figure 45 can be obtained from the manufacturer datasheet. Branches M2 and M3 are related to time scales from several minutes to several weeks and more, so they can be neglected. [64]

As has been discussed, the supercapacitor bank consists of series and parallel connection of individual cells. Thus, the model for the whole bank of n_s series connections and n_p parallel connections is [64]

$$u_{sc}(t) = i_{sc}(t)R_s + u_c(t) + \sum_{k=1}^n u_{C_k^s} = y(t) \quad (68)$$

$$i_{sc}(t) = u(t) \quad (69)$$

$$u_{sc}^s(t) = n_s u_{sc}(t) = n_s y(t) \quad (70)$$

$$i_{sc}^m(t) = n_p i_{sc}(t) = n_p u(t) \quad (71)$$

$$\frac{du_c}{dt} = \frac{i_{sc}(t)}{C_0 + k_v u_c(t)} \quad (72)$$

$$\frac{du_{C_k^s}}{dt} = -\frac{u_{C_k^s}}{R_k^s C_k^s} + \frac{i_{sc}(t)}{C_k^s} \quad (73)$$

where $y(t)$ is bank output and $u(t)$ is bank input.

According to [64], for a 100 MW bank up to 100000 supercapacitor cells are needed. To simulate the nonlinear model depicted by (68) – (73), a model shown in Figure 46 can be created [64]. In the Figure 46, the gain $k_v = k_c$.

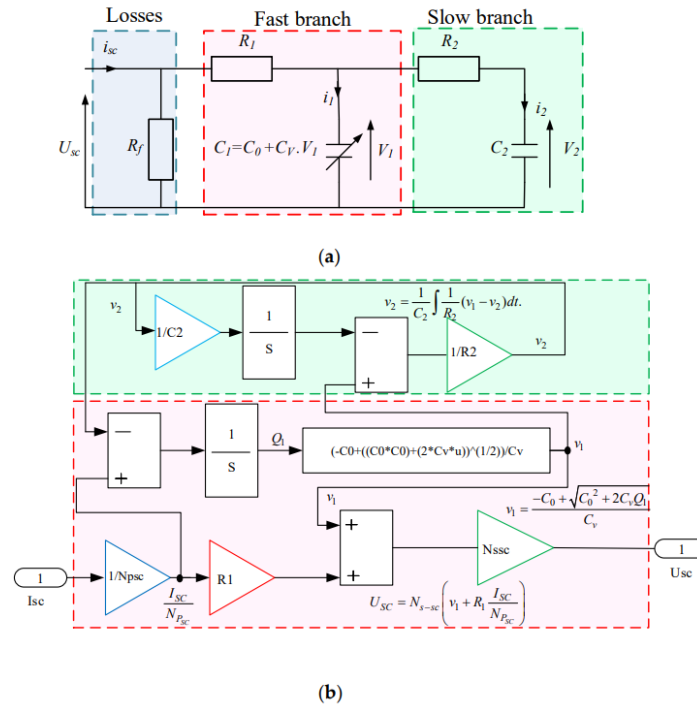


Figure 47. Faranda equivalent circuit a) and Simulink model b) [102]

Based on comparison conducted in [94] Zubieta model is the best options for simple and basic supercapacitor modelling. MathWorks also provides a ready-made Zubieta model for simulation. Supercapacitor bank can be easily simulated by introducing the number of series and parallel connections to the gain-blocks shown in Figure 47. Advantages of Zubieta and Faranda model include quite good accuracy and ease of simulation model implementation. Clear disadvantage is the need for parameter estimation from discharge tests.

3.2.5 Parallel model

Parallel model consists of many parallel branches where each parallel branch has a series connected variable resistor and capacitor. Implementation of a typical parallel model requires many measurements to identify the model parameters and is thus laborious. Maxwell Technologies has presented an implementation where the parameters can be derived based on datasheet information. In Maxwell model, there are three parallel branches and leakage resistance. For Maxwell model the parameters can be calculated based on Table 7. An example implementation in Simulink is showed in Figure 48.

Table 7. Supercapacitor scaling model [104]

R_1	$\frac{2}{3^p} ESR$	R_2	$\frac{2}{3} \phi^{-(2k-1)} ESR$	R_3	$\frac{2}{3} \phi^{-(2k+1)} ESR$	R_l	$\frac{V_r}{I_{leak}}$
C_1	$1.05 C_0$	C_2	$1.05 \phi^{+(2j+1)} C_0$	C_3	$1.05 \phi^{+(2j-1)} C_0$		
τ_1	$\frac{2.1}{3} C_0 ESR$	τ_2	$\frac{2.1}{3} \phi^{+2(1+j-k)} C_0 ESR$	τ_3	$\frac{2.1}{3} \phi^{+2(1+j-k)} C_0 ESR$		
ϕ	$\frac{1}{2}(\sqrt{5} - 1)$	$j = 2$	$k = 8$				

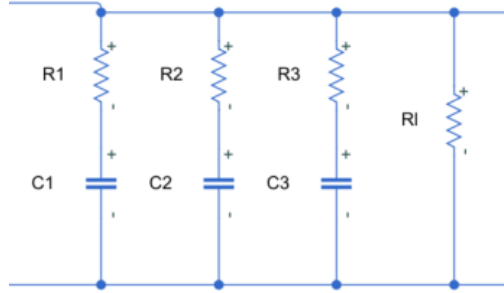


Figure 48. Simulink implementation of parallel model

In this thesis parallel model simulations are presented for comparison against other supercapacitor models but due to the lack of actual parameter estimation the model is not used in simulations with STATCOM.

3.2.6 Stern-Tafel model

Supercapacitor with non-linear capacitance can be modelled using Stern-Tafel model that is classified as an electrochemical model. Dynamics of a supercapacitor are taken into account by introducing double layer capacitance, Helmholtz's capacitance and Gouy-Chapman's capacitance depicted with following equations [94]

$$C_T = \frac{N_p}{N_s} \left(\frac{1}{C_H} + \frac{1}{C_{GC}} \right)^{-1} \quad (74)$$

$$C_H = \frac{N_e \epsilon \epsilon_0 A_i}{d} \quad (75)$$

$$C_{GC} = \frac{F Q_T}{2 N_e R T} \sinh \left(\frac{Q_T}{N_e^2 A_i \sqrt{8 R T \epsilon \epsilon_0 c}} \right) \quad (76)$$

where N_p is the number of parallel cells, N_s is the number of series connected cells, C_T is double layer capacitance, C_H is Helmholtz's capacitance, C_{GC} is Gouy-Chapman's capacitance, N_e is the number of electrode layers, ϵ is relative permittivity of electrolyte material $\frac{F}{m}$, ϵ_0 is free permittivity of space $\frac{F}{m}$, F is Faradays constant $\frac{C}{mol}$ c is the molar concentration in $\frac{mol}{m^3}$, d is molecular radius

in m^2 , T is operational temperature in K , A_i is interfacial area between electrode and electrolyte in m^2 , R is ideal gas constant in $\frac{J}{molK}$.

The rest of the model consists of a controlled voltage source, internal resistance and self-discharge current. Self-discharge current can be modelled with equation [94]

$$i_{self_dis} = N_e I_f e^{\left(\frac{\alpha F \left(\frac{V_{init}}{N_s} - \frac{V_{max}}{N_s} \right) - \Delta V}{RT} \right)} \quad (77)$$

where I_f is leakage current, α is charge transfer coefficient, V_{init} is initial voltage, V_{max} is maximum voltage and ΔV is over-potential.

For Simulink simulations, there is a ready-made supercapacitor model that is easily scalable according to the number of series and parallel connected cells. Figure 49 shows the equivalent circuit of the supercapacitor model. As was the case with Simulink battery model, also the supercapacitor is implemented as a controllable voltage source.

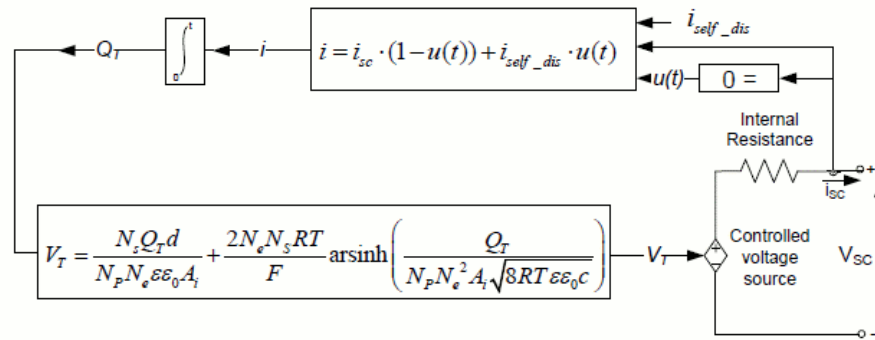


Figure 49. Simulink supercapacitor model based on controllable voltage source [105]

Supercapacitor voltage is modelled according to Stern equation. Stern equation for output voltage is

$$V_{sc} = \frac{N_s Q_T d}{N_p N_e \epsilon \epsilon_0 A_i} + \frac{2 N_e N_s R T}{F} \sinh^{-1} \left(\frac{Q_T}{N_p N_e^2 A_i \sqrt{8 R T \epsilon \epsilon_0 C}} \right) - R_{sc} i_{sc} \quad (78)$$

where $Q_T = \int i_{sc} dt$.

The Simulink model assumes a constant internal resistance and continuous current, it does not model temperature effects, aging or cell balancing and the charge distribution is constant for all voltage values. Advantage of Stern-Tafel model is that there is a ready-made simulation model that can be easily scaled to a supercapacitor bank configuration.

3.2.7 Comparing supercapacitor model results

The chosen models for comparison were basic RC model, state-space model, Zubieta model offered ready-made by Mathworks (MW), simplified Zubieta model constructed from elementary

blocks, detailed RC model, parallel model and Stern-Tafel model offered by MW. Voltage simulation results for different models are shown in Figure 50. The models were fed the same current shown in Figure 51. It should be noted that the models used only one cell and the initial voltage was chosen to be zero. The figures show that most of the models agree well with each other. Only the basic RC-model has significant deviation from the other models. Detailed RC model produces voltages that are significantly lower compared to other models.

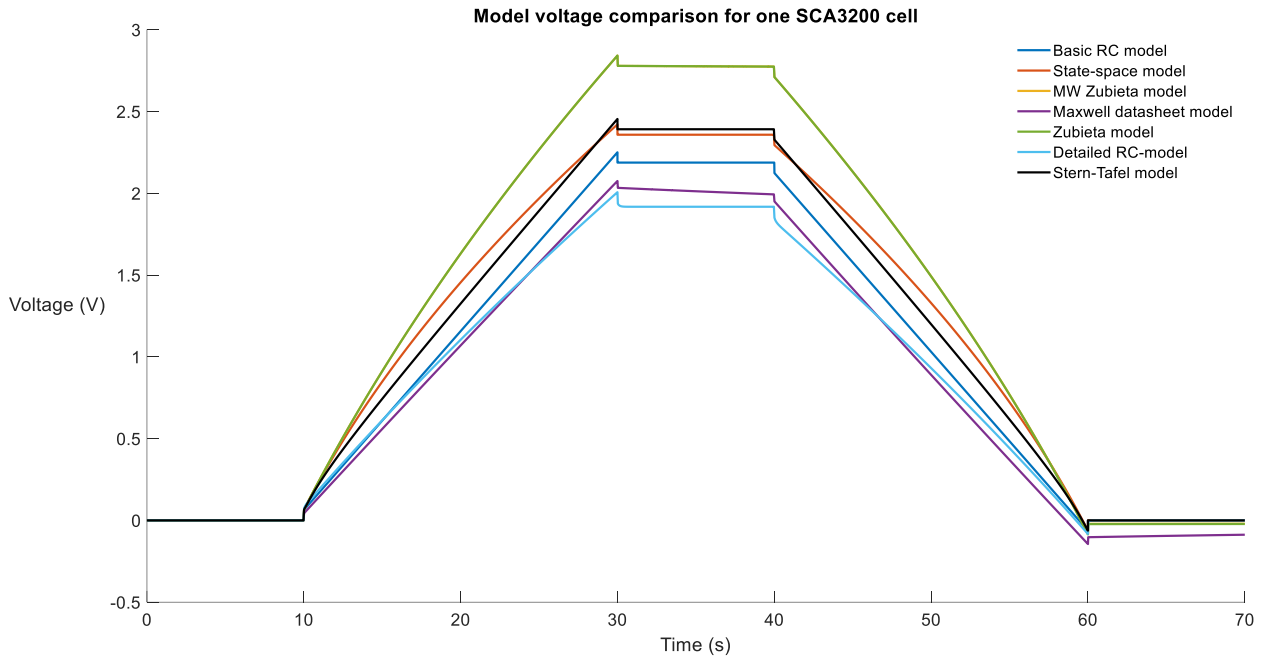


Figure 50. Supercapacitor model simulation results

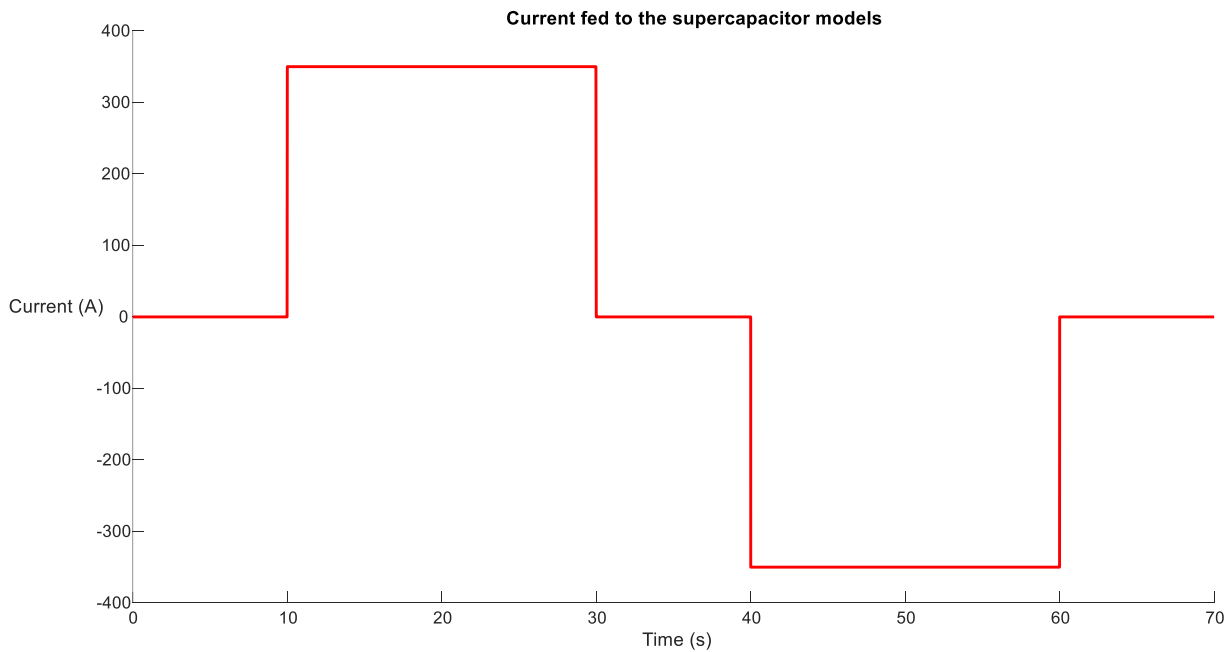


Figure 51. Injected supercapacitor current

Building a module from the cells is important and for that reason a simulation where there are 1000 cells in series and 10 strings in parallel were simulated. Results are shown in Figure 52. Based on Figure 52, it is clear to see that the detailed RC model produces wrong results compared to other models. For this reason, the model is not used in later simulations. The effect of voltage dependent capacitance can clearly be seen as the models that take it into account reach much higher voltages as the capacitance is smaller. For this reason, knowing realistic values for the voltage dependent capacitance is crucial as it clearly has significant effect on large supercapacitor systems. The two Zubieta models produce the same voltage behavior.

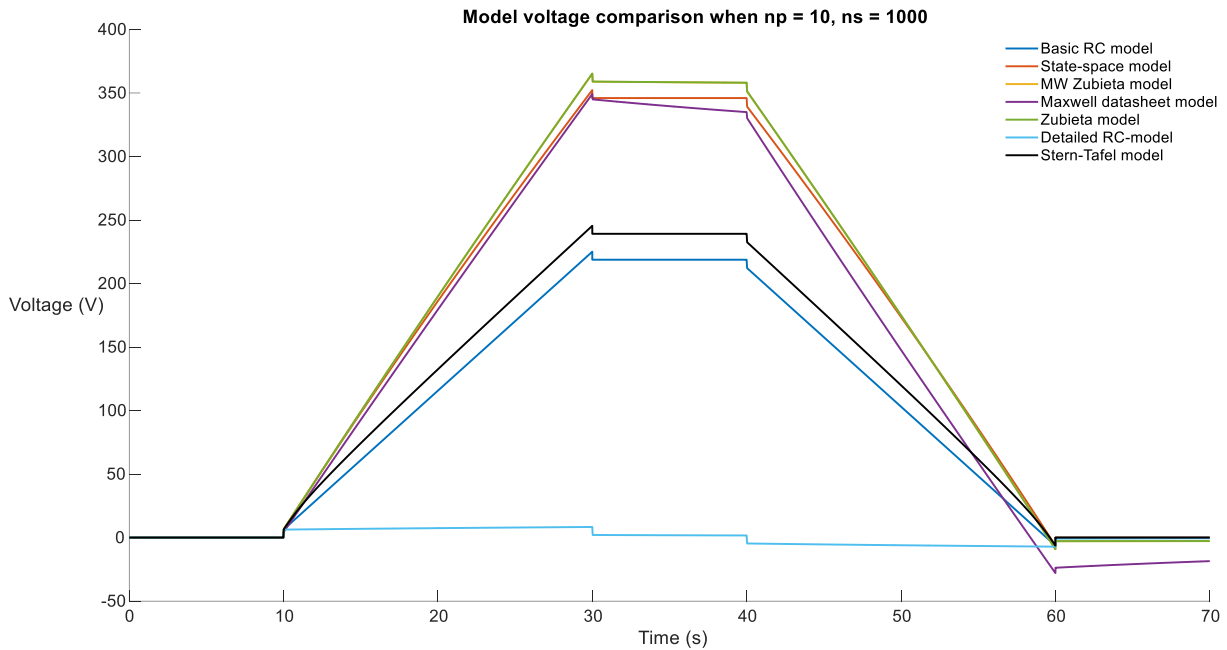


Figure 52. Supercapacitor module simulation

In the previous simulations an initial voltage of zero volts was assumed. However usually the supercapacitor will not be discharged completely empty so the simulation should have an initial voltage level. In Figure 53 simulation results based on initial voltage 1.5 V are shown. It can be seen that the cell voltage exceeds the rated voltage, but it is expected as the used current remained the same as in Figure 51. The Maxwell datasheet produces significantly larger voltages than the other models, so it is not used for further analysis.

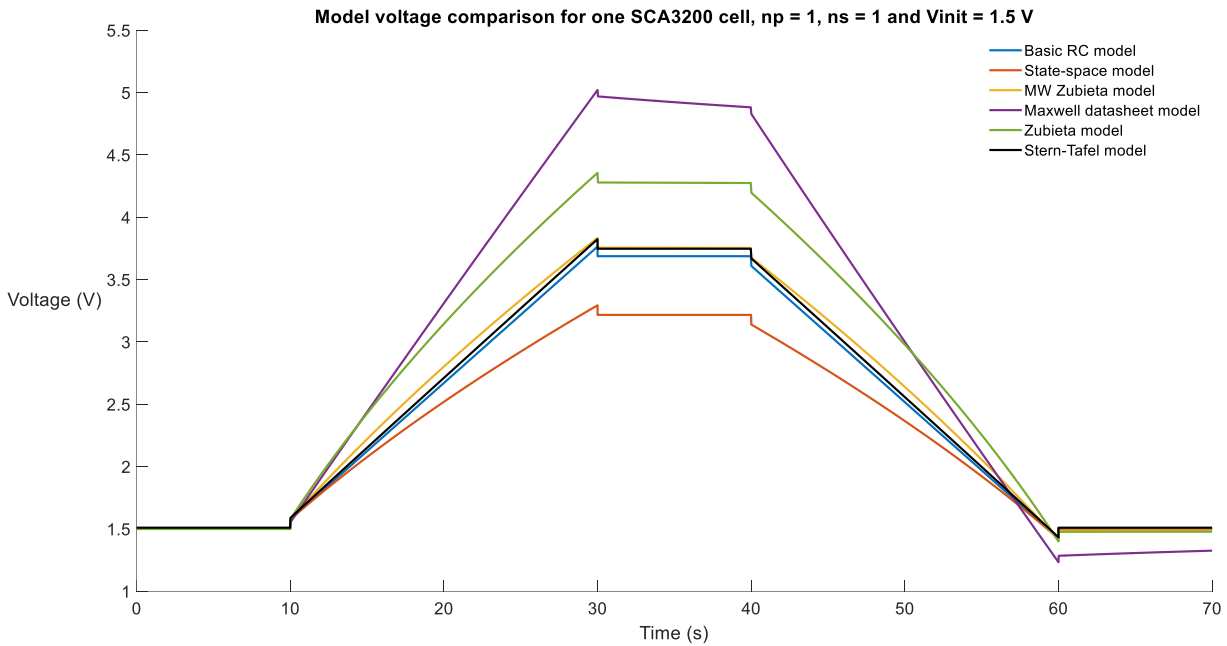


Figure 53. Supercapacitor simulations with initial voltage of 1.5 V

An important simulation case consists of constant power discharge as the requirement for STAT-COM included a demand of 100 MW for 1.25 seconds and 200 MW for 0.5 seconds. Based on simulation results, the constant power simulations can have significant stability problems. Supercapacitor maximum power is limited by its internal series resistance. Maximum deliverable power is given by (20). If the load power is higher than the maximum power provided by supercapacitor at a specific voltage, simulation will lead to an unstable situation and the voltage collapses [58]. To avoid instability, enough series and parallel connections should be used. Constant power discharge results are shown in Figure 54.

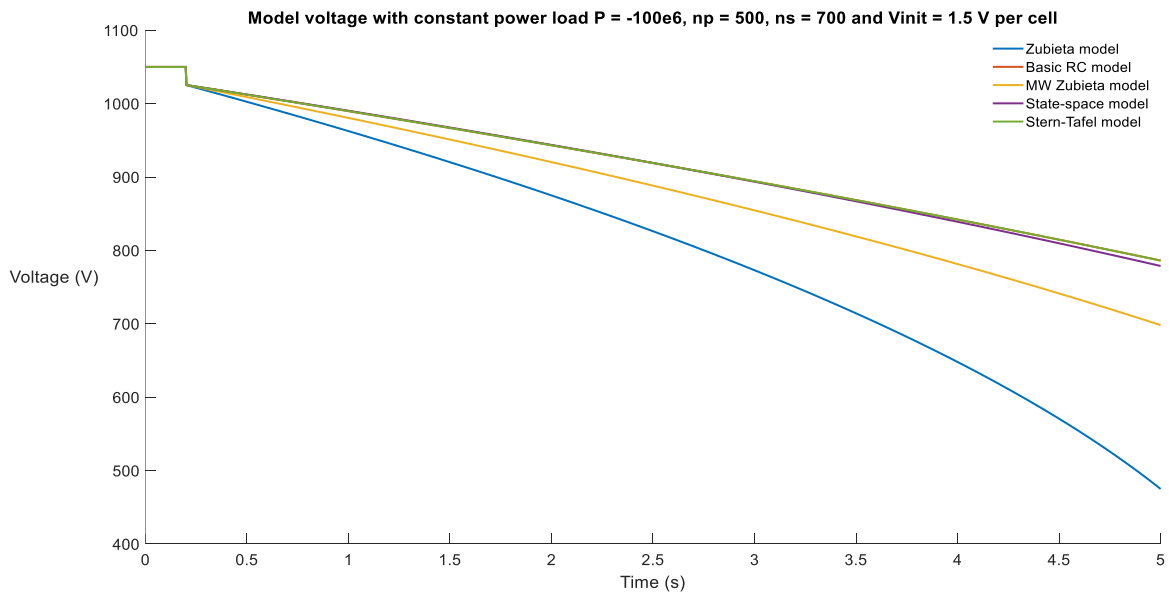


Figure 54. Constant power discharge simulation

Based on Figure 54, Zubieta, state-space, Stern-Tafel and simple RC models should be used in the final STATCOM simulations based on their similar results in all tests and fast simulation time. Especially the state-space and Zubieta models are used as they can address the voltage dependent capacitance. For future RTDS implementations, one should also think about the complexity of implementation and possible computational delays caused by the supercapacitor model simulation. The chosen simulation models are deemed to be simple, so the computational delay should not be too great.

As was discussed, the models used in this thesis do not accurately model the frequency behavior of a physical supercapacitor. If more detailed models are needed, then EIS measurements should be conducted. The EIS equivalent circuit models for supercapacitors are very complex as they can have up to 14 parameters, so also the parameter identification will be burdensome and time consuming [106]. When supercapacitors and batteries are purchased for the grid-forming STATCOM project more detailed frequency models can be constructed if it is deemed necessary. In the simulations of Chapter 3.2 inductance of the supercapacitors, connections as well as the additional connection resistances were neglected. In the STATCOM simulations some estimate for these values should be given to have more realistic simulation results.

Frequency behavior of the supercapacitor model impedance was studied using sinusoidal current excitation signals with different frequencies. The resulting voltage was measured and based on the fast Fourier transform the frequency response was calculated. The implemented models only consisted of resistors and capacitors so the expected behavior is that in high frequencies the capacitance should decrease so that the model resembles only a resistor. For the Bode-plots only one cell was used, and the initial voltage was chosen to be 0 V. Excitation signal consisted of only an AC-component and the amplitude was chosen to be 350 A. Perturbation frequencies consisted of 21 frequencies between 0.1 – 1000 Hz. The Bode-plots are shown in Figure 55. Note that all of the Zubieta-models produced the same Bode-plot so only one of them is visible. With the Maxwell model there is a significant deviation in the magnitude on high frequencies when compared

to the other models. Based on the phase, the supercapacitor models have only resistance at high frequencies as was expected.

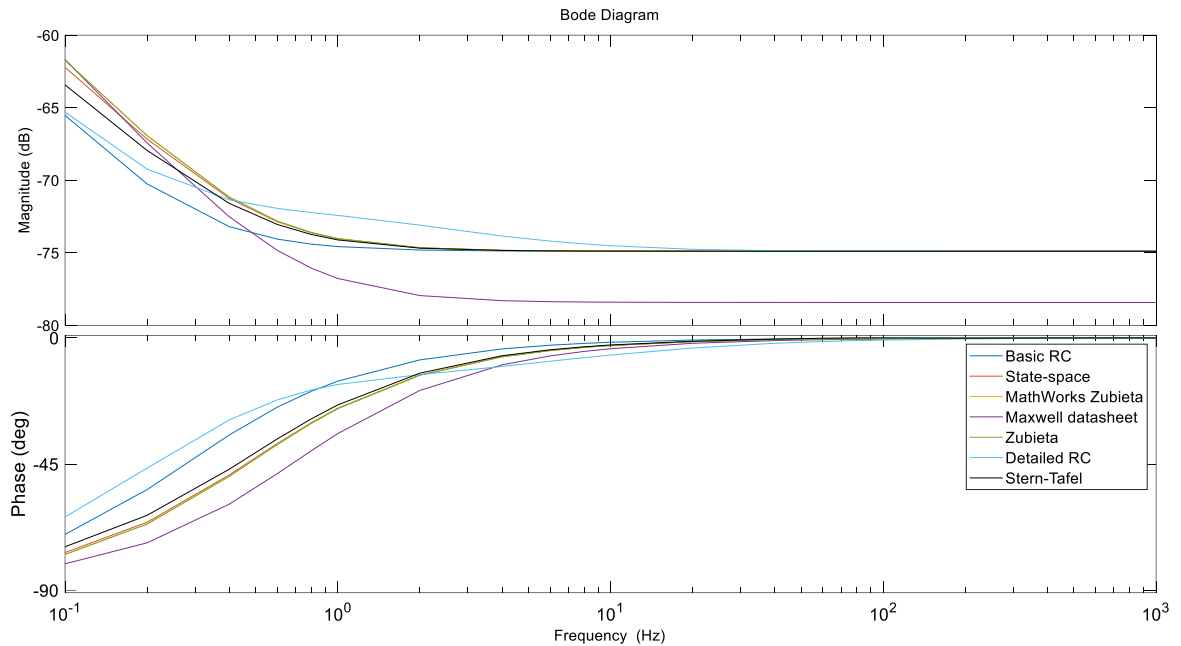


Figure 55. Supercapacitor model Bode-plots. Excitation amplitude 350 A and initial voltage 0 V

Many of the used supercapacitor models have voltage dependent capacitance, so to test if that has any effect on the frequency response, an excitation signal with amplitude of 1 A and 350 A was tested together with different initial voltages. With larger excitation current amplitude, the effect on the voltage should be greater than with small amplitude excitation signals and thus the voltage dependent capacitance could show significant difference in the results. Results are shown in Figures 56-58.

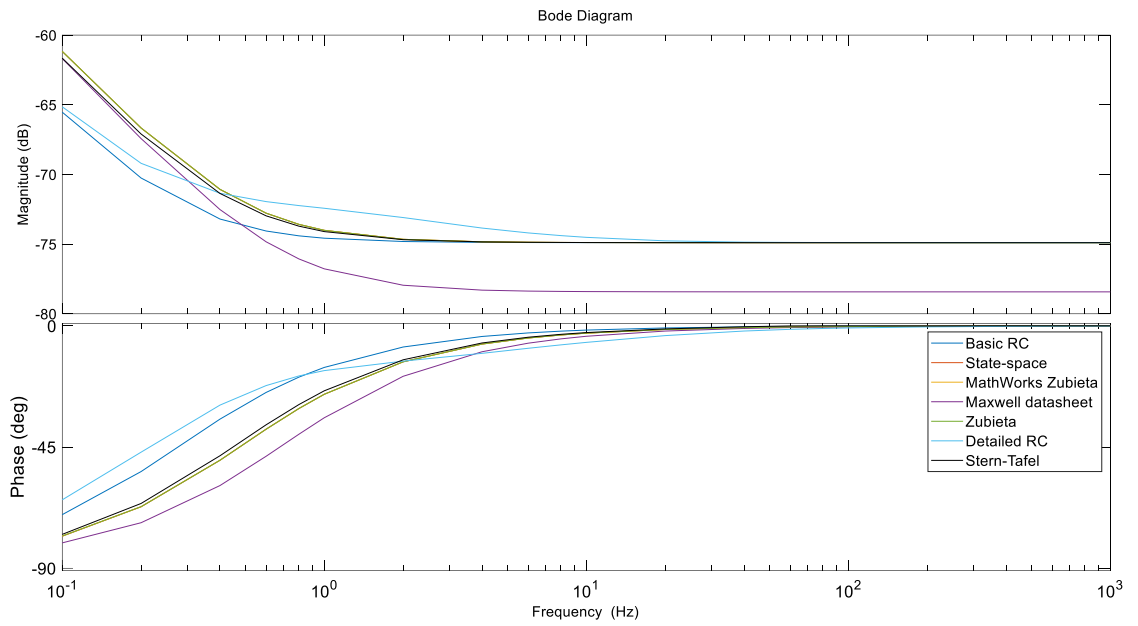


Figure 56. Bode-plot when excitation signal amplitude is 1 A and initial voltage is 0 V

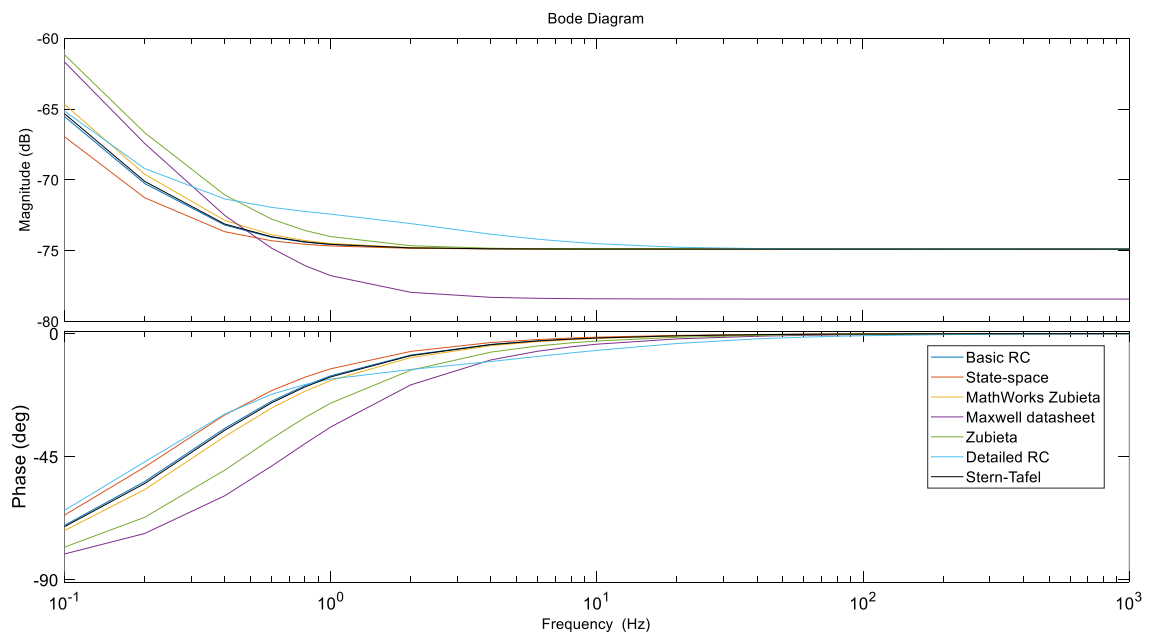


Figure 57. Bode-plot when excitation signal amplitude is 1 A and initial voltage 2.13 V

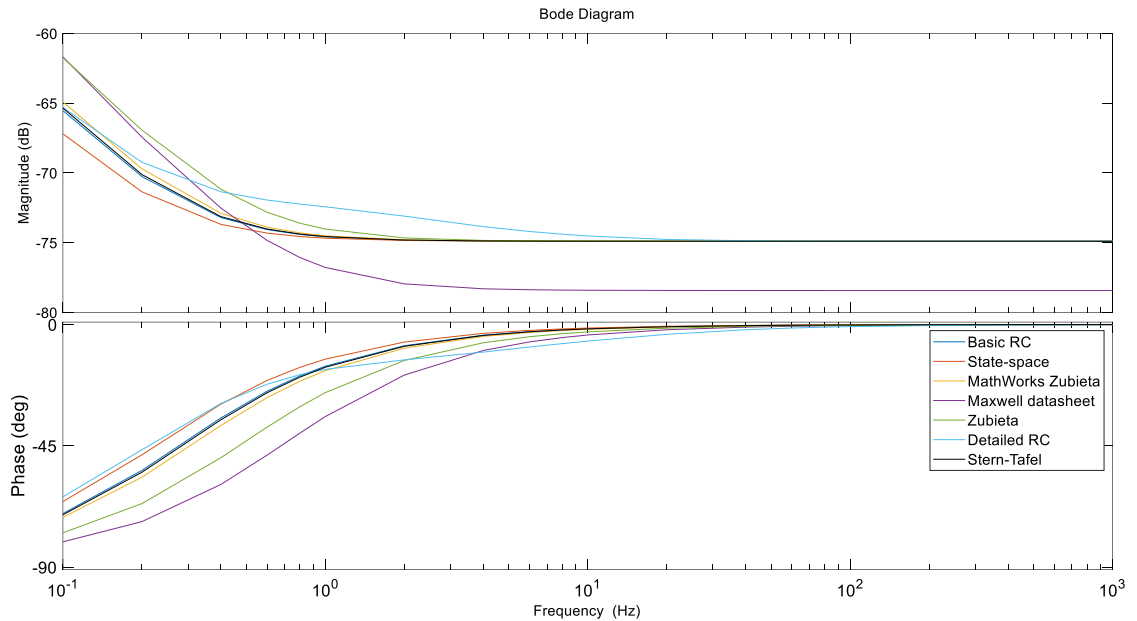


Figure 58. Bode-plot when excitation signal amplitude is 350 A and initial voltage 2.13 V

As can be seen from Figures 55-58, the excitation signal amplitude does not seem to have noticeable effect. However, the initial voltage seems to have significant effect on the impedance. More precise comparison for MW Zubieta model is shown in Figure 59. The same analysis holds true. A comparison can be made to the measurements of a 3000 F 3 V cell shown in Appendix D. Initial voltage of the measured supercapacitor cell was 0.7 V and the excitation amplitude of sine sweep was 20 A. The difference compared to supercapacitor simulation models is that after 100 Hz, the supercapacitor starts to behave as an inductor. The behavior is seen from the phase of the impedance as it starts to increase close to 90 degrees. Based on the frequency response analysis, the supercapacitor should not be used in high frequency AC applications as the capacitive behavior of supercapacitors diminishes at high frequencies.

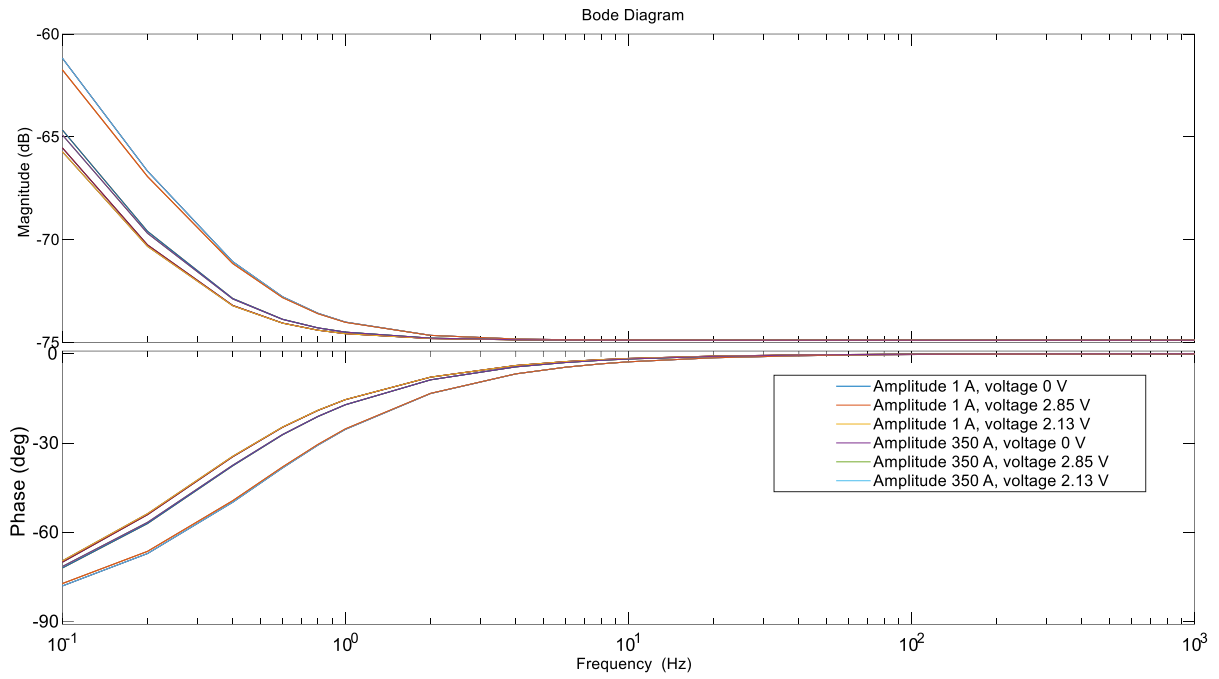


Figure 59. *MathWorks Zubieta model Bode-plot with different excitation signal amplitudes and initial supercapacitor voltages*

4. STATCOM SIMULATIONS

The supercapacitor and Li-ion battery model are added to a simplified STATCOM Simulink model for simulations. In this thesis the STATCOM is fitted with one energy storage option at a time while in reality, based on economic studies and possible requirements for longer discharge times, a hybrid solution might be more optimal. It is assumed that the temperature of the energy storage hall can be kept close to room temperature in order to guarantee long lifetime and nominal performance.

4.1 STATCOM models

Three STATCOM simulation models are used for different purposes. The first simulation model represents a single submodule without switching dynamics. The submodule energy storage is sized based on 0.83 MW of power requirement per submodule while respecting the maximum discharge current of around 2.5 kA for supercapacitors and 260 A for the LTO battery. 0.83 MW is calculated based on 100 MW active power that is distributed evenly to 120 submodules. Discharge time of 1.25 seconds is assumed. In a physical STATCOM there would be many submodules in series that could have an effect on the voltage balance and voltage ripple of the submodules. Still, the simplified model gives an idea how the voltage and current behave in an ideal case so that approximate sizing and cost estimations can be done. The simulation model uses three ideal voltage sources as the converter to generate the active and reactive power to the network. Based on the injected or absorbed active power and the energy storage voltage, a current can be calculated that is then injected to the energy storage thus affecting the internal voltage of the storage. The control structure of the model consists of cascaded reactive and active power controllers, voltage controller and current controllers. The model can be used for grid-forming control situations. A simplified block diagram of the model is shown in Figure 60.

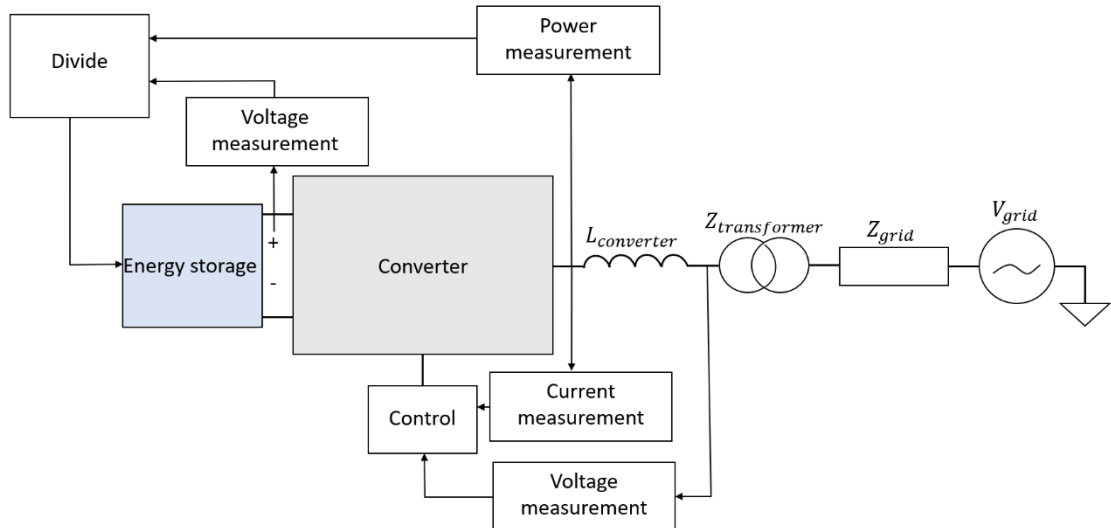


Figure 60. Submodule model structure

The second model considers a common DC-link implementation based on a double-star topology using a common DC-link storage as shown in Figure 61. The STATCOM valves are modelled with ideal voltage sources that have a voltage according to the control. DC-link voltage is measured from the energy storage. In this simulation case the model is sized based on 100 MW for 1.25 seconds requirement. In the simulations 60 kV DC-link voltage was used in order to avoid large valve currents. The control is based on grid-following structure.

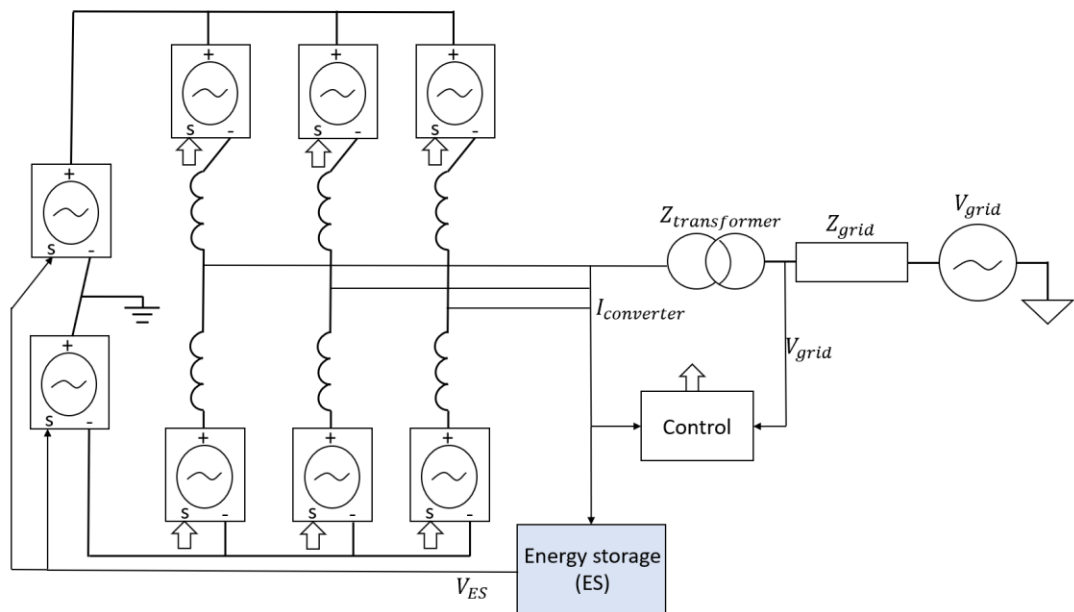


Figure 61. Common DC-link model structure

The third model takes into account the switching behavior for the submodule implementation. Using the model, it is investigated whether the replacement of a traditional submodule capacitor with a supercapacitor stack has any effect on the operation of the model. With this model only reactive power was controlled.

As was discussed, the simulations are not realistic as they do not consider any DC-DC converters, realistic DC-link voltage control or in the two first cases the switching behavior. Still, the objective of the simulations is to find out how the voltage and current of the energy storages behave which can be done using simplified simulation models.

4.2 Energy storage sizing

Energy storage sizing for the different simulation models is crucial. The sizing is done based on BOL conditions but modified accordingly if the EOL simulations do not fulfil the requirements.

4.2.1 Submodule energy storage sizing

It is decided that the STATCOM has 40 submodules per phase leg. This means that the total maximum power of 200 MW and nominal power of 100 MW would be divided between 120 submodules. For this reason, on average one submodule should be able to produce 1.7 MW of power for 0.5 seconds and 0.83 MW of power for 1.25 seconds. The following sizing and simulation results are designed based on the 0.83 MW requirement per submodule, but the same principles also apply for higher power requirements. With large power requirements, there needs to be a cost comparison between upgrading one STATCOM to be able to meet the high-power requirements against building two STATCOMs with lower ratings.

The energy storage should be able to inject and absorb the same amount of power and thus the initial voltage of the supercapacitors and batteries needs to be chosen carefully. Submodule maximum voltage is chosen to be 2000 V while the nominal voltage is chosen to be 1600 V. In the submodule implementation the voltage is allowed to decrease down to 1 kV. This means that the useful voltage range of the supercapacitor is between 1-2 kV. Based on (17), the energy balance can be used to solve for the capacitance. Maximum energy is calculated based on 100 MW for 1.25 s which gives

$$E_{tot} = P_{nom}t = 100 \text{ MW} \cdot 1.25\text{s} = 125 \text{ MJ} \quad (79)$$

For one submodule supercapacitor, the energy requirement is thus 1.04 MJ. The required capacitance is

$$C_{SM} = \frac{2E_{SM}}{(V_{max}-V_{min})^2} = 2.08 \text{ F} \quad (80)$$

where $V_{max} = 2000 \text{ V}$, $V_{min} = 1000 \text{ V}$ and $E_{SM} = 1.04 \text{ MJ}$.

Maximum current based on the active power from the submodule energy storage is written as

$$I_{SM,max} = \frac{P_{nom}}{V_{min}} = \frac{0.83 \text{ MW}}{1 \text{ kV}} = 830 \text{ A} \quad (81)$$

Minimum current is given by

$$I_{SM,min} = \frac{P_{nom}}{V_{max}} = \frac{0.83 \text{ MW}}{2 \text{ kV}} = 415 \text{ A} \quad (82)$$

It should be noted that the maximum current for active power generation needs to be summed on top of the current required for reactive power injection. Thus, the active power current could increase the ratings of the IGBT switches. It is assumed that the submodule converter can tolerate the added current.

Based on the maximum one second current rating of a SkelMod 102V88F module, the minimum supercapacitor voltage can be calculated as

$$V_{SC,min} = \frac{0.83 \text{ MW}}{2.69 \text{ kA}} = 308.6 \text{ V} \quad (83)$$

Using Skeleton modules as the basic building blocks, the nominal submodule voltage requires 21 series connected modules, where one module has 36 cells in series each with an initial voltage of 2.13 V. This would mean that the overall capacitance would be 4.2 F as one module has 88 F capacitance rating. Minimum energy of the supercapacitor storage is

$$E_{SC,min} = \frac{1}{2} \left(\frac{C_{sc}}{n_s} \right) V_{SC,min}^2 = 0.2 \text{ MJ} \quad (84)$$

where $C_{sc} = 88 \text{ F}$ and $n_s = 21$.

Thus, the nominal energy capacity of one submodule supercapacitor needs to be more than the sum of required energy of the submodule during injection and the minimum storage energy. If a DC-DC converter can be used, then the number of series connected modules could be significantly reduced as the number of series connected modules can be calculated from

$$E_{SC,nom} = \frac{1}{2} \left(\frac{C_{sc}}{n_s} \right) (n_s V_{SC,nom})^2 \geq \frac{1}{2} \left(\frac{C_{sc}}{n_s} \right) V_{SC,min}^2 + E_{SM} \quad (85)$$

where $E_{SM} = 0.83 \text{ MW} \cdot 1.25 \text{ s} = 1.0 \text{ MJ}$ is the submodule energy.

If the module initial voltage is 100 V, the number of supercapacitor modules in series is 4. If the submodule initial voltage is decreased down to 87 V to allow for injection and absorption of active power, the required number of series connected modules is 6. This means that the required number of series connected modules is much less than compared to the situation where DC-DC converters are not used. The rest of this thesis focuses on the simulation results without the use of DC-DC converters, so the number of supercapacitor modules in series is large.

Using the sizing without DC-DC converters means that 21 modules are connected in series. The series connected modules create enough capacitance and no parallel connected strings of modules are needed based on the calculations. However, based on simulations in Section 4.3 the self-made Zubieta model voltage drops below the low voltage limit, so the number of parallel strings is increased to two with EOL conditions. This means that without DC-DC converter, 1512 supercapacitor cells are needed with EOL conditions and 756 for BOL conditions.

For a 13 Ah battery with maximum C-rate of 20, the maximum current is 260 A. Based on the ratings, 3 parallel connections are needed to reduce the maximum submodule current to an appropriate level. 720 series connected battery cells with initial SOC of 50 % are needed to reach voltage of 1600 V and to allow for symmetrical capability for energy absorption and injection. For

one submodule, total of 2160 cells are needed. Sizing was tested using simulations where a constant power was fed to the energy storage and based on the energy storage voltage, a current was calculated that was served as the energy storage input. Simulation results are shown in Figure 62 where the energy storages were first discharged with power of 0.83 MW for 1.25 seconds, then rested for 0.5 seconds, charged for 1.25 seconds with power of 0.83 MW, rested for 0.5 seconds and again charged with the power of 0.83 MW for 1.25 seconds. Thus, the simulations show that with the designed sizing, all of the energy storage voltages are able to stay within the specified limits while being able to absorb and inject the required power. Beginning of life conditions were assumed in the simulation.

In the simulations of Figure 63, the initial voltage of the supercapacitors was 2.13 V and the initial SOC of the battery model was 50 %. EOL simulations were also tested, and it was noted that the number of parallel battery strings needs to be increased to 4 and the number of parallel supercapacitors strings to two in order to fulfil the voltage and current requirements. From figures 62 and 63 it is clear to see the difference between the equivalent series resistance of batteries and supercapacitors as the battery resistance is much larger and thus causes a large voltage drop at the start of discharge. Depending on the supercapacitor model, the voltage change during discharge has significantly different behavior. With self-made Zubieta model, the voltage decreases the fastest while with state-space model the voltage only decreases around 100 V. Because of the difference between the models, the sizing should be done based on the worst-case model which in this case is the self-made Zubieta model.

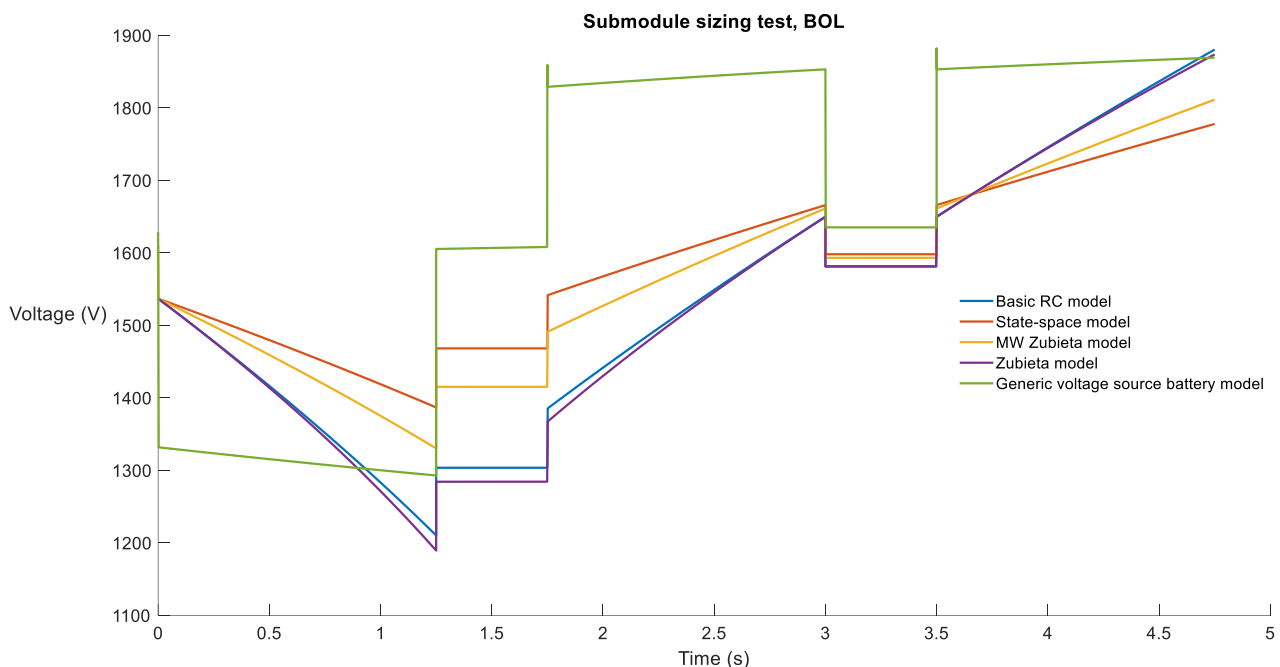


Figure 62. Constant power test for energy storage models with BOL conditions

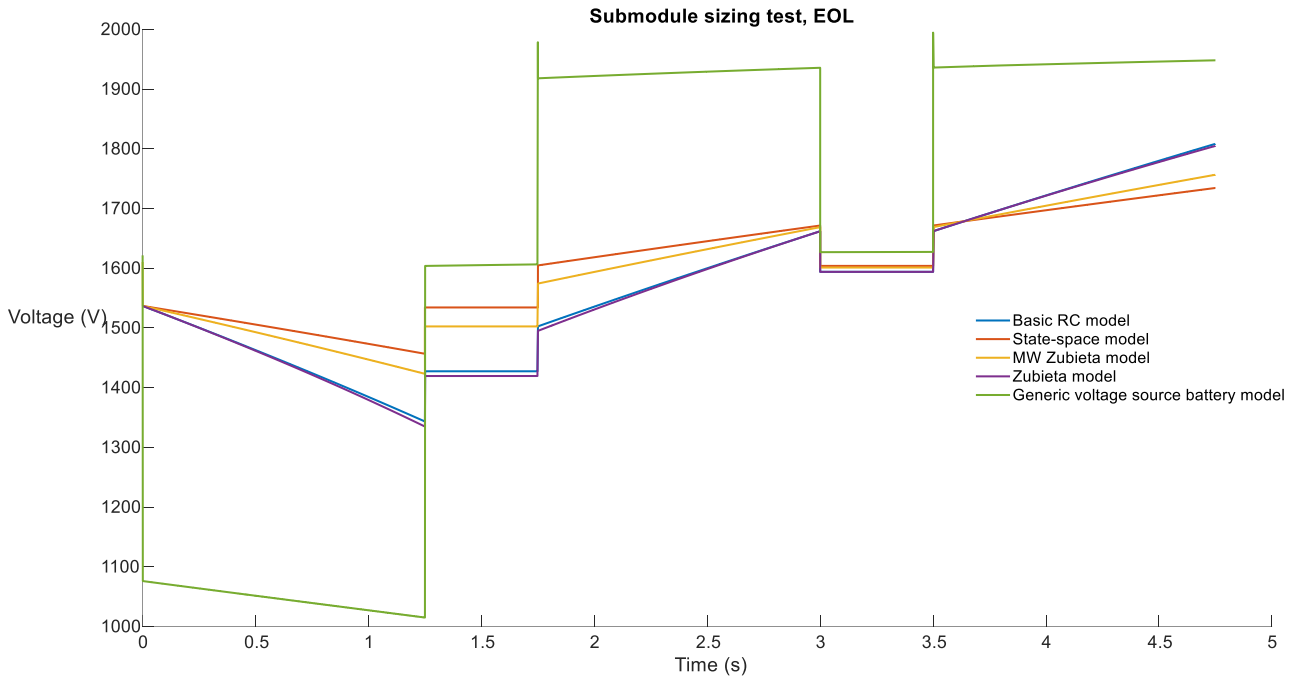


Figure 63. Constant power test for energy storage models with EOL conditions

Simple cost estimation can be done using freely available price data. If minimum order quantity is over 1000 cells, the LTO battery cell price is 8.23 € [107]. Similarly, SCA3200 cells cost around 54 € if at least of 100 cells are ordered. Based on the number of required series and parallel connected cells the energy storage cost is estimated on Table 8. It should be noted that purchasing large quantities directly from the manufacturer could allow for greatly reduced prices. Also, cost of installation, cooling, measurement devices etc. is not estimated. In practical installation redundancy should be assured so the actual cost could be much higher. If a DC-DC converter would be used, the supercapacitor cost for the whole system would be 1.45 million € because only 216 supercapacitor cells per submodule would be needed. However, purchasing or developing converters with appropriate ratings would introduce additional costs.

Table 8. Submodule implementation cost

Product	Price per cell (€/cell)	Number of cells, BOL	Cost per submodule (€)	Cost for 120 submodules (€)	Cost for 120 submodules, EOL (€)
3200 F supercapacitor cell	56	756	42.34 thousand	5.08 million	10.16 million
LTO Li-ion battery cell	8.23	2160	17.78 thousand	2.13 million	2.84 million

4.2.2 Common DC-link energy storage sizing

As has been discussed, the submodule implementation has significant downsides. Based on Figure 63, if a DC-DC converter is not used, during discharge the voltage will decrease down to 1000 V which means that there needs to be reserve submodules that are connected to compensate for the decreased voltage unless multiple parallel battery strings are used to decrease the difference between minimum and maximum voltages. With supercapacitors, the effect of voltage change does not have as significant effects but on the other hand the price is much higher.

To increase the safety of the STATCOM valves and decrease the overall complexity of the system, a common DC-link implementation should be considered. Double-star topology with a common DC-link is one potential topology as the topology allows the use of the already existing submodules without major modifications, allows for easy temperature control of the energy storage and produces the requested active power only from the common DC-link so the submodule control is simpler. Drawback of the common DC-link implementation is that the supercapacitors and batteries are not designed for such high voltages which would be requested in the common DC-link implementation. Usual maximum supercapacitor and battery module voltage ratings to ground are in the range from 1-3 kV and the common DC-link would in the worst-case have to be up to 75 kV. One beneficial characteristic of double-star topology with full-bridge submodules is that the common DC-link voltage value can be chosen freely [108]. However, if the DC-link voltage is chosen to be small, the current that would flow through the valves based on the requested maximum power of 100 MW for 1.25 s or 200 MW for 0.5 s would be too large for the converters to handle. For this reason, a balancing between the energy storage insulation to reach high voltages and the maximum allowable current for the converters needs to be made.

In order to reach high voltages, one option is to connect the modules up to voltages of tens of kilovolts using insulation between ground and the other modules. This can be done if the energy storages are placed in a rack and the rack is isolated from ground potential via external insulator poles. The racks should also be insulated from each other, and any metallic parts of the racks should be tied to the rack potential. A middle point connection between the series connected modules and the rack cabinet could be used as this would decrease the voltage stress. Rack to rack cabling should fulfill the same insulation requirements and the energy storage monitoring communication should be done using for example fiberoptic communication. Energy storage modules should not have any conductive parts in floating potentials to avoid any partial discharges. In the following analysis it is assumed that the previously described insulation can be done.

For this thesis, the common DC-link nominal voltage was assumed to be 60 kV with a maximum of 65 kV and minimum of 40 kV. Using (80) with the high voltage values gives overall capacitance of 0.4 F. To reach the voltage of 60 kV, there needs to be 28170 supercapacitor cells with initial voltage of 2.13 V and 26800 LTO battery cells with 50 % SOC. Based on the maximum power of 100 MW and chosen minimum voltage, the maximum current is 2.5 kA. This means that no parallel strings of supercapacitors are needed but 10 parallel strings of batteries are required. Based

on the simulations in Section 4.4, the number of parallel supercapacitor strings was changed to two and the number of battery strings to nine for BOL conditions. For EOL conditions number parallel battery strings need to be increased up to 15 while the number of parallel supercapacitor strings needs to be increased to 4. Common DC-link implementation cost analysis is shown in Table 9.

Table 9. *Common DC-link energy storage cost*

Product	Price per cell (€/cell)	Number of cells, BOL	Total cost, BOL (€)	Total cost, EOL (€)
3200 F supercapacitor cell	56	56340	3.16 million	6.31 million
LTO Li-ion battery cell	8.23	241200	1.99 million	3.31 million

Based on Table 9 it can be seen that over 4 times more battery cells are needed but the individual cell price for batteries is just around 15 % of the supercapacitor cell price.

4.3 Submodule simulation results

Using the STATCOM simulation model based on ideal voltage sources and active and reactive power control, the dynamic behavior of the energy storage can be analyzed in more detail based on Figures 64 and 65. At 0.5 seconds active power injection is started which causes a small transient phenomenon based on the controller interaction. After, the transient, constant power of 0.83 MW is fed to the grid for 1.25 seconds after which the energy storage waits idle for one second. Between 2.75 seconds and 4 seconds, 100 MW of power is absorbed to the STATCOM energy storage which causes the voltage to increase. After four seconds, the energy storage is again idling for one second.

The STATCOM model reactive power reference was set to zero so that only active power is controlled. Figure 64 shows the submodule energy storage BOL voltage simulation results with different supercapacitor models and one battery model. The results highlight that there is significant difference between different supercapacitor models as the voltage with self-made Zubieta model reaches significantly lower voltage values than the other supercapacitor models. It should be noted that the voltage from the supercapacitor was not used to control the ideal voltage sources, rather the model used a constant voltage of 60.5 kV for the output voltage.

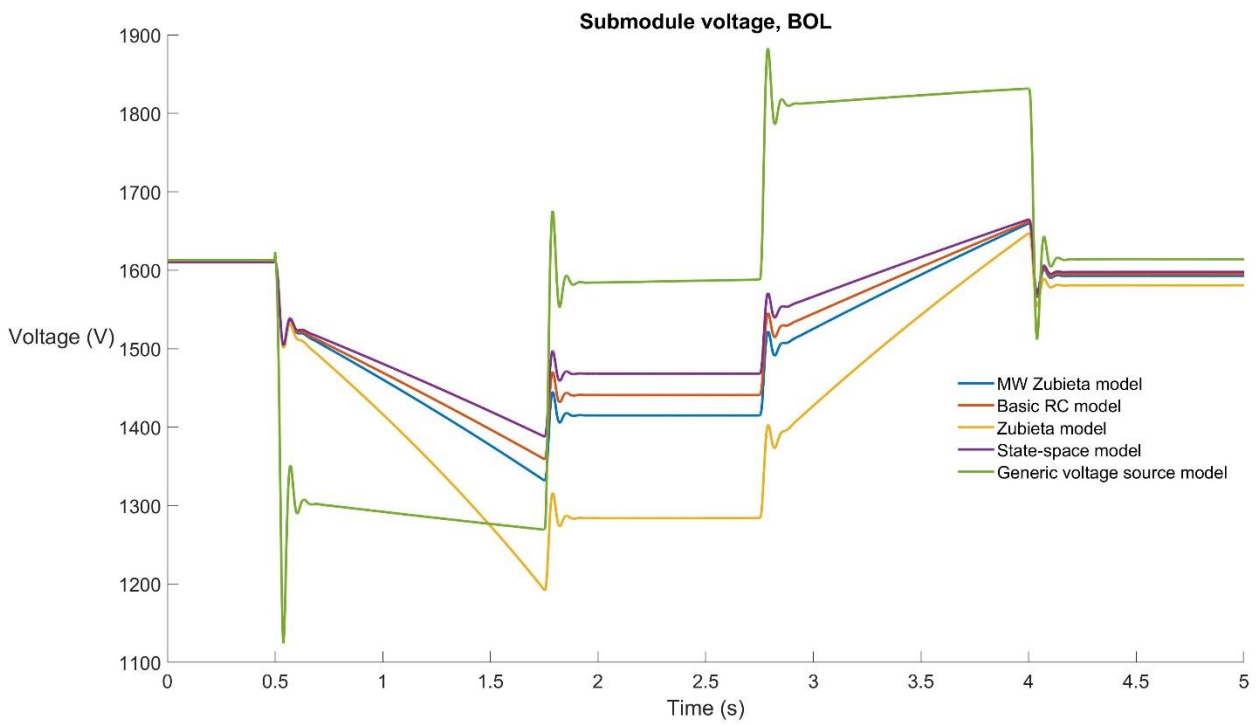


Figure 64. Submodule voltage simulation results with one battery and four supercapacitor models

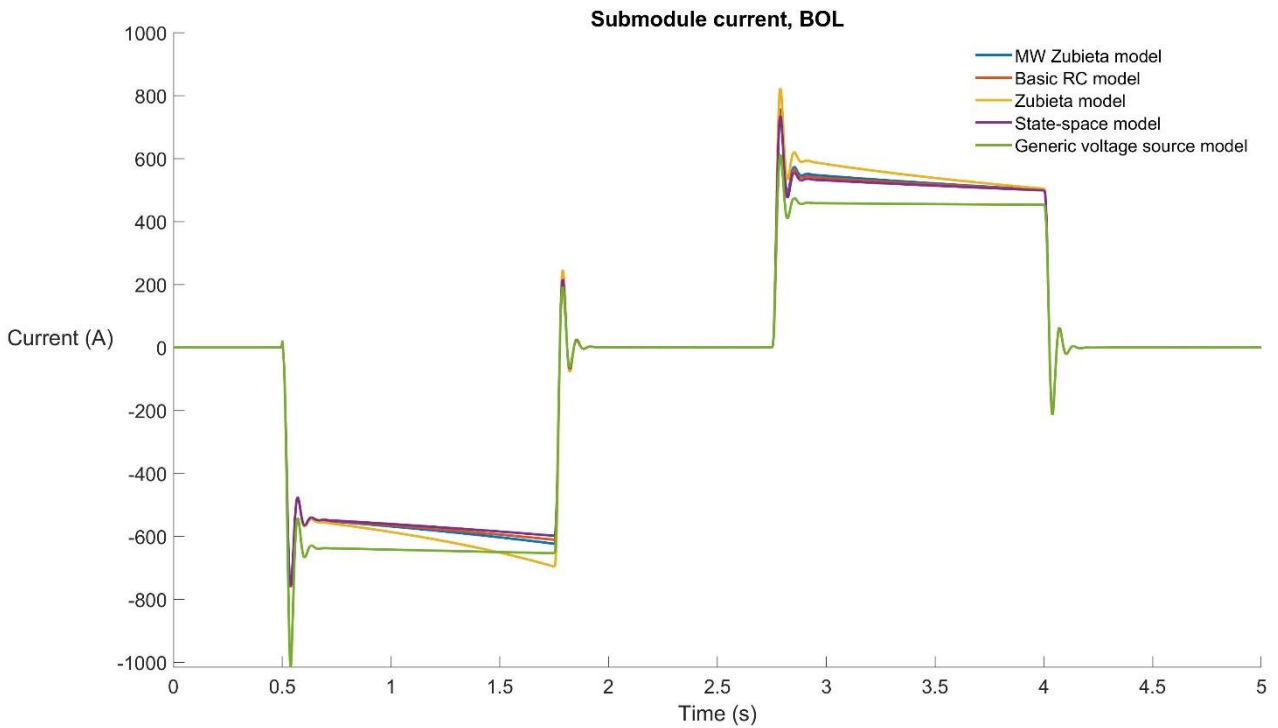


Figure 65. Submodule current with one battery and four supercapacitor models

Based on Figure 65, the BOL current in the models stays within given limits. At the start of active power injection at 0.5 seconds, the battery current exceeds the given limit of 260 A momentarily but otherwise the current per battery string is less than 260 A. With EOL conditions, the voltage and current limits are not exceeded, but as was discussed, the sizing needs to be increased with additional parallel string of batteries or supercapacitors.

Based on the results, the supercapacitors and batteries can be sized to meet the limits that the submodule implementation has while providing enough active power. Both energy storage options should be integrated using a DC-DC converter to allow for constant output voltage. However, the DC-DC converter ratings need to be sized accordingly as the energy storage current increases with the discharge time when constant voltage is used as the converter output. The supercapacitor voltage profile is quite flat with the required sizing, so the battery does not have significant benefits over the supercapacitors. On the contrary, the supercapacitors have significantly smaller heat generation and safer technology, so careful economic analysis should be conducted when deciding between the energy storage technology for a submodule implementation.

4.4 Common DC-link simulation results

Common DC-link simulations were done using a double-star model. Simulation results for discharge with power of 100 MW for 1.25 seconds are shown in Figure 66. At 0.3 seconds STATCOM starts to feed reactive power to the grid causing a sudden increase in the energy storage current which causes a large voltage drop. At 0.8 seconds 100 MW active power transfer is initialized causing a sudden voltage drop due to high current flowing through the energy storage equivalent series resistance.

Based on Figure 66, it is clear that with batteries there is a large initial voltage drop of over 10 kV which most likely will have a significant impact on the STATCOM operation. After the initial voltage drop, the battery voltage decreases linearly during the discharge. Change in the voltage during the discharge is under 2 kV. Supercapacitors on the other hand have significantly lower initial voltage drop of around 3.3 kV while the voltage drop during discharge is between 6.5-15.5 kV depending on the supercapacitor model. As the differences between the supercapacitor simulation model can be significant, the model validation using a real supercapacitor cell is important. With the chosen sizing, all of the models produce acceptable voltage behavior.

When EOL conditions are used, number of series connected supercapacitor strings needs to be increased to four and the number of parallel battery strings needs to be increased to 15 which would increase the costs substantially if DC-DC converters would not be used. This means that the capacity decrease and equivalent series resistance increase of batteries have more significant effect on the sizing and costs than the supercapacitor capacitance fade and equivalent series resistance increase.

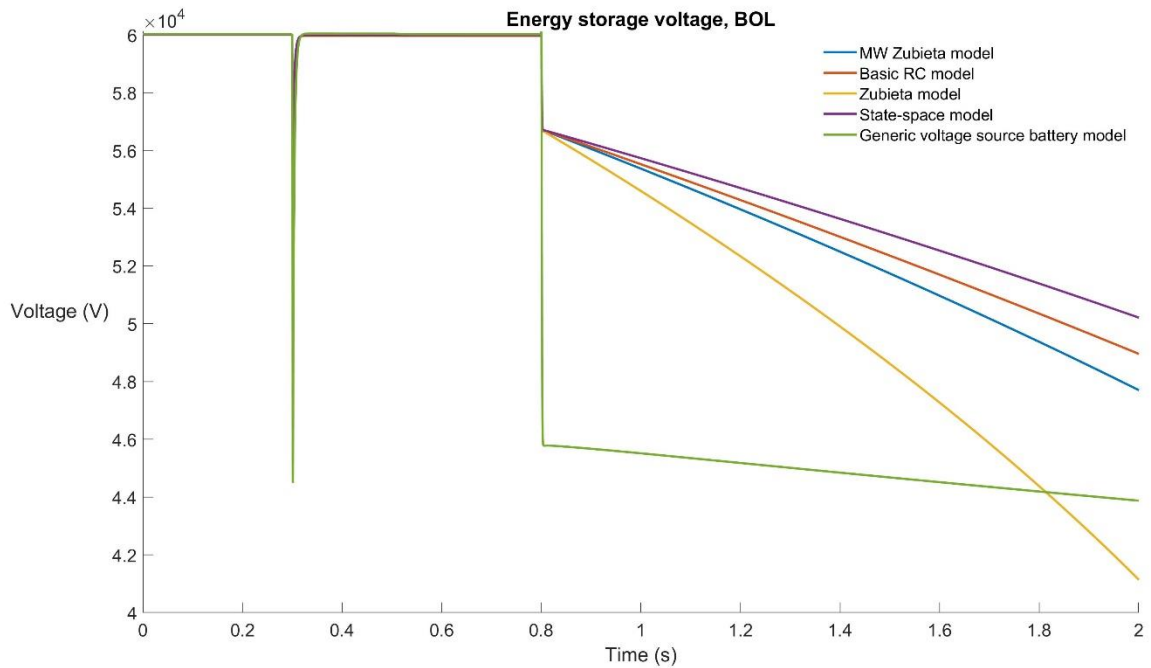


Figure 66. Common DC-link voltage simulation results with BOL conditions

Figure 67 shows the simulated energy storage currents during the discharge with BOL conditions. With 9 series connected battery strings, the maximum battery string discharge current is 277 A which can be assumed to be close enough to the 260 A maximum cell current requirement.

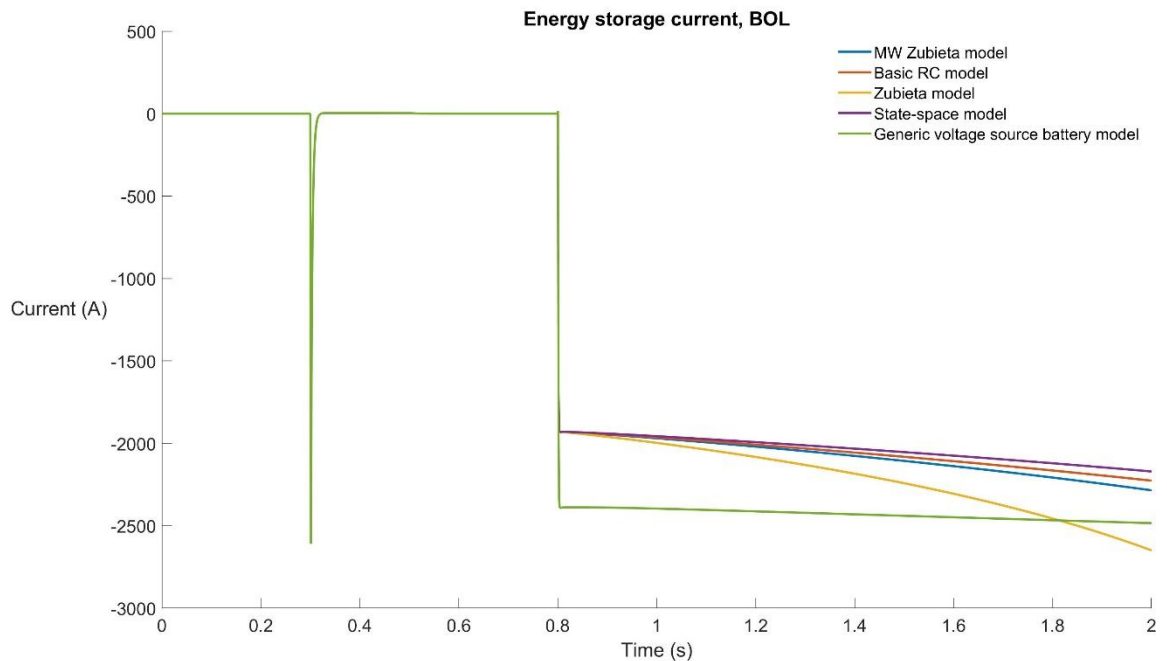


Figure 67. Simulated energy storage currents with BOL conditions

For supercapacitors the current values are well within the individual supercapacitor cell and module ratings for one second. With EOL conditions and sizing, the initial voltage drop caused by ESR is down to 42 kV and the supercapacitor voltage decreases faster towards the low voltage

boundary of 40 kV. However, based on the simulation results, both BOL and EOL conditions can meet the power requirements and current limits. In the common DC-link option, the initial voltage drop of several kV is not acceptable so a high-power converter should be implemented if possible.

4.5 Switching STATCOM model simulation results

The STATCOM models used in previous tests were heavily simplified as the models do not have switching characteristics. To get an idea of the effect of switching to a supercapacitor, a Stern-Tafel supercapacitor model was fitted into the submodules of a switching STATCOM model. Simulating the STATCOM model using a supercapacitor model gives an idea of the increase in computational time by first running the model with regular capacitors and then with different supercapacitor and battery models.

Structure of the STATCOM model is not disclosed, but the STATCOM only controls reactive power. For this reason, the supercapacitors are never discharged completely but rather the voltage fluctuates with a certain ripple around a mean value. In the simulation case, the reactive power was ramped between minimum and maximum value, so no fault situations were simulated. Supercapacitor capacitance was chosen to be small, 7 mF, to see the ripple effect without active power injection. Nominal submodule voltage was chosen to be 1600 V. Simulation result for one submodule supercapacitor voltage is shown in Figure 68.

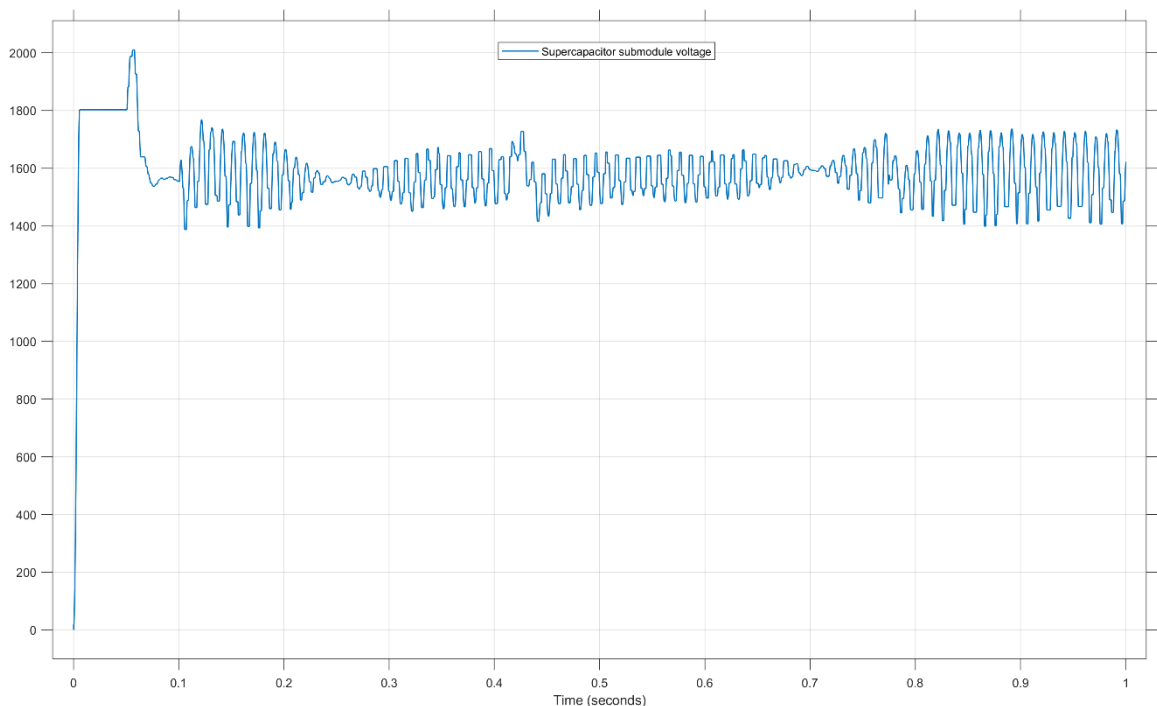


Figure 68. *Supercapacitor voltage in a submodule*

Based on the test, it was seen that the STATCOM model works with the supercapacitor model and that the ripple is quite small with the chosen sizing of 7 mF. The effect of such a ripple on the supercapacitor lifetime needs to be analyzed in more detail in the future together with a realistic

active power injection while using DC-DC converters. It was observed that the simulation times on average were 1.47 p.u. compared to the normal capacitor simulation time.

5. CONCLUSIONS

This thesis investigates the possible energy storage options for high-power STATCOM applications and based on the analysis develops simple simulation methods. Li-ion batteries, supercapacitors, flywheels and SMES were analyzed more closely as they present the best energy storage options for the STATCOM device based on a literature review. However, flywheels and SMES have significant disadvantages related to complexity, cost and reliability so the focus is given to supercapacitors and Li-ion batteries. Supercapacitors are seen as the best option for the high-power requirements because of the safety and proven implementation to STATCOMs. Batteries have also been used in STATCOM applications and the cost is significantly lower compared to supercapacitors, so more detailed analysis on the total cost of ownership should be made. In the future also hybrid solutions might need to be considered if the application requirements change. A hybrid energy storage would require much more complex control logic to enable power sharing among the energy storages. One possible reason for change of requirements is that with more stored energy it would also be possible to attend to a greater number of grid-scale markets than just the short-term inertia-based market.

Supercapacitor and battery operation is highly dependent on a few variables. For batteries, the most important factor is the state of charge. In addition, also temperature, charge/discharge current value and cycle life have an effect on the performance. The complex operational characteristics of Li-ion batteries make simple modelling and monitoring difficult. Supercapacitor performance is mainly dependent on temperature and cell voltage so sufficient ambient conditions and intermediate voltage level need to be maintained in order to reach long operation lifetimes. Main benefit of a Li-ion battery over a supercapacitor is the abundance of energy in addition to the flat voltage profile. Downsides consist of safety concerns, energy oversizing for the demanded power, slow recharge time and increased heat generation. For maintenance, discharging the batteries completely will take a long time, unlike with the supercapacitors. Supercapacitors can provide large currents very fast but the low cell voltages and linear voltage behavior might limit the applicability in some cases.

Based on the supercapacitor model comparison, a few different models should be used to get an understanding on average how the energy storage should be sized as the model results can have significant differences. Generally, a Zubieta model is seen as a good option, but based on the parameter values and number of included RC circuits, the Zubieta model results could vary significantly. Model parameter identification and simulation result validation against real supercapacitor and battery cells is needed before more detailed analysis can be done. Generic battery voltage source model can capture the battery voltage behavior in charging and discharging situations. For more accurate simulations based on multiple state variables, a six-parameter equivalent circuit model should be used for Li-ion batteries. Both batteries and supercapacitors can be modelled more accurately using EIS, but the method requires burdensome measurements.

Energy storage simulations together with simplified STATCOM model gives information about the energy storage sizing requirements as well as current and voltage behavior of the energy storage. Battery sizing in terms of parallel connections is limited by the maximum charge and discharge currents that are assumed to be equal. Supercapacitor sizing in terms of parallel connections is affected by the required capacitance. Based on the energy oversizing and flat voltage profile, the battery voltage is quite constant during charging and discharging while the voltage drop at the start of the charge is very significant. Supercapacitors have a lot smaller equivalent series resistance, so the initial voltage change and heating at the start of charging and discharging is smaller, but the voltage change during charging and discharging is higher than with batteries. If the voltage change is seen to be too great, a DC-DC converter should be integrated between the energy storage and the STATCOM.

Especially with the submodule implementation, a DC-DC converter would significantly reduce the number of series connected supercapacitor modules and the costs. Submodule implementation allows for lower energy storage voltages, but the overall system complexity increases. Common DC-link implementation allows for easier control of the storage, but the high series voltage requires good insulation and could possibly introduce other issues such as electromagnetic interference. Based on the simulation results, both submodule and DC-link implementation options are able to fulfil the requirements while respecting the given operational limits. However, more detailed simulation cases and STATCOM models are needed before decisions about the applicability of the energy storages can be made.

Overall, common DC-link implementation is seen as the better option based on ease of control, ease of maintenance and safety. Based on simulation results, battery-based solutions have significantly lower cost, but it should be kept in mind that discharges with high currents will influence the calendar and cycle lifetime of the battery more than the supercapacitors. Supercapacitors do not suffer from large discharge currents if the temperature of the cells can be maintained close to nominal values. However, in this thesis the load cycle was not known so lifetime simulations were not possible.

For future research, more complex energy storage models could be used that include temperature modelling, accurate frequency related behavior and cell balancing. In addition, realistic inductance values should be added to the battery and supercapacitor models to see how that affects the response time and resonance frequency. During this thesis only supercapacitor cells were available for impedance measurement, so more accurate parameter identification was not possible. Especially for batteries, more sophisticated simulation software than Simulink could be used to allow for temperature modeling and operation with regards to multiple state variables. Also, the model for STATCOM should be more detailed to account for more realistic simulations. The next step is to use a MMC model with active power control and DC-DC converters for the STATCOM. MMC model would be a switching model and thus it would introduce ripple to the energy storage that can have significant effect on the energy storage performance. In this thesis, mainly very simple simulation tests were conducted. In the future more complicated simulations scenarios,

such as faults, unbalanced grid events etc. should be considered to see how they can affect the energy storage behavior and sizing. In addition, a small-scale mockup of a high voltage energy storage integrated with a valve should be built as it could reveal new phenomena that are not taken into account in this thesis.

REFERENCES

- [1] P. Christensen *et al.*, “High Penetration of Power Electronic Interfaced Power Sources and the Potential Contribution of Grid Forming Converters – Technical report,” 2020.
- [2] G. Denis, T. Prevost, M.-S. Debry, F. Xavier, X. Guillaud, and A. Menze, “The Migrate project: the challenges of operating a transmission grid with only inverter-based generation. A grid-forming control improvement with transient current-limiting control,” *IET renewable power generation*, vol. 12, no. 5, pp. 523–529, 2018,
- [3] S. F. Tarannum and S. S. Kamble, “A Study on Application of Static Synchronous Compensator (STATCOM) in Power Quality Improvement,” in *Proceedings - International Conference on Smart Electronics and Communication, ICOSSEC 2020*, 2020, pp. 1003–1006.
- [4] X. P. Zhang, C. Rehtanz, and B. Pal, “Flexible AC Transmission Systems: Modelling and Control,” *Power Systems*, vol. 11, pp. 3–4, 2012,
- [5] M. Farhadi and O. Mohammed, “Energy Storage Technologies for High-Power Applications,” *IEEE Transactions on Industry Applications*, vol. 52, no. 3, pp. 1953–1961, 2016,
- [6] ENTSO-E, “Voltage Source Converters.” <https://www.entsoe.eu/Technopedia/techsheets/voltage-source-converters> (accessed Jan. 15, 2022).
- [7] ENTSO-E, “Static Synchronous Compensator (STATCOM).” <https://www.entsoe.eu/Technopedia/techsheets/static-synchronous-compensator-statcom> (accessed May 13, 2022).
- [8] J. M. Maza-Ortega, E. Acha, S. García, and A. Gómez-Expósito, “Overview of power electronics technology and applications in power generation transmission and distribution,” *Journal of Modern Power Systems and Clean Energy*, vol. 5, no. 4, pp. 499–514, 2017,
- [9] A. Yazdani and R. Iravani, *Voltage-Sourced Converters in Power Systems: Modeling, Control, and Applications*. IEEE Press/John Wiley, 2010.
- [10] T. Geyer, *Model Predictive Control of High Power Converters and Industrial Drives*. John Wiley & Sons, 2016.
- [11] J. Chivite-Zabalza, J. Perrier, M. Boden, T. Xu, and J. Outram, “Development of a full-bridge sub-module for HVDC and STATCOM markets,” *PCIM Europe*, pp. 1–7, 2017.
- [12] V. Spudic and T. Geyer, “Model Predictive Control Based on Optimized Pulse Patterns for Modular Multilevel Converter STATCOM,” *IEEE Transactions on Industry Applications*, vol. 55, no. 6, pp. 6137–6149, 2019,
- [13] G. J. M. de Sousa and M. L. Heldwein, “Concentrated submodules model for modular multilevel converters,” in *Proceedings - 2017 IEEE Southern Power Electronics Conference, SPEC 2017*, 2018, vol. 2018-January, pp. 1–6.
- [14] S. K. Chaudhary, A. F. Cupertino, R. Teodorescu, and J. R. Svensson, “Benchmarking of modular multilevel converter topologies for ES-STATCOM realization,” *Energies (Basel)*, vol. 13, no. 13, pp. 1–22, 2020,
- [15] E. Behrouzian and M. Bongiorno, “Investigation of Negative-Sequence Injection Capability of Cascaded H-Bridge Converters in Star and Delta Configuration,” *IEEE Trans Power Electron*, vol. 32, no. 2, pp. 1675–1683, 2017,
- [16] A. Shukla and A. Nami, “Multilevel converter topologies for STATCOMs,” *Power Systems*, vol. 90, pp. 35–82, 2015,
- [17] E. Acha, *FACTS modelling and simulation in power networks*. Wiley, 2004.
- [18] A. Chakraborty, S. K. Musunuri, A. K. Srivastava, and A. K. Kondabathini, “Integrating STATCOM and battery energy storage system for power system transient stability: A review and application,” *Advances in Power Electronics*, vol. 2012, pp. 1–12, 2012,
- [19] Q. Wang, B. Mao, S. I. Stolarov, and J. Sun, “A review of lithium ion battery failure mechanisms and fire prevention strategies,” *Progress in Energy and Combustion Science*, vol. 73. Elsevier Ltd, pp. 95–131, Jul. 01, 2019.
- [20] R. Kötz, P. W. Ruch, and D. Cericola, “Aging and failure mode of electrochemical double layer capacitors during accelerated constant load tests,” *Journal of Power Sources*, vol. 195, no. 3, pp. 923–928, Feb. 2010,
- [21] K. Ilves, S. Norrga, L. Harnefors, and H. P. Nee, “On energy storage requirements in modular multilevel converters,” *IEEE Transactions on Power Electronics*, vol. 29, no. 1, pp. 77–88, 2014,

- [22] Aiping. Yu, "Electrochemical supercapacitors for energy storage and delivery : fundamentals and applications," *Boca Raton, Fla: Taylor & Francis*. Taylor & Francis, Boca Raton, Fla, pp. 5–8, 2013.
- [23] Z. Melhem, *Electricity Transmission, Distribution and Storage Systems*, 1st edition. Philadelphia, PA: Woodhead Pub, 2013.
- [24] M. H. Rashid, *Power Electronics Handbook*. Butterworth-Heinemann, 2007.
- [25] Yang Liu, Shuitao Yang, Shao Zhang, and Fang Zheng Peng, "Comparison of synchronous condenser and STATCOM for inertial response support," in *2014 IEEE Energy Conversion Congress and Exposition (ECCE)*, 2014, pp. 2684–2690.
- [26] X. Luo, J. Wang, M. Dooner, and J. Clarke, "Overview of current development in electrical energy storage technologies and the application potential in power system operation," *Applied Energy*, vol. 137, pp. 511–536, 2015,
- [27] P. Sanjeevikumar, C. Sharmeela, J. B. Holm-Nielsen, and P. Sivaraman, "Power quality in modern power systems," *Academic Press*. Academic Press, London, United Kingdom, pp. 287–291, 2021.
- [28] J. Pikkarinen, "How Temperature Affects Ultracapacitors and Batteries," *Skeleton Technologies*, Nov. 28, 2016. <https://www.skeletontech.com/skeleton-blog/how-temperature-affects-ultracapacitors-and-batteries> (accessed Feb. 24, 2022).
- [29] P. Weicker, "A systems approach to lithium-ion battery management," *Boston: Artech House*. Artech House, Boston, pp. 38–39, 2013.
- [30] Y. Wu, *Lithium-Ion Batteries: Fundamentals and Applications*, 1st Edition., no. 1. Florida: CRC Press, 2015.
- [31] ABB, "DynaPeaQ ® Energy Storage System-A UK first," 2011. Accessed: Mar. 08, 2022. [Online]. Available: <https://library.e.abb.com/public/5c6dc4bd73860eb7c125793a0043a0e9/A02-0224%20E%20LR.pdf>
- [32] K. C. Divya and J. Østergaard, "Battery energy storage technology for power systems-An overview," *Electric Power Systems Research*, vol. 79, no. 4. pp. 511–520, 2009.
- [33] J. Sihvo, "SOH Estimation of Li-Ion Batteries Based on Broadband Impedance Measurements and Equivalent Circuit Model Analysis," Tampere University, 2021.
- [34] T. Singh and S. Kumar, "MODELING AND SIMULATION OF ELECTROCHEMICAL SUPERCAPACITOR FOR HIGH POWER DELIVERY," *International journal of advanced research (Indore)*, vol. 5, no. 6, pp. 509–516, 2017,
- [35] M. C. Argyrou, P. Christodoulides, and S. A. Kalogirou, "Energy storage for electricity generation and related processes: Technologies appraisal and grid scale applications," *Renewable & sustainable energy reviews*, vol. 94, pp. 804–821, 2018,
- [36] M. Morris, "COMPARISON OF RECHARGEABLE BATTERY TECHNOLOGIES," 2012. [Online]. Available: <https://www.researchgate.net/publication/281931837>
- [37] M. Bluejay, "Rechargeable Batteries - compared and explained in detail," 2021. <https://michaelbluejay.com/batteries/rechargeable.html> (accessed Feb. 28, 2022).
- [38] J. Garche, C. Dyer, P. T. Moseley, Z. Ogumi, D. A. J. Rand, and B. Scrosati, *Encyclopedia of Electrochemical Power Sources*. Oxford: Elsevier Science & Technology, 2009.
- [39] Battery University, "BU-201: How does the Lead Acid Battery Work?" 2021. Accessed: May 26, 2022. [Online]. Available: <https://batteryuniversity.com/article/bu-201-how-does-the-lead-acid-battery-work>
- [40] M. Moorthi, "Lithium Lithium Titanate Titanate Based Batteries Batteriesfor High Rate and High Cycle Life Applications," *NEI Corporation*. Accessed: May 26, 2022. [Online]. Available: https://www.neicorporation.com/white-papers/NEI_White_Paper_LTO.pdf
- [41] Beyond Oil Solar, "Nickel Iron Battery (Industrial Series)." 2016. Accessed: Mar. 14, 2022. [Online]. Available: <https://beyondoilsolar.com/product/nickel-iron-battery-industrial-series/>
- [42] ZincFive, "Data Sheet SubC Nickel-Zinc Batteries," 2019.
- [43] Grepow, "Nickel-Metal Hydride(NiMH) Battery." Accessed: Mar. 14, 2022. [Online]. Available: <https://www.grepow.com/page/nimh-battery.html>
- [44] B. Hariprakash, A. K. Shukla, and S. Venugoplan, *SECONDARY BATTERIES – NICKEL SYSTEMS | Nickel–Metal Hydride: Overview*. 2009.
- [45] Toshiba, "High-power type cells," *Product specifications*. Accessed: May 26, 2022. [Online]. Available: <https://www.global.toshiba/ww/products-solutions/battery/scib/product/cell/high-power.html>
- [46] R. Tjandra, S. Thanagasundram, K. J. Tseng, and A. Jossen, "Improved lithium-ion battery model with hysteresis effect," in *2014 IEEE Transportation Electrification Conference and*

- Expo: Components, Systems, and Power Electronics - From Technology to Business and Public Policy, ITEC 2014*, Jul. 2014, pp. 1–8.
- [47] M. E. Fuller, "A battery model for constant-power discharge including rate effects," *Energy Conversion and Management*, vol. 88, pp. 199–205, 2014,
- [48] David. Linden and T. B. Reddy, "Handbook of batteries," *McGraw-Hill*, vol. 3rd ed. McGraw-Hill, New York (N.Y.), 2002.
- [49] A. I. Stan, M. Swierczynski, D. I. Stroe, R. Teodorescu, and S. J. Andreasen, "Lithium ion battery chemistries from renewable energy storage to automotive and back-up power applications - An overview," in *2014 International Conference on Optimization of Electrical and Electronic Equipment, OPTIM 2014*, 2014, pp. 713–720.
- [50] D. Rastler, "Electricity Energy Storage Technology Options: A White Paper Primer on Applications, Costs, and Benefits," 2010.
- [51] A. Cooke, D. Strickland, and K. Forkasiewicz, "Energy storage for enhanced frequency response services," in *2017 52nd International Universities Power Engineering Conference, UPEC 2017*, 2017, vol. 2017-January, pp. 1–6.
- [52] A. B. Ch and S. Maiti, "Modular multilevel E-STATCOM considering distributed energy storage at the dc link," in *2016 IEEE 7th Power India International Conference, PIICON 2016*, 2017, pp. 1–6.
- [53] L. Zhang, X. Hu, Z. Wang, F. Sun, and D. G. Dorrell, "A review of supercapacitor modeling, estimation, and applications: A control/management perspective," *Renewable & sustainable energy reviews*, vol. 81, pp. 1868–1878, 2018,
- [54] S. Ma *et al.*, "Temperature effect and thermal impact in lithium-ion batteries: A review," *Progress in Natural Science: Materials International*, vol. 28, no. 6. pp. 653–666, 2018.
- [55] A. Kirchev, "Chapter 20 - Battery Management and Battery Diagnostics," in *Electrochemical Energy Storage for Renewable Sources and Grid Balancing*, Elsevier B.V, 2015, pp. 411–435.
- [56] J. Gao, B. Gong, Q. Zhang, G. Wang, Y. Dai, and W. Fan, "Study of the surface reaction mechanism of Li₄Ti₅O₁₂ anode for lithium-ion cells," *Ionics (Kiel)*, vol. 21, no. 9, pp. 2409–2416, Sep. 2015,
- [57] L. Wang, Z. Wang, Q. Ju, W. Wang, and Z. Wang, "Characteristic Analysis of Lithium Titanate Battery," in *Energy Procedia*, 2017, vol. 105, pp. 4444–4449.
- [58] P. J. Grbović, *Ultra-Capacitors in Power Conversion Systems: Analysis, Modeling and Design in Theory and Practice*. John Wiley & Sons Inc, 2013.
- [59] Supramaniam. Srinivasan, "Fuel Cells From Fundamentals to Applications," *Springer US*, no. 1st ed. Springer US, New York, NY, pp. 27–34, 2006.
- [60] G. L. Plett, "Battery management systems volume I: battery modeling," *Artech House*. Artech House, Boston, Mass, pp. 303–305, 2015.
- [61] K. K. Kar, *Handbook of Nanocomposite Supercapacitor Materials I Characteristics*, 1st ed. 2020. Cham: Springer International Publishing, 2020.
- [62] P. Luan *et al.*, "Epidermal Supercapacitor with High Performance," *Advanced Functional Materials*, vol. 26, no. 45, pp. 8178–8184, Dec. 2016,
- [63] D. Linzen, S. Buller, E. Karden, and R. W. de Doncker, "Analysis and evaluation of charge-balancing circuits on performance, reliability, and lifetime of supercapacitor systems," *IEEE Transactions on Industry Applications*, vol. 41, no. 5, pp. 1135–1141, 2005,
- [64] M. Krpan, I. Kuzle, A. Radovanovic, and J. v. Milanovic, "Modelling of Supercapacitor Banks for Power System Dynamics Studies," *IEEE Transactions on Power Systems*, vol. 36, no. 5, pp. 3987–3996, 2021,
- [65] L. Zubieta and R. Bonert, "Characterization of double-layer capacitors for power electronics applications," *IEEE Transactions on Industry Applications*, vol. 36, no. 1, pp. 199–205, Jan. 2000,
- [66] Eaton, "Supercapacitor modules application guidelines," *Technical Note*, no. 10888. Eaton, 2019. Accessed: Feb. 18, 2022. [Online]. Available: <https://www.eaton.com/content/dam/eaton/products/electronic-components/resources/technical/eaton-supercapacitor-modules-application-guidelines.pdf>
- [67] R. Kötzt, P. W. Ruch, and D. Cericola, "Aging and failure mode of electrochemical double layer capacitors during accelerated constant load tests," *Journal of Power Sources*, vol. 195, no. 3, pp. 923–928, 2010,

- [68] Maxwell Technologies, "Ultracapacitor safety data sheet (SDS)," 2015. Accessed: Apr. 13, 2022. [Online]. Available: https://library.e.abb.com/public/5184a587e60d4f1ea541de4f4d3d676d/Maxwell%20Ultra-cap%20Safety_Datasheet_3000389_EN_2.pdf
- [69] M. A. ben Fathallah, A. ben Othman, and M. Besbes, "Modeling a photovoltaic energy storage system based on super capacitor, simulation and evaluation of experimental performance," *Applied Physics A: Materials Science and Processing*, vol. 124, no. 2, pp. 1–10, 2018,
- [70] M. Amiryar and K. Pullen, "A Review of Flywheel Energy Storage System Technologies and Their Applications," *Applied sciences*, vol. 7, no. 3, p. 286, 2017,
- [71] M. M. Rahman, E. Gemechu, A. O. Oni, and A. Kumar, "The development of a techno-economic model for the assessment of the cost of flywheel energy storage systems for utility-scale stationary applications," *Sustainable energy technologies and assessments*, vol. 47, p. 101382, 2021,
- [72] M. H. Mostafa, S. H. E. Abdel Aleem, S. G. Ali, Z. M. Ali, and A. Y. Abdelaziz, "Techno-economic assessment of energy storage systems using annualized life cycle cost of storage (LCCOS) and levelized cost of energy (LCOE) metrics," *J Energy Storage*, vol. 29, p. 101345, 2020,
- [73] EATON, "Supercapacitor modules frequently asked questions." <https://www.eaton.com/us/en-us/products/electronic-components/faq/supercapacitor-modules-frequently-asked-questions.html> (accessed Mar. 15, 2022).
- [74] Md. R. Islam, F. Rahman, and W. Xu, *Advances in solar photovoltaic power plants*, 1st ed. Springer Berlin Heidelberg, 2016.
- [75] G. Sathish Kumar, V. Agnes Idhaya Selvi, and K. Pandiyan, "Design and analysis of ML-VSC based SMES with improved power quality features," *Materials Today: Proceedings*, pp. 1–6, 2021,
- [76] M. G. Molina, P. E. Mercado, and E. H. Watanabe, "Static synchronous compensator with superconducting magnetic energy storage for high power utility applications," *Energy Conversion and Management*, vol. 48, no. 8, pp. 2316–2331, 2007,
- [77] M. G. Molina and P. E. Mercado, "Comparative evaluation of performance of a STATCOM and SSSC both integrated with SMES for controlling the power system frequency," in *2004 IEEE/PES Transmission and Distribution Conference and Exposition: Latin America*, 2004, pp. 535–541.
- [78] M. Soltani and S. H. Beheshti, "A comprehensive review of lithium ion capacitor: development, modelling, thermal management and applications," *J Energy Storage*, vol. 34, p. 102019, 2021,
- [79] A. Chu and P. Braatz, "Comparison of commercial supercapacitors and high-power lithium-ion batteries for power-assist applications in hybrid electric vehicles: I. Initial characterization," *J Power Sources*, vol. 112, no. 1, pp. 236–246, 2002,
- [80] LIGHTING GLOBAL, "Lithium-ion Battery Overview," *Technical Notes*, no. 10, 2012, Accessed: Feb. 18, 2022. [Online]. Available: <https://www.lightingglobal.org/resource/lithium-ion-battery-overview/>
- [81] N. Kularatna, "Energy storage devices for electronic systems : rechargeable batteries and supercapacitors," *Elsevier Science & Technology*. Academic Press, London, England, pp. 35–35, 2015.
- [82] X. Zhang, J. Wu, and G. Kang, "SOC estimation of Lithium battery by UKF algorithm based on dynamic parameter model," *2016 13th International Conference on Ubiquitous Robots and Ambient Intelligence, URAI 2016*, pp. 945–950, 2016,
- [83] M. Bercibar, I. Gandiaga, I. Villarreal, N. Omar, J. van Mierlo, and P. van den Bossche, "Critical review of state of health estimation methods of Li-ion batteries for real applications," *Renewable & sustainable energy reviews*, vol. 56, pp. 572–587, 2016,
- [84] M. Petzl, M. Kasper, and M. A. Danzer, "Lithium plating in a commercial lithium-ion battery - A low-temperature aging study," *Journal of Power Sources*, vol. 275, pp. 799–807, 2015,
- [85] C. Zhang, W. Allafi, Q. Dinh, P. Ascencio, and J. Marco, "Online estimation of battery equivalent circuit model parameters and state of charge using decoupled least squares technique," *Energy*, vol. 142, pp. 678–688, Jan. 2018,
- [86] J. Meng, G. Luo, M. Ricco, M. Swierczynski, D. I. Stroe, and R. Teodorescu, "Overview of Lithium-Ion battery modeling methods for state-of-charge estimation in electrical vehicles," *Applied Sciences (Switzerland)*, vol. 8, no. 5, pp. 659–659, 2018.

- [87] M. Tomasov, M. Kajanova, P. Bracinik, and D. Motyka, "Overview of Battery Models for Sustainable Power and Transport Applications," in *Transportation Research Procedia*, 2019, vol. 40, pp. 548–555.
- [88] O. Tremblay, L. A. Dessaint, and A. I. Dekkiche, "A generic battery model for the dynamic simulation of hybrid electric vehicles," *VPPC 2007 - Proceedings of the 2007 IEEE Vehicle Power and Propulsion Conference*, pp. 284–289, 2007.
- [89] C. M. Shepherd, "Theoretical Design of primary and secondary cells Part III - Battery discharge equation," *Electrochemistry Branch Chemistry Division*, pp. 3–15, 1963.
- [90] MathWorks, "Generic battery model," *MathWorks*, 2008. <https://se.mathworks.com/help/physmod/sps/powersys/ref/battery.html> (accessed Feb. 18, 2022).
- [91] A. I. Stroe, M. Swierczynski, D. I. Stroe, and R. Teodorescu, "Performance model for high-power lithium titanate oxide batteries based on extended characterization tests," in *2015 IEEE Energy Conversion Congress and Exposition, ECCE 2015*, Oct. 2015, pp. 6191–6198.
- [92] A. I. Stroe, D. I. Stroe, M. Swierczynski, R. Teodorescu, and S. K. Kær, "Lithium-Ion battery dynamic model for wide range of operating conditions," in *Proceedings - 2017 International Conference on Optimization of Electrical and Electronic Equipment, OPTIM 2017 and 2017 Intl Aegean Conference on Electrical Machines and Power Electronics, ACEMP 2017*, Jul. 2017, pp. 660–666.
- [93] S. Madani, E. Schaltz, and S. Knudsen Kær, "An Electrical Equivalent Circuit Model of a Lithium Titanate Oxide Battery," *Batteries (Basel)*, vol. 5, no. 1, p. 31, 2019.
- [94] H. Miniguano, A. Barrado, C. Fernández, P. Zumel, and A. Lázaro, "A general parameter identification procedure used for the comparative study of supercapacitors models," *Energies (Basel)*, vol. 12, no. 9, p. 1776, 2019.
- [95] A. B. Cultura and Z. M. Salameh, "Modeling, Evaluation and Simulation of a Supercapacitor Module for Energy Storage Application," in *Proceedings of the International Conference on Computer Information Systems and Industrial Applications*, 2015, vol. 18, pp. 1–7.
- [96] T. C. Reddy, K. K. Reddy, B. Venkatesh, M. Muthusamy, and A. V. Pillai, "Simulation of supercapacitor energy storage system with Bi DC-DC converters," in *Journal of Physics: Conference Series*, 2019, vol. 1362, no. 1, p. 12055.
- [97] L. Zhang, X. Hu, Z. Wang, F. Sun, and D. G. Dorrell, "A review of supercapacitor modeling, estimation, and applications: A control/management perspective," *Renewable & sustainable energy reviews*, vol. 81, pp. 1868–1878, 2018.
- [98] Skeleton Technologies, "SkelCap supercapacitor." 2021. Accessed: Feb. 21, 2022. [Online]. Available: <https://www.skeletontech.com/skelcap-sca-ultracapacitor-cells>
- [99] I. N. Jiya, N. Gurusinge, and R. Gouws, "Electrical circuit modelling of double layer capacitors for power electronics and energy storage applications: A review," *Electronics (Switzerland)*, vol. 7, no. 11. MDPI AG, p. 268, Nov. 01, 2018.
- [100] Lennart Ljung and Torkel Glad, *Control Theory*, 1st edition. CRC Press, 2018.
- [101] M. Şahin, "Modelling of Supercapacitors Based on Simplified Equivalent Circuit," *CPSS Transactions on Power Electronics and Applications*, vol. 6, no. 1, pp. 31–39, Mar. 2021.
- [102] Z. Cabrane and S. H. Lee, "Electrical and Mathematical Modeling of Supercapacitors: Comparison," *Energies (Basel)*, vol. 15, no. 3, p. 693, 2022.
- [103] A. Lahyani, P. Venet, A. Guermazi, and A. Troudi, "Battery/Supercapacitors Combination in Uninterruptible Power Supply (UPS)," *IEEE Transactions on Power Electronics*, vol. 28, no. 4, pp. 1509–1522, 2013.
- [104] J. Miller, P. McCleer, and M. Cohen, "ENERGY BUFFERS," *Maxwell Technologies White Paper*. pp. 5–7. Accessed: Mar. 25, 2022. [Online]. Available: https://www.tecate-group.com/white_papers/200904_WhitePaper_EnergyBuffers.pdf
- [105] MathWorks, "Supercapacitor," *MathWorks*, 2013. <https://se.mathworks.com/help/physmod/sps/powersys/ref/supercapacitor.html> (accessed Feb. 18, 2022).
- [106] G. Navarro, J. Nájera, J. Torres, M. Blanco, M. Santos, and M. Lafoz, "Development and Experimental Validation of a Supercapacitor Frequency Domain Model for Industrial Energy Applications Considering Dynamic Behaviour at High Frequencies," *Energies (Basel)*, vol. 13, no. 5, p. 1156, 2020.
- [107] Alibaba.com, "2.5V 16AH Long Deep Cycle Life Lithium Titanate Battery Rechargeable LTO Battery Cell." https://www.alibaba.com/product-detail/2-5V-16AH-Long-Deep-Cycle_1600070539605.html (accessed May 18, 2022).

- [108] K. Ilves, S. Norrga, and H.-P. Nee, "On energy variations in modular multilevel converters with full-bridge submodules for Ac-Dc and Ac-Ac applications," in *2013 15th European Conference on Power Electronics and Applications (EPE)*, 2013, pp. 1–10.
- [109] Battery University, "Types of Lithium-ion," *BU-205*. <https://batteryuniversity.com/article/bu-205-types-of-lithium-ion> (accessed Feb. 18, 2022).
- [110] B. Priyono, P. W. Winowatan, A. Z. Syahrial, Faizah, and A. Subhan, "Optimizing the performance of Li₄Ti₅O₁₂/LTO by addition of silicon microparticle in half cell lithium-ion battery anode," in *IOP Conference Series: Earth and Environmental Science*, Jan. 2018, vol. 105, no. 1, p. 12121.
- [111] K. Saarentausta, "Selection and sizing of electrical energy storage for a hybrid working machine based on the work cycle," Master's Thesis, Lappeenranta-Lahti University of Technology LUT, 2020.

APPENDIX A

Table a: Characteristics of electrical energy storage technologies, [5][26][32][58]

Technology	ZnBr	Regenerative fuel cell	Supercapacitor	SMES	Solar fuel	Hydrogen fuel cell	Liquid air storage
Energy density (W/l)	30-65	20-30	10-30	0.2-6	500-10000	500-3000	4-6 times CAES at 200 bar
Power density (W/kg)	Less than 25	Less than 2	100000+	1000-4000	-	500+	-
Specific energy (Wh/kg)	30-80	15-30	0.05-5	0.5-70	800-100000	150-10000	214
Specific power (W/kg)	45-100	-	3000-100000	500-2000	-	5-800	-
Daily discharge (%)	Small	Almost zero	5-40	10-15	Almost zero	Almost zero	Small
Lifetime (years)	5-10	10-15	10-30	20-30	-	5-20+	25+
Cycling time (cycles)	2000+	-	100000+	100000+	-	1000-20000+	-
Discharge efficiency (%)	60-70	-	95-98	95	-	59	-
Cycle efficiency (%)	65-80	60-75	84-97	95-98	20-30	20-66	55-80+
Response time	Less than ¼ cycle	20 ms	Milliseconds	Milliseconds	-	Seconds	Minutes
Temperature region (°C)	0, 40	0, 40	-40, 65	-50, 60	-	-	-

Technol- ogy	Large- scale CAES	Fly- wheel	Lead- acid	Li-ion	NaS	NiCd	VRB
Energy density (W/l)	2-6	20-80	50-90	150-500	150-300	15-150	16-33
Power density (W/kg)	0.5-2	1000-5000	100-400	1500-10000	140-180	80-600	Less than 2
Specific energy (Wh/kg)	30-60	5-100	25-50	75-200	100-240	45-80	10-30
Specific power (W/kg)	-	400-1500	75-300	150-2000	90-230	150-300	166
Daily discharge (%)	Almost zero	Over 20% per hour	0.1-0.3	0.1-0.3, 1 & 5	Almost zero	0.2-0.6	Very low
Lifetime (years)	20-40	Over 15	5-15	5-16	10-20	3-20	5-20
Cycling time (cycles)	8000-12000	Over 20000	200-1800	1000-10000, up to 20000	2500-4000	2000-3500	12000+
Discharge efficiency (%)	70-79	90-93	85	85	85	85	75-82
Cycle efficiency (%)	42-70	90-95	63-90	90-97	75-90	60-83	65-85
Response time	Minutes	Less than 1 cycle, seconds	Milliseconds	Milliseconds	Milliseconds	Milliseconds	Less than ¼ cycle
Temperature region (°C)	-	-40, 40	-5, 5	-20, 60	-	-40, 60	0, 40

APPENDIX B

Table b: Comparison of Li-ion chemistries. Cost per power is calculated using maximum peak pulse power [45][49][80][109][110][111]

Chemistry	Specific capacity (mAh/g)	Nominal voltage (V)	Energy density (Wh/l)	Cycle life (cycles)	Cost (\$/kWh)	Cost (\$/kW)	Continuous discharge rate (C)	Properties
LCO	200	3.7	400–640	500–1000	357	-	2-3	High safety risk, good lifetime
LMO	146	3.8	100–120	1000	380-260	-	1-10	Cheaper and safer than LCO and LNO
NCA	180-240	3.6	400-640	500–3000	315	-	1-3	High energy, high density, expensive
NMC	145	3.6	250-640	2000–3000	420	50	2-3, power cells over 30	High voltage, good specific energy, high safety risk, good lifetime
LFP	170	3.3	325	over 3000	80-580	526	1-25	Long lifetime, high stability, basic low cost
LTO	114	2.2	177	over 5000	1005	117	10-75	Negligible volume expansion, stable electrochemical operation, high thermal stability, expensive, power cell

APPENDIX C

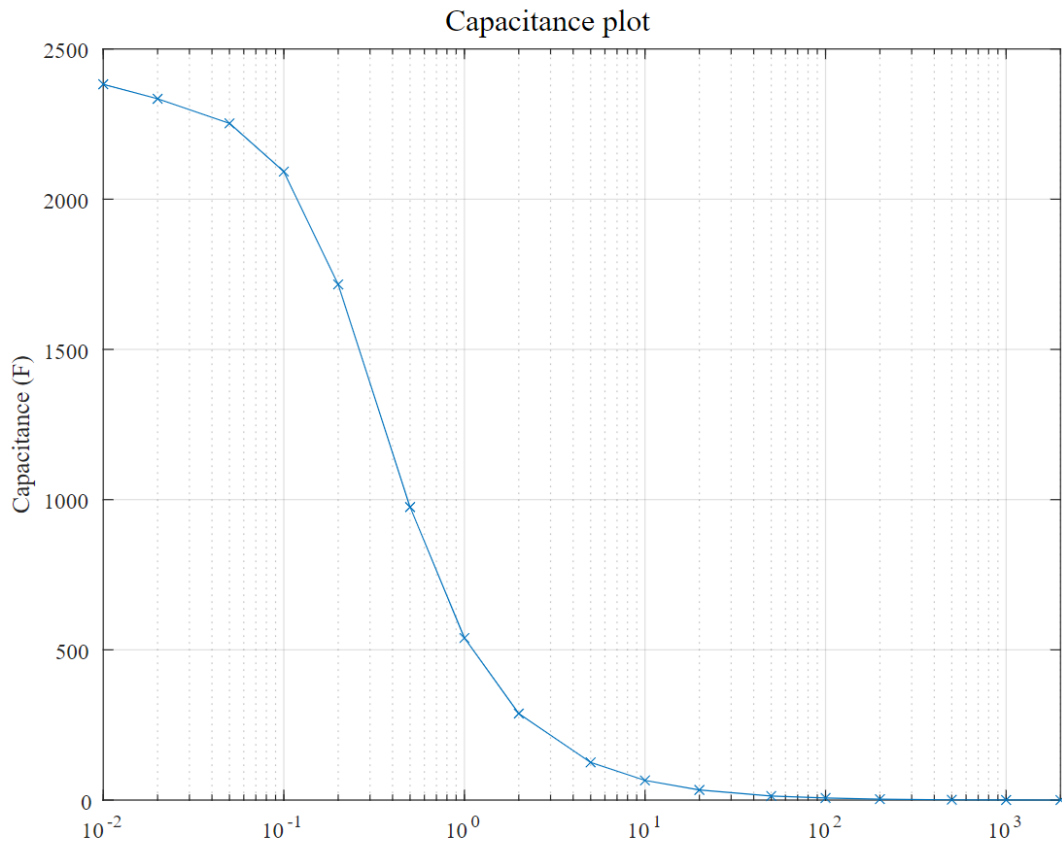


Figure C: Frequency dependent supercapacitor capacitance for a 3 V, 3000 F cell. Initial voltage 0.7 V

APPENDIX D

Impedance Bode plot

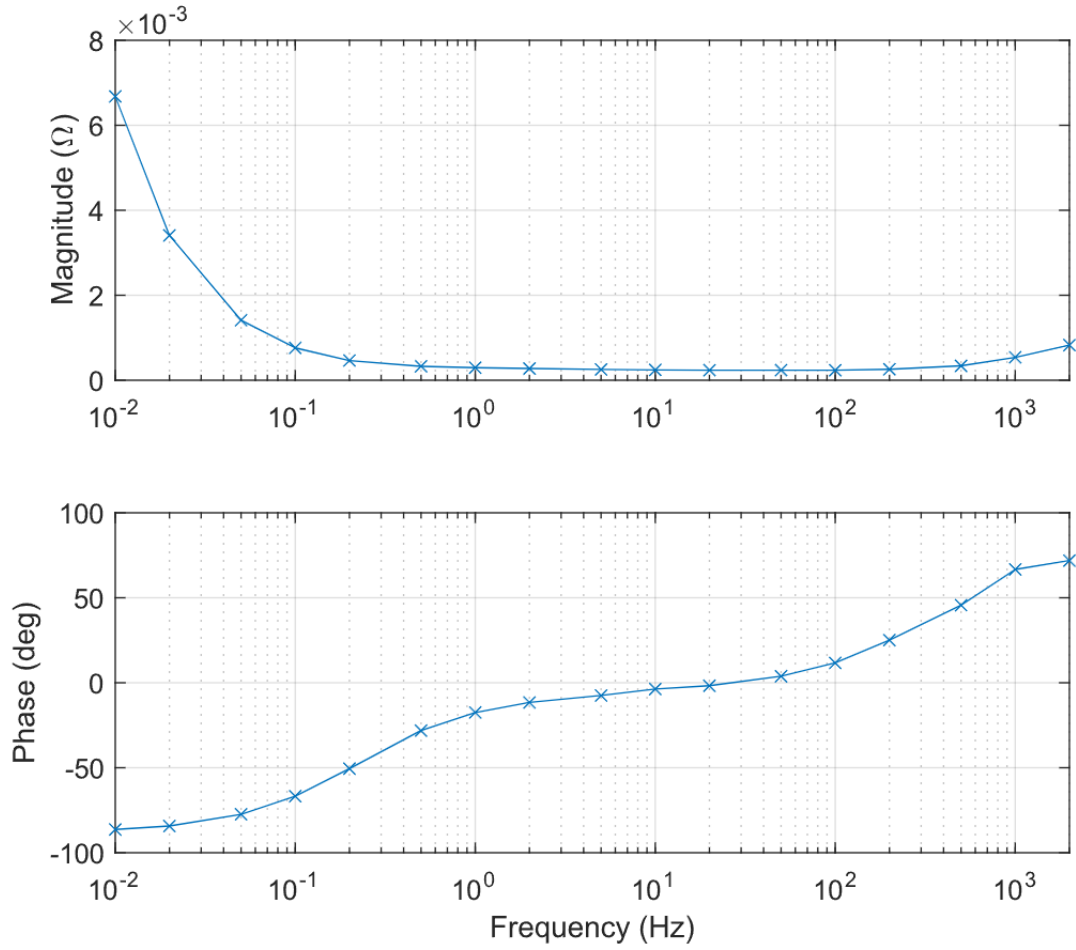


Figure D: 3 V, 3000 F Supercapacitor impedance. Initial voltage 0.7 V